POLITECNICO DI TORINO

UNIVERSIDAD POLITÉCNICA DE MADRID

ISTITUTO NAZIONALE DI RICERCA METROLOGICA

Politecnico di Torino

Master's Double Degree in

Mechatronic Engineering and Industrial Engineering

Master's Degree Thesis

Influence of Indenter Geometry and Force Alignment in Brinell, Vickers and Knoop Hardness Tests

Supervisors

Prof. Gianfranco Genta

Andrea Prato

Alessandro Germak

Candidate

Pablo Rodríguez

Academic Year 2025/2026 Turin, 23 March 2026

"One accurate measurement is worth a thousand expert opinions."
GRACE MURRAY HOPPER

Acknowledgements

Thank you to Andrea for welcoming me with his characteristic kindness from the first day I arrived at INRiM, for answering all my questions at all times, and for making me feel at home during this short but intense period dedicated to research.

Thank you to Alex for always helping me whenever any problem came up in the lab.

Thanks also to Claudio, Sergio, Daniele, and the others for those conversations and good times while playing cards during breaks.

Thanks to Prof. Gianfranco for always being attentive and available to me despite his busy schedule.

And finally, thanks to my family and friends who, even though a long distance separates us, have always made me feel their love from Spain during this journey.

This project is dedicated to you.

Grazie mille.

Abstract

The aim of the present work is to investigate the role of indenter geometry and force misalignment in Brinell, Vickers, and Knoop hardness tests. A geometrical modelling approach is used in the analysis of the impact of indenter geometry deviations on the process of indentation.

The geometrical model was tested under two different conditions: $V = \text{const}$ and $d = \text{const}$. These conditions represent two different descriptions of the indentation process from a geometrical and metrological point of view.

The results of the analysis of these two cases enable the calculation of the sensitivity of hardness to geometry deviations.

An experimental analysis of the impact of force misalignment under controlled tilt conditions was also conducted. The results of the experimental analysis were treated using weighted total least squares (WTLS) regression models in order to estimate the sensitivity coefficients and evaluate the statistical significance of the trends.

Contents

List of Figures

List of Tables

Nomenclature

Most important parameters

F	Applied test force [N]
D	Diameter of the Brinell indenter [mm]
α (1)	Angle between opposite faces in Vickers indenter [deg]
α (2)	Angle between opposite long diagonal edges in Knoop indenter [deg]
β	Angle between opposite short diagonal edges in Knoop indenter [deg]
ω	Rotation angle of the sample around the vertical axis [deg]
θ	Tilt angle of the sample with respect to the horizontal plane [deg]
d	Diameter of indentation [mm]
h	Indentation depth [mm]
A_s	Surface area of the indentation [mm^2]
V	Volume of the indentation [mm^3]
HBW	Brinell hardness number
HV	Vickers hardness number
HK	Knoop hardness number

Abbreviations

BVK	Brinell, Vickers and Knoop
VIM	International Vocabulary of Metrology
INRiM	Istituto Nazionale di Ricerca Metrologica
NMI	National Metrology Institute
EURAMET	European Association of National Metrology Institutes
TracInd BVK-H	Traceability for Indentation measurements in BVK Hardness
EMPIR	European Metrology Programme for Innovation and Research
CIPM	Centro Italiano per la Promozione della Mediazione
PTB	German National Metrology Institute
TÜBİTAK UME	Turkish National Metrology Institute
ČMI	Czech National Metrology Institute

BEV	Austrian National Metrology Institute
INM	Moldovan National Metrology Institute
IMBiH	Bosnian National Metrology Institute
ZAG	Slovenian National Metrology Institute
GUM (1)	Polish National Metrology Institute
GUM (2)	Guide to the Expression of Uncertainty in Measurement
ISO	International Organization for Standardization
ASTM	American Society for Testing and Materials
IEC	International Electrotechnical Commission
NIST	National Institute of Standards and Technology
SI	International System of Units
WP	Work Package
NA	Numerical Apertures
HBW	Brinell Hardness Wolfram
HV	Vickers Hardness
HMV	Micro-Vickers Hardness
HK	Knoop Hardness
HM	Mohs Hardness
PHS DW & PRIMARY	The Hardness Standardization Machine
MHSM	Micro Hardness Standardization Machine
WTLS	Weighted Total Least Squares
CCC	Calibration Curves Computing
BIPM	Bureau International des Poids et Mesures
KCDB	Key Comparison Database
FEM	Finite Element Methods

Chapter 1

Introduction

Measurement is one of the basic principles of engineering and a fundamental pillar in the decision-making process for those working in this field. These decisions are vitally important not only for product design and quality, but also for reliability and the associated costs. Evidence of this can be found in what Barbato states in his book:

> *"The management of measurement and testing activities is complex and demanding and cannot be reduced to a simplistic approach"* [1].

What may look like a simple routine action is actually part of a more complex situation. It is necessary to understand what is measured, why it is measured and how confident the result is. For this reason, measurement should not be considered only as a number but as useful information to achieve a final objective.

In this work, measurements are based on the concept of hardness, which is particularly relevant because it clearly represents the meaning of the measurement results and is considered one of the most important factors in the characterization of metals in industrial applications.

Hardness is measured through tests that are widely used for two main reasons: the speed with which they can be performed and their easy adaptation to routine inspections. Among the most commonly used methods, Brinell, Vickers and Knoop (BVK) hardness tests are employed to analyse how a material behaves when subjected to plastic deformation. The hardness values obtained provide information on whether a material is more

or less resistant, which in the industrial field translates into greater control of product quality and design.

One of the key aspects to take into account is that each hardness measurement depends on the method used. A specific hardness value is obtained based on a set of defined conditions and procedures. Therefore, test methods that may appear similar or equivalent at first sight may lead to different values due to elements such as the type of indenter, the applied load or the measurement system. This becomes evident when hardness values obtained in different calibration laboratories are compared, where even small differences may become significant.

From a metrological point of view, hardness measurements do not simply consist of following a set of standardised procedures and tests. It is also necessary to understand the measurement model and the quantities that influence the result, as defined in the International Vocabulary of Metrology (VIM), in particular through the concepts of *measurement model* and *influence quantity* [2]. Without this understanding, the results of the measurements may not be fully reliable. As a consequence, the hardness values obtained may not be easily comparable or properly traceable, especially in applications where high accuracy is required.

In this context, it is also relevant to mention the Istituto Nazionale di Ricerca Metrologica (INRiM), which is the National Metrology Institute of Italy. It works on research in metrology and on maintaining national measurement standards [3]. The present work has been carried out mainly in the INRiM hardness laboratory, which collaborates with both industrial clients and international calibration laboratories. These activities aim to improve measurement methodologies and reduce the associated uncertainties.

This thesis has been developed within the framework of the European research project 22RPT01 TracInd BVK-H, whose main objective is to improve the traceability and reliability of Brinell, Vickers and Knoop hardness measurements by studying the phenomena associated with indentation measurements and developing more consistent and reliable methodologies. In particular, the project addresses several factors that influence hardness testing and may contribute to inconsistencies between National Metrology Institutes (NMIs) [4]. At INRiM, several of these factors are being investigated, including the effects of creep and temperature [5, 6].

This thesis focuses specifically on two other parameters that can significantly affect hardness testing methods. In particular, it analyses the response of hardness to small variations in the geometry of the indenters and to misalignment of the force vector applied during the test. These two factors act directly on the testing machine and therefore influence the measurement process itself, unlike other influencing factors more related to environmental conditions or material characteristics.

Hardness tests using BVK methods are ideally performed assuming a perfectly defined indenter geometry and a load applied exactly perpendicular to the surface of the test specimen. However, under real laboratory conditions these ideal assumptions are rarely fully achieved. Small geometrical imperfections in the indenter and slight misalignments of the applied force with respect to the machine axis may occur. Even when these deviations remain within standardised tolerances, they may still produce noticeable variations in the geometry of the indentation and therefore in the measured hardness value.

For this reason, it is important to distinguish between the ideal measurement test defined in standards and the real measurement test carried out in laboratory conditions. A more realistic description of the indentation process can be obtained by quantifying the sensitivity of hardness measurements to small variations in the geometrical parameters of the test. In this work, particular attention is given to the determination of sensitivity coefficients describing how hardness varies as a function of changes in indenter geometry and force alignment. In addition, a consistent evaluation of the associated measurement uncertainties is performed, following the principles defined in the Guide to the Expression of Uncertainty in Measurement (GUM) [7].

The main objective of this thesis is to investigate and contribute to the development of more robust and reliable BVK hardness testing models from a metrological point of view. It also aims to improve the comparability of results and the traceability of measurements, not only between different NMIs and calibration laboratories, but also across the industrial sector, by considering the influence that geometrical imperfections in the indenter and misalignment of the applied force have on hardness measurements.

Chapter 2

Theoretical and Normative Background

2.1 Introduction to indentation hardness

By pressing an indenter into a material, it is possible to determine its indentation hardness, which is a mechanical property that measures how resistant a material is when plastic deformation occurs. In practice, a force is applied perpendicular to the surface of the material using a penetrator, resulting in an mark whose geometry is then measured using a microscope. This measurement of the dimensions of the deformed surface allows the hardness value to be calculated. This hardness value remains constant for a given material, as long as certain test conditions are satisfied. However, the hardness value varies significantly depending on the method used, the range of the applied load and the measurement scale [8].

Depending on the type of application, indentation hardness tests are classified into three main ranges: macroscopic, microscopic, and nanoscopic. Table 2.1 shows the different ranges of application according to ISO 14577-1 [8].

Table 2.1: Classification of indentation ranges according to ISO 14577-1

Range	F	h
Macro	2 N $\leq F \leq$ 30 kN	–
Micro	$F <$ 2 N	$h >$ 0.2 μm
Nano	–	$h \leq$ 0,2 μm

where:

- $\boldsymbol{F}$: applied force (N or kN)
- $\boldsymbol{h}$: penetration depth (μm)

Microscopic and nanoscopic testing is mainly used in the scientific field to investigate phenomena at the local scale (small areas in the material or thin layers). In contrast, in industrial applications, the evaluation of properties such as material homogeneity, ductility and wear resistance are present in macro-hardness tests [1, 4].

In historic terms, methods for measuring hardness have progressively developed from both a quantitative and qualitative point of view. Going back to 1822, the first documented attempt to classify the resistance of materials was made by German geologist Friedrich Mohs, who developed a scale (still used today) that classified materials from softest (HM = 1) to hardest (HM = 10) based on the ability of one material to scratch another [9]. A more detailed appreciation can be observed in Figure 2.1.

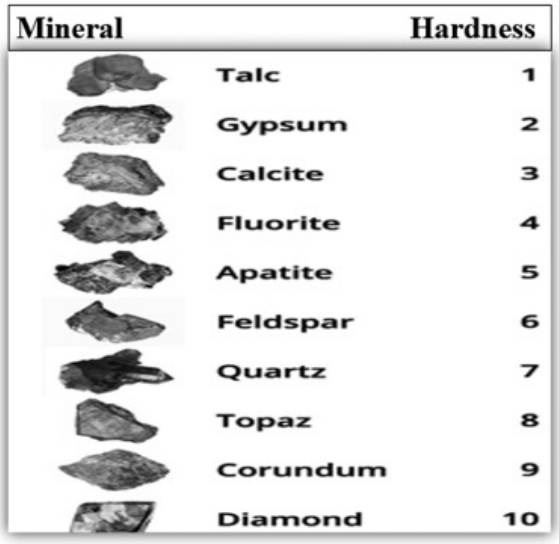

Figure 2.1: The Mohs hardness (HM) of ten defining minerals [10]

It was not until 1900 that the bases for indentation hardness were established when the first quantitative indentation method was presented by Swedish engineer Johan A. Brinell. His proposal consisted of applying a load to a hardened steel ball indented on the surface of a material, generating a mark whose geometry allowed the hardness of the material to be calculated [11]. This achievement, whose main motivation was to evaluate the rolling resistance of train wheels, was very well received due to the industrial expansion of the moment, promoted by the growth of mass production and greater demands on quality control. It was from this point onwards that new techniques such as Rockwell, Vickers and Knoop were developed, each adapted to different materials, hardness ranges and penetration depths. According to Walley, indentation hardness became a fundamental tool in engineering and materials science thanks to the consolidation of the first national laboratories and metrology institutes such as the National Bureau of Standards (now NIST), playing a key role in the traceability and standardisation of these testing methods [12].

Although each of the BVK methods uses a different indenter geometry and specific measurement parameters, they all share the fundamental principle that defines *hardness by indentation*:

> *"Hardness number is calculated using the indenter load L and the actual surface area of the impression A_c"* [13].

$$H = \frac{L}{A_c} \tag{2.1}$$

where:

- $\boldsymbol{H}$: hardness value (MPa or kgf/mm^2)
- $\boldsymbol{L}$: applied load during the test (N)
- $\boldsymbol{A_c}$: contact area of the indentation (mm^2)

The International Organization for Standardization (ISO) is very important in defining the standards of these methods. It helps to ensure metrological traceability, comparability and repeatability of measurements between different laboratories all over the world. This thesis is strongly based on the specific standards that regulate BVK indentation hardness testing:

- **ISO 6506**: Brinell hardness of metallic materials [14–16]

- **ISO 6507**: Vickers hardness of metallic materials [17–19]
- **ISO 4545**: Knoop hardness of metallic materials [20–22]

These standards provide essential information such as indenter geometries, permitted load ranges, application times, tolerances, test surface requirements, calibration procedures and hardness tester verification.

This theoretical and normative context provides the basis for the three indentation testing methods that will be covered in this thesis: Brinell, Vickers, and Knoop, which will be explained in detail in the following sections, together with their standardised formulas, technical principles, test conditions, and practical applications.

2.1.1 Brinell hardness

The Brinell hardness test consists of indenting the surface of a metallic material using a spherical tungsten carbide ball under a specified test force, and then measurements are taken from the size of the indentation. This method is one of the first standardised indentation hardness scales and is currently defined by ISO 6506-1 [14], under the denomination HBW (Brinell Hardness Wolfram).

In the Brinell method, the reduction in the influence of surface irregularities is characterised by the large diameter of the indenter. This is why they are found in low and medium hardness materials such as non-ferrous alloys, structural steels, castings and surfaces with a certain degree of roughness [23].

According to ISO 6506-1, the Brinell hardness value is defined as the applied force divided by the area of the spherical surface of the indentation mark. HBW is calculated using the expression:

$$HBW = 0.102 \cdot \frac{2F}{\pi D^2 \left(1 - \sqrt{1 - \frac{d^2}{D^2}}\right)} \tag{2.2}$$

Where:

- $\boldsymbol{F}$: test force (N)
- $\boldsymbol{D}$: diameter of the sphere (mm)

- ***d*** : mean diameter of the indentation (mm)

The mean diameter of the indentation d is obtained as the average of two indentation diameters measured in perpendicular directions:

$$d = \frac{d_1 + d_2}{2} \tag{2.3}$$

Where d_1 and d_2 are the indentation diameters measured at approximately 90° to each other.

The depth of indentation h is expressed as a function of the spherical indenter of diameter D and the measured indentation diameter d as:

$$h = \frac{D}{2}\left(1 - \sqrt{1 - \frac{d^2}{D^2}}\right) \tag{2.4}$$

A clearer appreciation of parameters F, D, h, d_1, and d_2 can be seen in Figure 2.2.

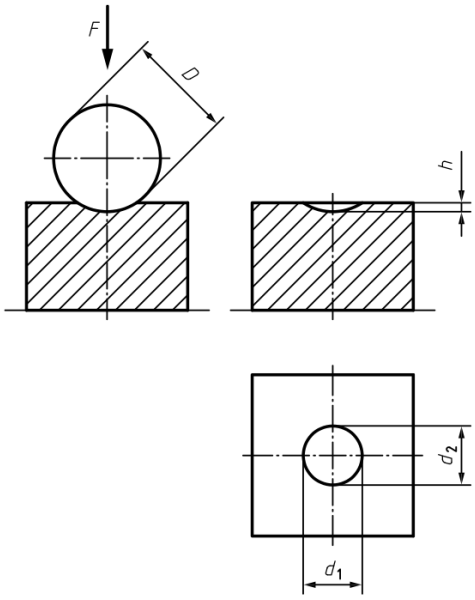

Figure 2.2: Brinell principle of test [14]

In Equation (2.2), the term $0.102 \cdot \frac{F}{D^2}$ is called *force-diameter index*. The factor $0.102 \approx$

$\frac{1}{9.80665}$ is applied to convert the test force from N to kgf ($1\,\text{kgf} = 9.80665\,\text{N}$) allowing the use of SI units.

An example of the HBW designation is shown below:

EXAMPLE

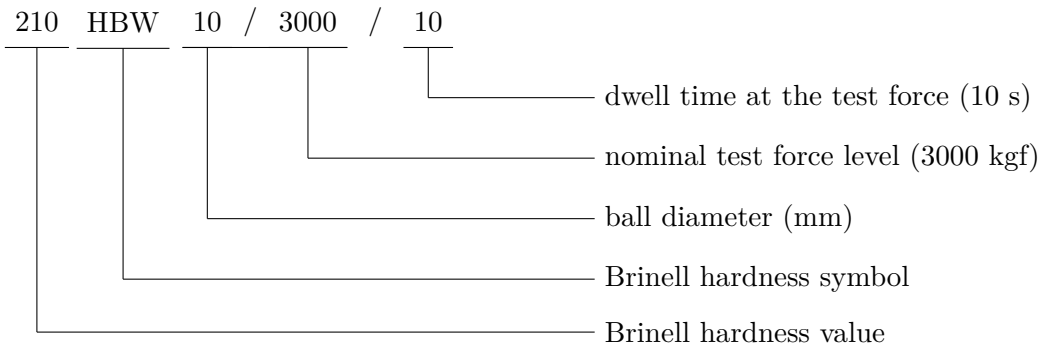

Standard parameters for the Brinell test

Following the ISO 6506-1, there are some conditions in Brinell hardness tests:

- **Indenter**: tungsten carbide ball which has diameters that vary from 1 mm to 10 mm.
- **Test force**: selected according to the indenter diameter and the tested material. Its approximate range extends from about 10 N to 30 kN and it is expressed using the notation HBW D/F.
- **Load application**: the force is applied progressively. The time between the initial application of the force and the moment when the full test force is reached is 7 s (within the limits established by the standard).
- **Dwell time**: the target duration at maximum force is 14 s (within the limits established by the standard).
- **Indentation validity**: the average diameter of the indentation must be approximately between $0.24D$ and $0.6D$.
- **Thickness and preparation of the test piece**: the thickness of the test piece shall be at least 8 times the depth of the indentation, in order to minimise any influence from the opposite surface during the test.
- **Test conditions**: the test is carried out at ambient temperature, with a reference temperature of $(23 \pm 5)\,^{\circ}\text{C}$. The minimum distances between the indentations and with respect to the edges of the test piece must also be observed.

Test procedure

In accordance again with the standard, the Brinell test consists of the following basic steps:

1. Application of the load F in a perpendicular direction to the surface.
2. Maintenance of the load F during the specified time.
3. Removal of the load F and measurement of two perpendicular indentation diameters (d_1 and d_2).
4. Calculation of HBW using the standardised expression (Equation (2.2)).

Both the testing machine and the reference hardness blocks have to be properly verified and calibrated. These procedures are carried out in accordance with ISO 6506-2 [15] for the testing machine and ISO 6506-3 [16] for the reference blocks.

2.1.2 Vickers hardness

The Vickers hardness test consists of compressing the surface of a material with a diamond indenter that is shaped as a straight pyramid with a square base and a nominal angle of 136° between opposite faces. The test is performed by applying a specific force. Once removed, the indentation produced is measured to obtain the hardness value. This method is a standardised indentation hardness scale and is currently defined by ISO 6507-1 [17], under the denomination HV (Vickers Hardness).

The Vickers method uses a pyramid-shaped diamond indenter whose geometry remains practically constant for the whole range of test forces used. As a result, the Vickers test can be applied to materials with very different hardness levels, always using the same indenter geometry. For this reason, the Vickers method is commonly used on steels, heat-treated materials and superficially hardened components, as well as in cases where smaller and more defined indentations are required than those obtained with spherical indenters [23].

According to ISO 6507-1 and similarly to the Brinell hardness test, the Vickers hardness value is defined as the relation between the applied force and the surface area of the indentation. HV is calculated using the expression:

$$\boxed{HV = \frac{1}{g_n} \frac{2F \sin\left(\frac{\alpha}{2}\right)}{d^2}} \tag{2.5}$$

Where:

- $\boldsymbol{F}$: test force (N)
- $\boldsymbol{d}$: arithmetic mean of the two indentation diagonals (mm)
- $\boldsymbol{\alpha}$: mean angle between opposite faces of the pyramidal indenter
- $\boldsymbol{g_n}$: standard acceleration because of gravity (9.80665 $\mathrm{m/s^2}$)

For the nominal indenter angle $\alpha = 136°$, the expression becomes:

$$\boxed{HV \approx 0.1891 \cdot \frac{F}{d^2}} \tag{2.6}$$

The mean diagonal length d is obtained as the arithmetic mean of the two indentation diagonals measured in perpendicular directions, according to the same definition used in Equation (2.3).

Where d_1 and d_2 are the diagonal lengths measured at approximately 90° to each other.

A clearer appreciation of parameters F, α, d_1, and d_2 can be seen in Figure 2.3.

In Equation (2.5), the factor $\frac{1}{g_n}$ is applied to convert the test force from N to kgf ($1\,\mathrm{kgf} = 9.80665\,\mathrm{N}$) allowing the use of SI units.

An example of the HV designation is shown below:

Standard parameters for the Vickers test

Following the ISO 6507-1, there are some conditions in Vickers hardness tests:

- **Indenter**: a diamond pyramid with square base and a nominal angle of about 136° between opposite faces.
- **Test force**: selected according to the tested material. Its approximate range is from 0.01 N to 1 kN and it is expressed using the notation HV F.

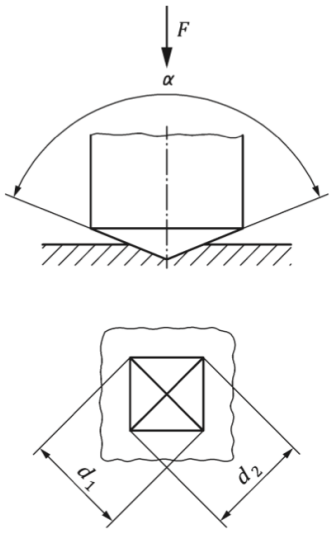

Figure 2.3: Vickers principle of test [17]

EXAMPLE

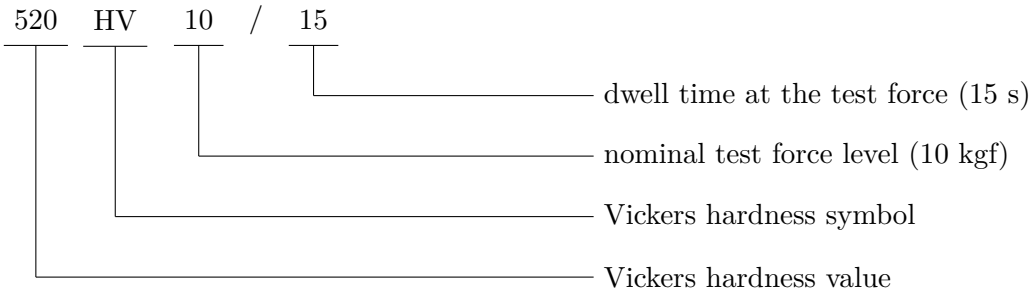

- **Load application**: as in the Brinell hardness test, the force is applied gradually and the time between the first contact and the moment when the full test force is reached is about 7 s. For Vickers and low-force Vickers hardness tests, the indenter must contact the test piece with a velocity not higher than 0.2 mm/s. For micro-Vickers hardness tests, the approach speed of the indenter must not exceed 0.070 mm/s.
- **Dwell time**: similarly to the Brinell hardness test, the target duration at maximum force is 14 s (within the limits established by the standard). If the material exhibits time-dependent behaviour, a different dwell time may be specified and shall be indicated as part of the hardness designation.
- **Indentation validity**: the perimeter of the footprint needs to be clearly defined in the microscope's field of view and the long diagonal needs to be measured at a zoom level that covers approximately 25% to 75% of the optical field of view. In Table

2.2 can be seen that d must be between 0.020-1.400 mm to ensure the resolution requirements from ISO 6507-1.

- **Thickness and preparation of the test piece**: the thickness should be at least about 1.5 times d. The thickness should not be less than 1 mm and h is 1/7 times d ($h \approx 0.143d$). Similarly to the Brinell hardness test, the surface should be clean, flat and well supported.
- **Test conditions**: as for the Brinell hardness test, the Vickers test is performed at ambient temperature, with a reference temperature of $(23 \pm 5)\,°C$. Minimum distances between indentations and with respect to the edges of the test piece must also be respected (Figure 2.4).

Table 2.2: Resolution of the diagonal measuring system in Vickers [17]

Diagonal length, d (mm)	**Resolution of the measuring system**
$0.020 \leq d < 0.080$	0.0004 mm
$0.080 \leq d \leq 1.400$	0.5 % of d

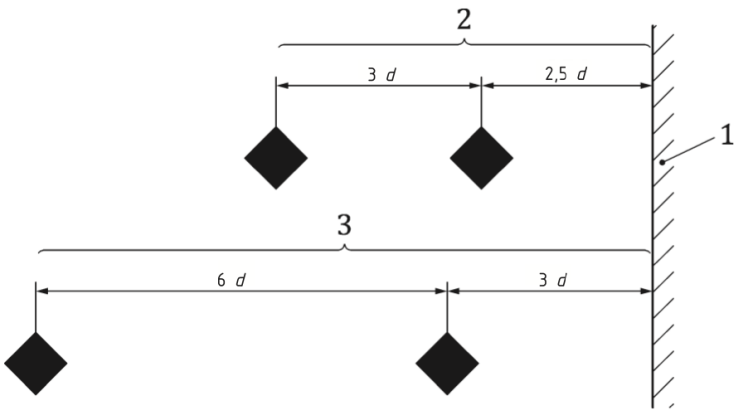

Figure 2.4: Minimum spacing of Vickers indentations [17]

Where:

1. edge of the test piece
2. copper, copper alloys and steel
3. light metals, lead and tin and their alloys

Test procedure

In accordance again with the standard, the Vickers hardness test follows the same basic procedure as the Brinell hardness test. The difference exists in the geometry of the indenter and in the hardness calculation, this time based on the Vickers hardness expression (Equation (2.5) or Equation (2.6)).

Both the testing machine and the reference hardness blocks have to be properly verified and calibrated. These procedures are carried out in accordance with ISO 6507-2 [18] for the testing machine and ISO 6507-3 [19] for the reference hardness blocks.

2.1.3 Knoop hardness

The Knoop hardness test consists of making a mark on the surface of the material using a diamond indenter shaped like a rhomboidal pyramid and then measuring the size of the indentation. Different from the Vickers test, the Knoop indenter is very elongated, which distinguishes it from the latter. The angles between the opposite edges at the apex are nominally equal to $\alpha = 172.5°$ in the direction of the long diagonal and $\beta = 130°$ in the direction of the short diagonal. Once the load is removed, only the long diagonal d of the indentation is measured for the hardness evaluation. This method is a standardised indentation hardness scale and is currently defined by ISO 4545-1 [20], under the denomination HK (Knoop Hardness).

The elongated indentation allows little-depth indentations to be formed for a certain applied force, making the Knoop method particularly useful for thin layers and coatings (surface treatments) as well as for brittle materials where it is important to reduce cracking and substrate influence. This is also one of the reasons why the Knoop hardness test is typically used in the microhardness force range [23].

According to ISO 4545-1, the Knoop hardness value is defined as the ratio between the test force and the projected area of the indentation, assuming that the indenter is a pyramid with a rhombus shape. HK is calculated using:

$$\boxed{HK = \frac{1}{g_n} \frac{F}{c\, d^2}} \tag{2.7}$$

Where:

- $\boldsymbol{F}$: test force (N)
- $\boldsymbol{d}$: length of the long diagonal of the indentation (mm)
- $\boldsymbol{c}$: indenter constant relating projected area to d^2
- $\boldsymbol{g_n}$: standard acceleration because of gravity (9.80665 m/s^2)

The indenter constant c is defined from the indenter angles as:

$$c = \frac{1}{2} \frac{\tan\left(\frac{\beta}{2}\right)}{\tan\left(\frac{\alpha}{2}\right)} \qquad \Rightarrow \qquad c \approx 0.07028 \text{ for nominal } \alpha = 172.5°,\ \beta = 130° \tag{2.8}$$

By inserting the nominal value of c into Equation (2.7), the expression becomes:

$$\boxed{HK \approx 1.451 \cdot \frac{F}{d^2}} \tag{2.9}$$

A clearer appreciation of parameters F, α, β, d, and d_s can be seen in Figure 2.5, where d_s is the length of the short diagonal of the indentation, expressed in millimetres.

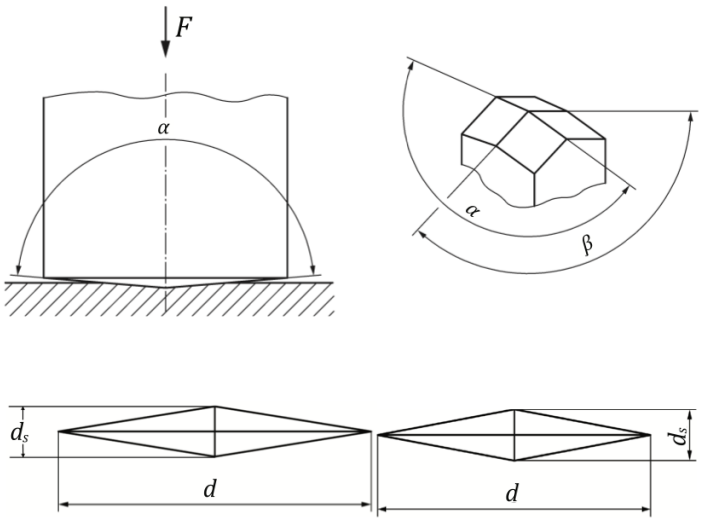

Figure 2.5: Knoop principle of test [20]

In Equation (2.7), the factor $\frac{1}{g_n}$ is applied to convert the test force from N to kgf. In accordance with ISO 4545-1, the use of the actual values for angles α and β instead of the nominal values may be considered for the calculation of Knoop hardness in order to

reduce uncertainty.

An example of the HK designation is shown below:

EXAMPLE

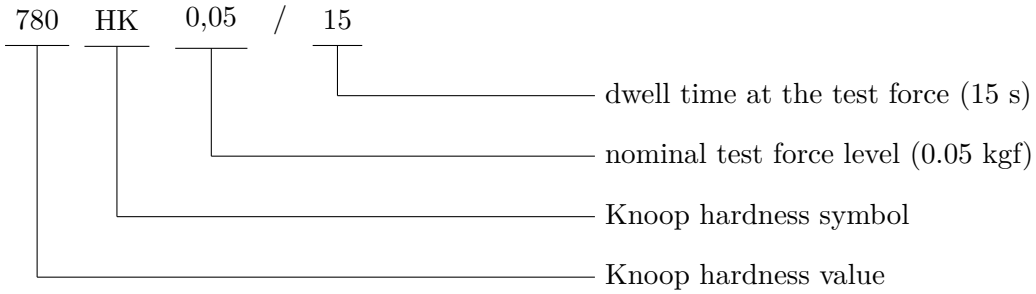

Standard parameters for the Knoop test

Following the ISO 4545-1, there are some conditions in Knoop hardness tests:

- **Indenter**: diamond pyramid with a rhomboidal base where the nominal angles between opposite edges are $\alpha = 172.5°$ for the long diagonal and $\beta = 130°$ for the short diagonal.
- **Test force**: selected according to the tested material. Its approximate range is from 0.01 N to 20 N and it is expressed using the notation HK F.
- **Load application**: as in the Brinell and Vickers hardness tests, the force is applied progressively. The time between the initial application of the force and the moment when the full test force is reached is 7 s (within the limits established by the standard). The approach speed of the indenter shall be ≤ 0.070 mm/s.
- **Dwell time**: similarly to the Brinell and Vickers hardness tests, the target duration at maximum force is 14 s (within the limits established by the standard). As in Vickers, if the material exhibits time-dependent behaviour, a different dwell time may be specified and shall be indicated as part of the hardness designation.
- **Indentation validity**: similarly to the Vickers hardness test, the perimeter of the indentation shall be clearly defined in the microscope field of view and the diagonal shall be measured using a magnification such that it occupies approximately 25% to 75% of the optical field of view. In Table 2.3 can be seen that d must be between 0.020 and 0.080 mm to ensure the resolution requirements from ISO 4545-1.
- **Thickness and preparation of the test piece**: the thickness should be at least about 1/3 of d. The variable h is approximately 1/30 times d ($h \approx 0.033d$). As for the other indentation methods, the surface should be clean, flat and properly

supported.

- **Test conditions**: as for the Brinell and Vickers hardness tests, the Knoop test is performed at ambient temperature, with a reference temperature of $(23 \pm 5)\,°C$. Minimum distances between indentations and with respect to the edges of the test piece shall also be respected. In this case, the spacing rules are expressed using both the long diagonal d and the short diagonal d_s, as illustrated in Figure 2.6.

Table 2.3: Resolution of the diagonal measuring system in Knoop [20].

Diagonal length, d (mm)	**Resolution of the measuring system**
$0.020 \leq d < 0.080$	0.0004 mm
$d \geq 0.080$	0.5 % of d

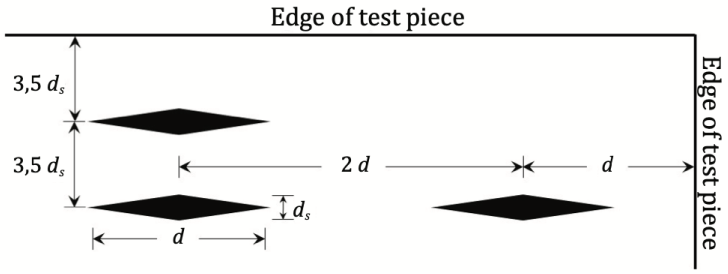

Figure 2.6: Minimum spacing of Knoop indentations [20]

Test procedure

In accordance again with the standard, the Knoop hardness test follows the same basic procedure as the Brinell and Vickers hardness tests. The difference exists in the geometry of the indenter and in the hardness calculation, this time based on the Knoop hardness expression (Equation (2.7) or Equation (2.9)). Contrary to the Vickers test, only the long diagonal of the indentation is measured. If the indentation appears asymmetrical, the long diagonal can be checked by measuring its two segments. Indentations showing excessive asymmetry shall be rejected in accordance with the standard.

Both the testing machine and the reference hardness blocks have to be properly verified and calibrated. These procedures are carried out in accordance with ISO 4545-2 [21] for the testing machine and ISO 4545-3 [22] for the reference hardness blocks.

2.2 Istituto Nazionale di Ricerca Metrologica (INRiM)

The *Istituto Nazionale di Ricerca Metrologica* (INRiM) is basically the National Metrology Institute of Italy [24]. It is a public research organisation that works in the field of metrology and carries out scientific research related to measurement science. One of its main roles is to maintain the national primary measurement standards and to ensure that they are comparable with those of other countries. INRiM also guarantees traceability to the International System of Units (SI). Moreover, INRiM is member of EURAMET (European Association of National Metrology Institutes) which supports collaboration and cooperation between different metrology institutes and infrastructures across Europe [25].

INRiM played an important role in this thesis. In its laboratories it was carried out experimental measurements using the equipment and technical support provided to obtain the corresponding measurements.

INRiM is also participating in the European TracInd project (see Section 2.3) coordinated by EURAMET, which focuses on improving traceability in hardness measurements, especially for BVK scales. Other national metrology institutes are also participating in this project, including PTB (Germany), TÜBİTAK UME (Turkey), ČMI (Czech Republic) and GUM (Poland), among others.

Metrological Traceability Pyramid

Metrological traceability is usually structured as a hierarchy which is often illustrated by a traceability pyramid. At the top of this pyramid (see Figure 2.7) are the SI and the national metrology institutes that produce and maintain the primary standards. At the base are the end users and their measuring instruments. This representation helps to visualise how traceability flows from the primary level to the end user through several intermediate levels.

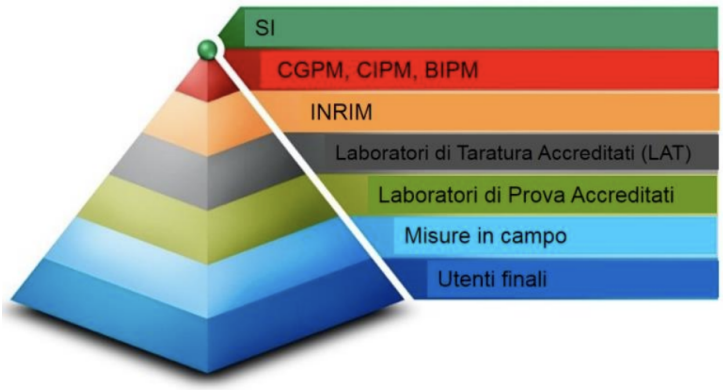

Figure 2.7: Hierarchy of metrological traceability [26]

Here are the main levels in this hierarchical traceability pyramid:

1. **National Metrology Institutes (NMIs)**: The top of the pyramid is composed by these institutions. They maintain the primary standards for SI units and perform research to implement and improve them. For example, INRiM, as Italy's NMI, establishes the national standards for units of measurement and guarantees their international equivalence. NMIs provide the highest level of reference standards and calibrations from which the entire traceability chain is derived.
2. **Accredited Calibration Laboratories**: These constitute the intermediate level of the pyramid. These laboratories (usually accredited according to ISO/IEC 17025) connect NMIs with industry and provide traceability to users [27]. Some specialise in the calibration of secondary reference standards (e.g. reference blocks), while others directly calibrate industrial testing machines. In all cases, their working standards are calibrated or verified against the NMI's primary standards, ensuring an uninterrupted chain of traceable calibrations.
3. **Industrial Instruments and Machines (End Users)**: At the bottom of the pyramid are the measuring instruments used in industrial environments, quality control laboratories and manufacturing companies. These instruments, such as hardness testers, gauges, scales, and coordinate measuring machines, are periodically calibrated either internally using working standards or by accredited calibration laboratories. The calibration of these instruments ensures that their measurements are traceable to national standards, what means that there is a documented link between the instrument reading and a higher-level reference standard.

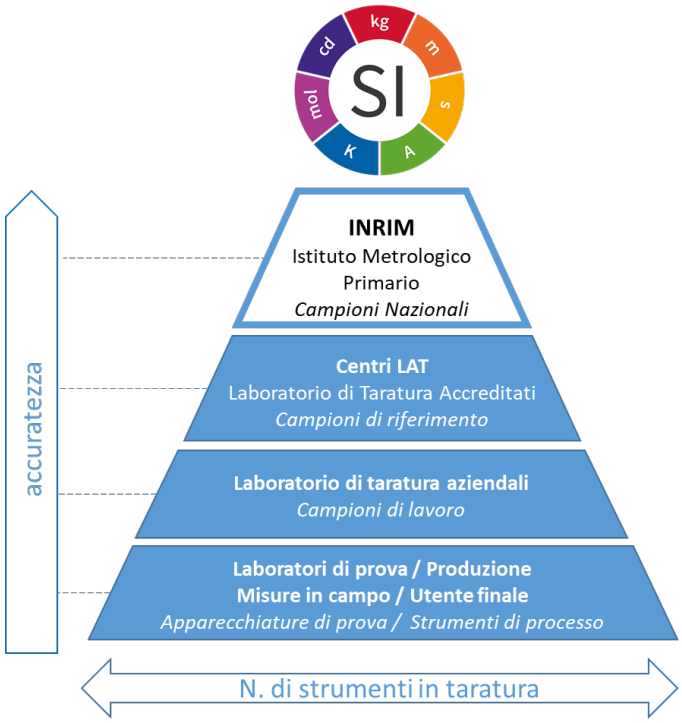

Figure 2.8: Metrological pyramid hierarchy from INRiM down to end users [28]

Thanks to this structured system, measurements performed in industry can be directly traced back to national primary standards. This makes it possible to ensure that the results obtained are both reliable and comparable.

2.3 Traceability in Brinell–Vickers–Knoop Hardness Measurements

BVK hardness methods are widely used for metallic materials. However, the traceability of their measurements presents some significant challenges. Different NMI's have observed inconsistent results in the calibration and verification of BVK hardness scales, revealing the need of a unified approach [29].

Figure 2.9: 22RPT01 TracInd BVK-H Project (EMPIR Programme) [4]

In response to these challenges, the European project *"Traceability for Indentation Measurements in Brinell–Vickers–Knoop Hardness"* (22RPT01 TracInd BVK-H) was started in 2023. The consortium consists of 14 entities from 9 countries and includes several European NMIs, such as INRiM (Italy), PTB (Germany), TÜBİTAK UME (Turkey), ČMI (Czech Republic), GUM (Poland), BEV (Austria), INM (Moldova), IMBiH (Bosnia and Herzegovina) and ZAG (Slovenia), together with academic and industrial partners. All participants are focused on improving the international traceability of BVK hardness scales [30].

Table 2.4 summarises the general distribution of tasks between the main partners of the project where WP refers to *Work Package* [31]:

Partner	**Main Role**
TÜBİTAK UME (Turkey)	Project coordination and automation of indentation measurement (WP4,WP6)
PTB (Germany)	Definition of the measured quantity and development of reference devices for indentation (WP1, WP2)
INRiM (Italy)	Traceability and uncertainty modelling framework: study of creep, temperature, indenter geometry and force alignment (WP3)
ZAG (Slovenia)	Dissemination and industrial linkages (WP5)
Other NMIs and partners	Production of reference blocks, validation activities and industrial support

Table 2.4: Main roles of the TracInd BVK-H partners [31]

The general objective of the TracInd BVK-H project is to establish a traceable, consistent and reliable indentation measurement methodology for the BVK scales. To achieve this goal, Table 2.5 [29, 31–33] presents five linked objectives and four expected impacts:

Main Objective	
Development of a more reliable and traceable framework for BVK hardness measurements	
Key Project Objectives	**Impact and Implications**
Definition of a standardised BVK hardness scale	**Industrial partners and final users**
Set uniform and repeatable standards for defining indentation limits and selecting appropriate test parameters.	More consistent hardness measurements and better alignment of instruments with international metrological requirements.
Establishment of traceable hardness reference standards	**Research and metrology environment**
Develop and characterise stable reference materials that guarantee the reproducibility of measurements at an industrial level.	Implementation of improved measurement methodologies and greater international comparability of BVK indentation results.
Structured traceability system from NMI to final users	**Standards at international level**
Develop sophisticated uncertainty models and technical guidelines for calibration and hardness testing procedures.	Contribution to the revision and unification of ISO and ASTM standards on hardness such as ISO 6506, ISO 6507 and ISO 4545 [14, 17, 20].
Digitalisation and automation of hardness testing	**Social, economic and ecological benefits**
Update the existing software tools and testing systems to make the measurement process more stable and less dependent on the person carrying out the measurement.	Reducing manufacturing costs through accurate testing, product reliability, and minimizing environmental and safety risks in critical applications.
Distribution and transfer of validated methodologies	
Promote collaboration between metrology institutes, industrial partners, and regulatory authorities to support the adoption of consistent hardness testing practices.	

Table 2.5: Objectives and expected impact of the TracInd BVK-H project [5, 6]

The need for this project became evident after several international hardness comparison studies. BVK hardness measurements lack a fully standardised measurement definition and unified equipment specifications, making it difficult to establish a common reference value and ensure consistent propagation of traceability [32].

In 2005, the CIPM (Italian Centre for the Promotion of Mediation) Brinell pilot study

CCM.H-P3 found considerable discrepancies between the NMIs results, which were attributed to variations in the indentation measurement parameters. For example, optical microscopes with different numerical apertures (NA) produced significant differences in indentation diameter measurements under identical hardness conditions. As a result, objectives with NA ≥ 0.4 are currently recommended to reduce these differences [29, 33].

However, inconsistencies persist not only between NMIs but also between secondary or industrial laboratories. At lower metrological levels, the problem is more pronounced due to the lower sophistication of equipment and insufficient control of the parameters that influence results.

The current discrepancies are due to a combination of metrological and technical factors that affect indentation measurement, which include [29, 33]:

1. **Indenter geometry:** Small deviations in the indenter geometry such as slightly rounded Vickers/Knoop tips or small diameter deviations in Brinell balls can change the projected contact area and therefore affect the measured hardness value. Variations between manufacturers and wear effects also contribute to measurement variability.
2. **Force alignment:** Misalignment between the indenter axis and the sample surface produces asymmetrical indentations and bias in measurement. Hardness testing machines must apply the load perpendicular to the surface. An angular deviation affects the projected dimensions of the indentation.
3. **Indentation creep:** During load application, certain materials continue to deform plastically over time (indentation creep). Prolonged dwell times can increase the size of the indentation. Therefore, variations in dwell time between laboratories result in measurable differences [5].
4. **Temperature effects:** The hardness of the material and the dimensions of the indentation vary with temperature. Current standards allow relatively large environmental ranges (15°C – 35°C) which can introduce variability if it is not controlled properly [6].
5. **Indentation measurement methods:** Different measurement systems (manual optical microscopes, semi-automatic software systems, 3D scanning techniques) introduce discrepancies. Edge detection depends on lighting, focus, and image processing algorithms. The lack of a standardised criteria for defining the boundaries of indentations continues to be a significant source of variability [31–33].

Traditional traceability is based on calibrating the optical system using length standards

such as micrometers and reference blocks. However, this approach only controls the 2D measurement component. In practice, the 3D characteristics of the indentations (depth and pile-up effects) cause variability between systems, even if they are all calibrated with the same length standard [29, 32].

2.4 Influence of Indenter Geometry and Force Alignment

Hardness tests are sensitive to various geometrical aspects of the indentation system. In particular, the exact geometry of the indenter and the correct alignment of the applied load with respect to the sample surface can influence the measured hardness values [34,35].

From a metrological point of view, these effects are mainly due to two causes:

- Deviations from the ideal geometry of the indenter (angles, radius of the tip or diameter of the ball)
- Angular misalignment between the load axis and the sample surface.

Both effects may slightly change the geometry of the indentation and therefore influence the values measured to calculate hardness, such as the indentation diameter, the diagonal length or the penetration depth. The following sections briefly overview the technical literature related to these two sources of error and present the geometrical interpretation adopted in this work.

2.4.1 Influence of Indenter Geometry

The geometry of hardness indenters is defined by international standards so the hardness measurements can be more reproducible. There are some examples (Figure 2.10):

- Vickers pyramid (angle of 136° between opposite faces)
- Rockwell diamond cone (vertex angle of 120° and a tip radius of 0.2 mm)
- Brinell ball

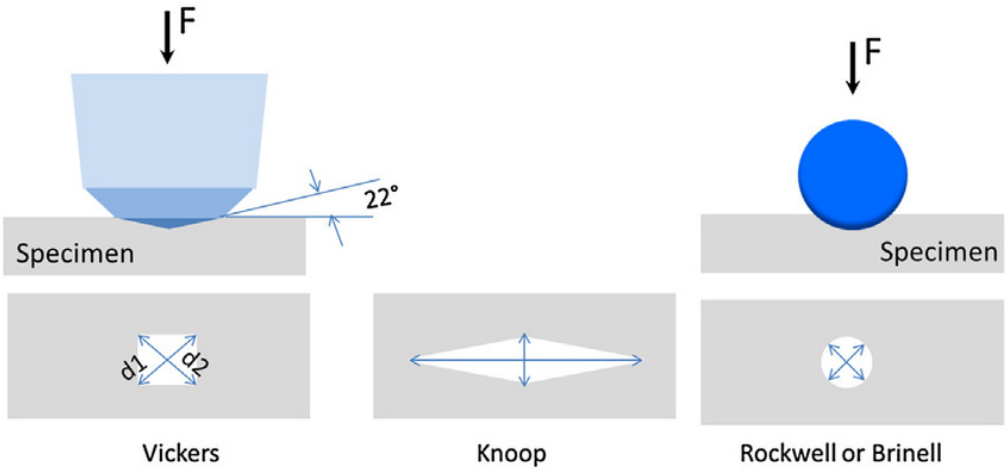

Figure 2.10: Schematic representation of typical hardness indenters and the corresponding indentation geometry [36]

It can be surprisingly, but small variations in the nominal geometry can make considerable errors in hardness. This is the reason why standards define strict tolerances for the geometrical parameters of indenters. As an example, the angle of a Vickers pyramid is typically limited to $\pm 0.5°$. On the other hand, the radius of a Rockwell diamond tip has micrometric tolerances [17].

The influence of these deviations have been investigated with experiments and simulations. El-Sherbiny et al. measured 9 Vickers indenters with small angular errors and observed that deviations in face angles affect hardness measurements [37]. Indenters with angles outside the tolerance produced HV values that deviated from the nominal value. This was also confirmed by finite element simulations (FEM).

In Rockwell tests, the geometry of the diamond cone is very important. Barbato reported that small variations in the tip radius or cone angle can produce differences in Rockwell C hardness values [38]. This also make sense with the rule of thumb proposed by Yamamoto [39], who states that the uncertainty associated with the geometry of the indenter in standard Rockwell machines is typically of the order of ± 1 HRC.

In Brinell tests, the geometry of the spherical ball is also very important. If the ball diameter deviates from the nominal value, the contact area and the resulting indentation depth are modified [40].

2.4.2 Influence of Force Alignment

The misalignment between the applied force and the normal direction of the block surface is another possible error that must be taken into account. This can cause the indentation become not totally symmetrical and because of that the hardness value measured can change [35].

In Rockwell, this effect is even more important because hardness depends on h. If there is an inclination of 1° it is sufficient to create a change in the hardness value, as Fidelus mentions in his paper [35]. And if the tilt angle becomes higher (around 2-5°) the HRC value decreases a lot.

In Brinell and Vickers tests, the effect is usually less pronounced, as hardness is obtained from optical measurements of the indentation dimensions. According to experimental results, inclinations of up to approximately 2° usually remain within the normal experimental dispersion of HV and HB measurements [35]. However, as misalignment increases, visible distortions in the indentation geometry may appear. In Vickers tests, for example, a significant difference between the two diagonals of the indentation is usually an indication of misalignment. Therefore, ASTM E384 considers highly asymmetrical indentations to be not valid measurements [41].

From a geometrical point of view, the effect of force misalignment can be interpreted through the projection of the indentation geometry on the sample surface. If the dimension of the indentation generated along the direction of the applied force is denoted by d, the dimension observed on the sample surface can be approximated as:

$$d_{\text{obs}} = d \cos\theta \tag{2.10}$$

Where θ is the angle the applied force makes with the surface normal.

This relationship shows that this configuration can make the indentation to be smaller. In Brinell and Vickers tests, hardness is inversely proportional to d^2 (see Equations 2.2 and 2.6), so even small changes in d_{obs} can produce noticeable differences in the calculated hardness.

Figure 2.11 illustrates this geometrical interpretation. The applied load vector $\mathbf{F}$ forms an angle θ with respect to the indenter axis, resulting in a projected indentation dimension

observed on the sample surface.

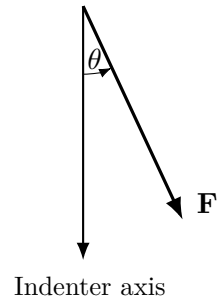

Figure 2.11: Misaligned applied load **F** forming an inclination angle θ with respect to the indenter axis

In summary, an inclination of the indenter or of the specimen means that the load is not perfectly axial, which may influence the hardness measurements. For small misalignments the effect is usually within the normal experimental uncertainty in Brinell and Vickers tests, but when the inclination becomes larger the deviations may become noticeable. For this reason, international standards recommend minimising angular misalignment and periodically checking the alignment of hardness testing machines [34, 35].

Chapter 3

Metrological modelling and methodology

3.1 Geometrical model with two boundary conditions

This section explains the geometrical–metrological models used for the BVK hardness tests. These models are later used as the base for the numerical simulations implemented in the software MATLAB. The objective is to see how the geometry of the indenter and some assumptions made during the measurements can influence hardness.

In this work the modelling is mainly based on the geometry of the indenter. The same geometrical description is used but considering two different boundary conditions. These two conditions correspond basically to two different interpretations of the indentation process.

Boundary condition 1: constant indentation volume

According to the first boundary condition, the indentation volume is supposed to remain constant during the indentation process [38, 42–44].

$$\boxed{V = V(h, p) = V_0} \tag{3.1}$$

Where:

- h : penetration depth
- p : set of geometrical parameters of the indenter (diameter, angles, etc.)

This hypothesis is based on geometry. The displaced volume produced by the indenter is supposed to be equal to a reference value (V_0). If the indenter geometry changes, then the penetration depth h needs to change also in order to keep that same volume.

Boundary condition 2: constant measured indentation dimension

In the second boundary condition the measured indentation dimension is supposed to stay constant.

$$\boxed{d = d_0 = \text{const}} \tag{3.2}$$

In this situation the indentation process itself is not explicitly modelled. Instead, the effect produced by variations in the indenter geometry is analysed using directly the hardness equation defined in the ISO standard.

In this case the geometrical dependence of hardness is already contained in the ISO analytical equation. The measured indentation parameter is assumed constant and the hardness value is recalculated according to that relation.

Looking at these two boundary conditions is relevant from a metrological point of view. The constant volume condition is related with the geometrical response of the indentation process, while the constant measured dimension condition corresponds more to the behaviour included in the hardness definitions of the standards.

In the next sections this modelling framework is used to analyse the Brinell, Vickers and Knoop hardness scales.

3.1.1 Brinell hardness model

This section presents the complete mathematical formulation adopted to analyse the influence of the indenter diameter on Brinell hardness measurements. The model reproduces

the theory implemented in the numerical simulations developed in the software MATLAB.

The analysis uses the geometry of the spherical indenter and also the indentation process. The same geometrical formulation is analysed considering the two boundary conditions defined in Section 3.1: the constant indentation volume ($V = \text{const}$) and the constant indentation diameter ($d = \text{const}$).

All geometrical relationships are derived explicitly in order to clearly identify the origin of each formula and the assumptions involved in the modelling procedure.

Geometrical description of the Brinell indentation

Figure 3.1 shows the geometrical construction used for the Brinell indentation model. In the model a sphere with radius R is intersected by the plane representing the surface of the sample at $z = z_p = R - h$. A Cartesian coordinate system is defined with origin O at the centre of the sphere. The material surface is represented as a plane intersecting the sphere at a distance h measured from the lowest point. This value h corresponds to the indentation depth. The portion of the sphere between the plane and the bottom corresponds to the displaced volume. The intersection between the plane and the sphere defines the indentation diameter d.

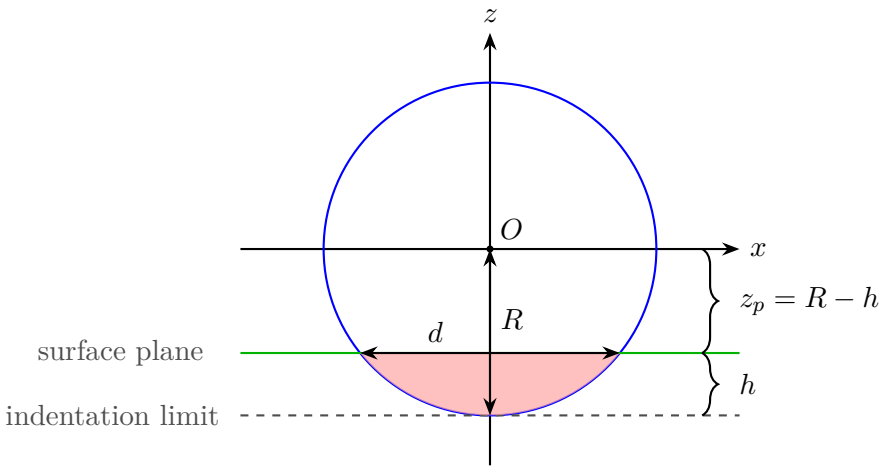

Figure 3.1: Sphere-plane intersection (Brinell geometry)

The Brinell indenter is considered to be a rigid sphere with diameter D and radius:

$$R = \frac{D}{2} \tag{3.3}$$

The equation corresponding to a sphere centred at the point O is given by:

$$x^2 + y^2 + z^2 = R^2 \tag{3.4}$$

The surface of the specimen is modelled as a plane, located at:

$$z_p = R - h \tag{3.5}$$

The intersection between the sphere and the plane is a circle corresponding to the indentation footprint. Substituting $z_p = R - h$ in the sphere equation gives:

$$\begin{aligned} x^2 + y^2 + z_p^2 = R^2 &\implies x^2 + y^2 + (R-h)^2 = R^2 \\ x^2 + y^2 = R^2 - (R-h)^2 &\implies x^2 + y^2 = 2Rh - h^2 \end{aligned} \tag{3.6}$$

Following the geometrical definition:

$$x^2 + y^2 = r^2 \tag{3.7}$$

By substituting the previous equations, the indentation radius r can be calculated:

$$r^2 = 2Rh - h^2 \implies r = \sqrt{2Rh - h^2} \tag{3.8}$$

The indentation diameter d, which is the value measured during the Brinell hardness test, is given by:

$$d = 2r \implies d = 2\sqrt{2Rh - h^2} \tag{3.9}$$

This relation establishes the geometrical relation between the indentation diameter d, the indenter radius R and the indentation depth h.

The penetration depth can be determined by solving h from the previous expression. If both sides are squared and regrouping terms, the following is obtained:

$$h^2 - 2Rh + \frac{d^2}{4} = 0 \tag{3.10}$$

The resulting solution from the quadratic equation is:

$$h = R \pm \sqrt{R^2 - \left(\frac{d}{2}\right)^2} \tag{3.11}$$

Since the condition $h < R$ must be satisfied for the penetration depth, the physically valid solution is:

$$h = R - \sqrt{R^2 - \left(\frac{d}{2}\right)^2} \tag{3.12}$$

Contact area and indentation volume

The real contact area between the indenter and the specimen is modelled as the lateral surface of a spherical cap of height h.

The area of the curved contact surface of the cap is given by the geometrical relationship [45]:

$$A_s = 2\pi Rh \tag{3.13}$$

The volume of the spherical cap is expressed as [46]:

$$\boxed{V = \frac{\pi h^2(3R - h)}{3}} \tag{3.14}$$

This volume is the geometrical volume of the material displaced by the indenter and it is used as an important variable for modelling the indentation process physically.

Brinell hardness definition

According to the ISO 6506-1 standard [14], the Brinell hardness number is given by:

$$HBW = 0.102\,\frac{F}{A_s} \tag{3.15}$$

Where:

- $\boldsymbol{F}$: applied test force (N)
- $\boldsymbol{A_s}$: curved contact area (mm^2)
- **0.102** : conversion factor from kgf to N

Substituting Eq. (3.13) into Eq. (3.15) gives:

$$HBW = 0.102\,\frac{F}{2\pi Rh} \tag{3.16}$$

Alternatively, hardness can be expressed depending on the measured indentation diameter d, giving the ISO formula indicated previously in Section 2.1.1 (Equation (2.2)):

$$\boxed{HBW = 0.102\,\frac{2F}{\pi D^2}\left(1-\sqrt{1-\frac{d^2}{D^2}}\right)} \tag{3.17}$$

Inversion of the ISO Brinell hardness formula

In order to apply the volume-constrained geometry, the nominal indentation diameter d_0 associated with a reference hardness value HBW_0 has to be determined. This can be done by inverting the ISO Brinell hardness equation with respect to the measured indentation diameter d.

Starting from Eq. (3.17) and restructuring the expression:

$$HBW = \left(\frac{0.204\,F}{\pi D}\right)\left(D-\sqrt{D^2-d^2}\right) \tag{3.18}$$

The algebraic inversion of this expression is reported in Appendix A.1. The resulting exact solution for the indentation diameter d is:

$$\boxed{d = \sqrt{2D\left(\frac{0.204\,F}{\pi D\,HBW}\right) - \left(\frac{0.204\,F}{\pi D\,HBW}\right)^2}} \tag{3.19}$$

Using this expression it is possible to obtain the nominal indentation diameter d_0 that corresponds to a reference hardness value HBW_0 in the ISO-based metrological model.

Constant indentation volume condition ($V = \text{const}$)

> *In the geometrical model based on volume conservation, it is assumed that the indentation volume remains the same as the reference value V_0.*

According to the constant indentation volume condition ($V = \text{const}$) introduced in Section 3.1, the indentation volume is assumed to remain equal to the reference value V_0 when small variations in the indenter diameter D occur:

$$\boxed{V(R, h) = V_0 = \text{const}} \tag{3.20}$$

For a nominal configuration defined by $(D_0, F, HBW_{\text{ref}})$, first the nominal indentation diameter d_0 is obtained by inverting the ISO hardness formula with Eq. (3.19). Then the parameters h_0 and V_0 are calculated:

$$h_0 = R_0 - \sqrt{R_0^2 - \left(\frac{d_0}{2}\right)^2} \tag{3.21}$$

$$V_0 = \frac{\pi h_0^2(3R_0 - h_0)}{3} \tag{3.22}$$

When the constant volume condition is used for the spherical cap, the following expression is obtained.

$$V(R_1, h_1) = \frac{\pi h_1^2(3R_1 - h_1)}{3} = V_0 \tag{3.23}$$

After rearranging the equation, a cubic equation for the penetration depth h_1 appears.

$$h_1^3 - 3R_1 h_1^2 + \frac{3V_0}{\pi} = 0 \tag{3.24}$$

The equation admits a closed analytical solution, which is obtained by reducing it to a depressed cubic and applying the trigonometric Cardano–Viète method [47] (see Appendix A.2).

The solution with physical meaning, which satisfies $0 < h_1 < 2R_1$, is the following:

$$\boxed{h_1 = R_1 + 2R_1 \cos\left[\frac{1}{3}\arccos\left(1 - \frac{3V_0}{2\pi R_1^3}\right) - \frac{2\pi}{3}\right]} \tag{3.25}$$

If the penetration depth h_1 is known, the indentation diameter d_1 can be calculated using the spherical geometry relations. Then the hardness value is obtained using Eq. (3.16):

$$HBW(D_1) = 0.102\,\frac{F}{2\pi R_1 h_1} \tag{3.26}$$

With:

$$R_1 = \frac{D_1}{2} \tag{3.27}$$

With this boundary condition HBW decreases with D, giving a negative slope. A larger indenter diameter produces a more superficial indentation for the same displaced volume. This behaviour can be observed in the numerical results of Figure 4.4.

Constant indentation diameter condition ($d = \text{const}$)

> *According to the ISO-based metrological formulation, the measured indentation diameter is considered to be the same as the nominal value d_0.*

$$\boxed{d = d_0 = \text{const}} \tag{3.28}$$

In this ISO metrological approach the measured indentation diameter is taken as equal to the nominal value d_0.

Therefore, the hardness value is calculated as:

$$HBW(D) = HBW(D, d_0, F) \tag{3.29}$$

So basically the ISO equation already contains the geometrical dependence of the hardness value.

With this hypothesis the model predicts a positive slope of HBW with respect to D, since the mathematical relation is already present in the ISO formulation. This behaviour also appears in the numerical results of Figure 4.4.

Sensitivity coefficient

The effect of the indenter diameter D on the hardness value can be described by the sensitivity coefficient:

$$\boxed{c_D = \frac{\partial HBW}{\partial D}} \tag{3.30}$$

Because obtaining this derivative analytically is not easy, the sensitivity coefficient is calculated numerically using a forward finite difference [48]:

$$\boxed{c_D \approx \frac{HBW(D + \Delta D) - HBW(D)}{\Delta D}} \tag{3.31}$$

3.1.2 Vickers hardness model

As in the Brinell case (Section 3.1.1), the mathematical model of the Vickers hardness test is written by explicitly analysing the geometrical contribution of the indenter. The model reproduces the theory implemented in the numerical simulations developed in MATLAB.

The analysis uses the exact geometry of the quadrangular pyramidal indenter used in

the Vickers hardness test and also the indentation process. As in the Brinell model, the same geometrical formulation is analysed considering the two boundary conditions introduced in Section 3.1, namely the constant indentation volume condition and the constant indentation diagonal condition.

All geometrical relationships are derived explicitly in order to identify where each equation comes from and what assumptions are behind the modelling procedure.

For the numerical application, a nominal reference state is first defined from a selected test force and a prescribed reference hardness value. Then the corresponding nominal diagonal, penetration depth and indentation volume are calculated and used as the starting point for the parametric analysis.

Geometrical description of the Vickers indentation

The Vickers indenter is modelled as a square-based pyramid. Its nominal geometry is defined by the face-to-face angle $\alpha_0 = 136°$ between opposite faces (ISO 6507-1 [17]).

After unloading, the indentation mark is assumed to be a square on the surface of the specimen, characterised by the average diagonal length d, obtained as the average of the two measured diagonals.

The geometrical construction used in the model is shown in Figures 3.2 and 3.3. In these figures the penetration depth is indicated as h. The square indentation has a lateral side length s and a diagonal length d. Their corresponding half lengths are $s/2$ and $d/2$.

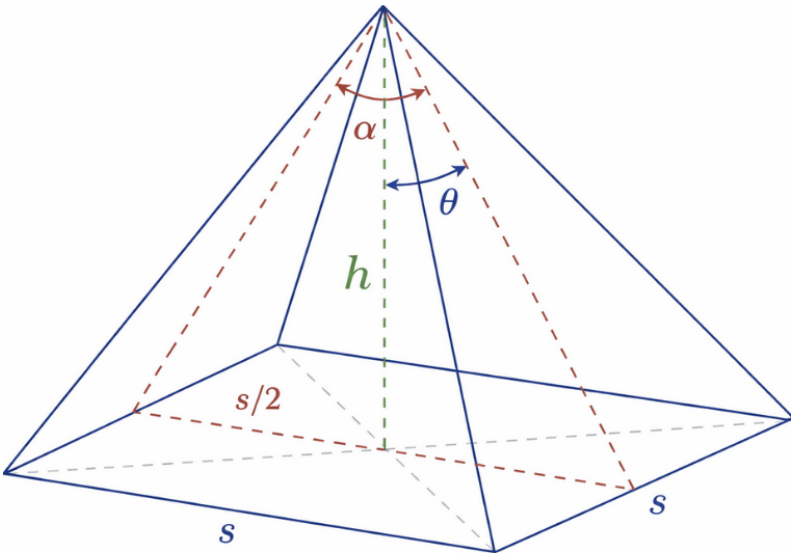

Figure 3.2: Geometrical construction adopted for the Vickers indenter model

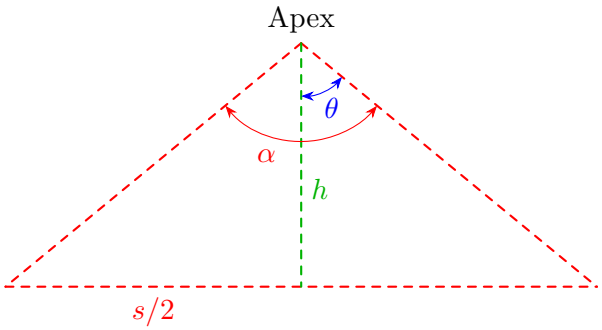

(a) Axial section of the Vickers indenter

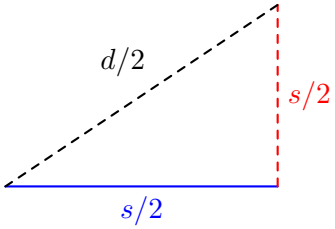

(b) Geometric relation between $d/2$ and $s/2$

Figure 3.3: Auxiliary geometrical relations used in the Vickers indentation model

Geometrical relationships between d, s and h

The indentation footprint is taken as a square with side length s. Using the Pythagorean theorem on half of the square [49], the relation between the diagonal and the side is obtained:

$$\left(\frac{d}{2}\right)^2 = \left(\frac{s}{2}\right)^2 + \left(\frac{s}{2}\right)^2 \quad \Rightarrow \quad d = \sqrt{2}\, s \quad \Rightarrow \quad s = \frac{d}{\sqrt{2}} \tag{3.32}$$

The pyramid slope is determined by the face-to-face angle α. If $\theta = \alpha/2$ is defined, then from the triangular section it follows that:

$$\tan\theta = \frac{s/2}{h} \tag{3.33}$$

The following auxiliary parameter is introduced:

$$a = \tan\theta = \tan\left(\frac{\alpha}{2}\right) \tag{3.34}$$

Substituting $s = d/\sqrt{2}$ from Equation (3.32), it is obtained:

$$a = \frac{s}{2h} = \frac{d}{2\sqrt{2}\,h} \quad \Rightarrow \quad \boxed{d = 2\sqrt{2}\,a\,h} \tag{3.35}$$

And equivalently:

$$\boxed{h = \frac{d}{2\sqrt{2}\,a}} \tag{3.36}$$

These expressions give the geometrical relation between the diagonal length d, the indentation depth h and the indenter geometry through the parameter a.

Projected area and indentation volume

The projected area is the area of the square footprint:

$$A_p = s^2 \tag{3.37}$$

Using $s = d/\sqrt{2}$ from Equation (3.32), this becomes:

$$A_p = \left(\frac{d}{\sqrt{2}}\right)^2 \quad \Rightarrow \quad A_p = \frac{d^2}{2} \tag{3.38}$$

These geometrical relations make it possible to describe the indentation volume depending on the indenter geometry and the penetration depth.

In this geometrical model based on volume conservation, the displaced volume is simply taken as the volume of a pyramid with base area A_p and height h [50].

$$V = \frac{1}{3} A_p h \tag{3.39}$$

Substituting Equation (3.38) gives:

$$V = \frac{1}{3} \left(\frac{d^2}{2} \right) h \tag{3.40}$$

Finally, using $d = 2\sqrt{2}ah$ from Equation (3.35), it follows that:

$$d^2 = 8a^2h^2 \quad \Rightarrow \quad V = \frac{1}{3} \left(\frac{8a^2h^2}{2} \right) h \quad \Rightarrow \quad \boxed{V = \frac{4}{3} a^2 h^3} \tag{3.41}$$

This expression is the one used for the indentation volume in the Vickers model.

Vickers hardness definition

ISO 6507-1 [17] defines the Vickers hardness as the applied force over the contact area of the indentation.

Considering the ideal Vickers geometry, this definition gives the standard hardness expression normally used:

$$\boxed{HV(\alpha) = \frac{1}{g_n} \frac{2F \sin\left(\frac{\alpha}{2}\right)}{d^2}} \tag{3.42}$$

Where F is expressed in N, d in mm, and $g_n = 9.80665$ N/kgf. When the nominal indenter angle is $\alpha_0 = 136°$, the expression simplifies and gives the common formula used for the Vickers hardness calculation:

$$\boxed{HV = \frac{0.1891\,F}{d^2}} \tag{3.43}$$

This simplified expression has already been shown previously in Equation (2.6).

Inversion of the ISO Vickers hardness formula

For the purposes of the model, it is useful to invert the nominal Vickers hardness expression in order to express the indentation diagonal as a function of the target hardness value and the applied test force:

$$HV = \frac{0.1891\,F}{d^2} \quad \Rightarrow \quad \boxed{d(HV, F) = \sqrt{\frac{0.1891\,F}{HV}}} \tag{3.44}$$

This inverted relation allows the calculation of the nominal diagonal corresponding to a reference hardness value for a given applied force.

Nominal state (d_0, h_0, V_0)

For a nominal test condition defined by the applied force, the reference hardness value and the nominal indenter angle, the nominal indentation diagonal is first obtained using the inverted hardness relation. From this value the corresponding slope parameter of the indenter is calculated:

$$a_0 = \tan\left(\frac{\alpha_0}{2}\right) \tag{3.45}$$

Then the nominal penetration depth is obtained from the geometrical relation between diagonal, depth and indenter geometry:

$$h_0 = \frac{d_0}{2\sqrt{2}\,a_0} \tag{3.46}$$

Finally, the nominal indentation volume is obtained from the expression previously derived for the Vickers indentation volume:

$$\boxed{V_0 = \frac{4}{3} a_0^2 h_0^3} \tag{3.47}$$

This nominal state represents the reference configuration used later in the parametric analysis.

Constant indentation volume condition ($V = \text{const}$)

> *In this formulation it is assumed that the indentation volume remains equal to the reference value V_0.*

According to the constant indentation volume condition introduced in Section 3.1, the indentation volume is assumed to remain constant even when small variations occur in the indenter angle.

$$\boxed{V(a(\alpha), h(\alpha)) = V_0 = \text{const}} \tag{3.48}$$

Using the expression of the indentation volume, this condition can be written in terms of the auxiliary parameter and the indentation depth:

$$\frac{4}{3} a(\alpha)^2 h(\alpha)^3 = \frac{4}{3} a_0^2 h_0^3 \quad \Rightarrow \quad a(\alpha)^2 h(\alpha)^3 = a_0^2 h_0^3 \tag{3.49}$$

Solving this relation gives the penetration depth as a function of the indenter angle:

$$\boxed{h(\alpha) = h_0 \left(\frac{a_0}{a(\alpha)} \right)^{2/3}} \tag{3.50}$$

The corresponding indentation diagonal is then calculated from the geometrical relation previously obtained:

$$d(\alpha) = 2\sqrt{2}\, a(\alpha)\, h(\alpha) \tag{3.51}$$

Replacing Equation (3.50) gives:

$$\boxed{d(\alpha) = d_0 \left(\frac{a(\alpha)}{a_0} \right)^{1/3}} \tag{3.52}$$

Once the indentation diagonal is known, the hardness value is calculated using the nominal Vickers hardness expression:

$$\boxed{HV_{V=\text{const}}(\alpha) = \frac{0.1891\, F}{d(\alpha)^2}} \tag{3.53}$$

Under the constant-volume condition, an increase of the face-to-face angle produces a larger indentation diagonal. Since hardness is inversely proportional to the square of the diagonal, the model predicts a negative slope of hardness with respect to the indenter angle. This behaviour can also be observed in the numerical results presented in Figure 4.10.

Constant indentation diagonal condition ($d = \text{const}$)

> *In the ISO-based metrological formulation, the measured indentation diagonal is assumed to remain equal to the nominal value d_0.*

$$\boxed{d = d_0 = \text{const}} \tag{3.54}$$

According to this condition, variations in the indenter angle do not modify the size of the indentation footprint.

Instead, the hardness value changes only through the geometrical factor contained in the ISO hardness definition.

Therefore, the angular dependence is introduced only through the analytical relation between applied force, indenter geometry and hardness:

$$\boxed{HV_{d=\text{const}}(\alpha) = \frac{1}{g_n} \frac{2F \sin\left(\frac{\alpha}{2}\right)}{d_0^2}} \tag{3.55}$$

Under the condition of constant diagonal, hardness changes only through the trigonometric factor associated with the indenter angle. Since this function increases with the angle in the range considered, the model predicts a positive slope of hardness with respect to the indenter angle. This behaviour also appears in the numerical results shown in Figure 4.10.

Sensitivity coefficient

The effect of the indenter geometry, represented here by the face-to-face angle α, on the hardness value can be described by the sensitivity coefficient:

$$\boxed{c_\alpha = \frac{\partial HV}{\partial \alpha}} \tag{3.56}$$

Because obtaining this derivative analytically is not straightforward, the sensitivity coefficient is calculated numerically using a forward finite difference [48]:

$$\boxed{c_\alpha \approx \frac{HV(\alpha + \Delta\alpha) - HV(\alpha)}{\Delta\alpha}} \tag{3.57}$$

In the numerical implementation developed in MATLAB, this coefficient is evaluated for different nominal hardness levels in order to quantify how sensitive the Vickers hardness result is to deviations in the indenter geometry.

Sensitivity to diagonal measurement error

In addition to the angular sensitivity coefficient c_α, the numerical implementation also includes a more general metrological study based on the sensitivity of the Vickers hardness value to the measured diagonal d.

Starting from the ISO Vickers hardness equation:

$$HV = \frac{0.1891\, F}{d^2} \tag{3.58}$$

The sensitivity coefficient with respect to the measured diagonal is defined as:

$$\boxed{c_d = \frac{\partial HV}{\partial d}} \tag{3.59}$$

Differentiating with respect to d gives:

$$\boxed{c_d = -\frac{2 \cdot 0.1891\, F}{d^3}} \tag{3.60}$$

This coefficient is evaluated in the numerical simulations for the complete set of ISO Vickers test forces considered in this work and for several nominal hardness levels.

In this way, it is possible to quantify the propagation of diagonal measurement errors to the final hardness value under different testing conditions.

Unlike the angular sensitivity coefficient c_α, which is linked to deviations in indenter geometry for a fixed reference configuration, the coefficient c_d provides a more direct metrological indicator associated with the measurement process itself. Because of that, it is especially useful for global comparisons across different Vickers scales.

3.1.3 Knoop hardness model

This subsection presents the mathematical formulation adopted to analyse the influence of indenter geometry on Knoop hardness measurements. As for Brinell and Vickers (Sections 3.1.1 and 3.1.2), the model reproduces the theory implemented in the numerical simulations developed in MATLAB.

The analysis uses the exact geometry of the rhomboidal pyramidal indenter used in the Knoop hardness test and also the indentation process. As in the Brinell and Vickers models, the same geometrical formulation is analysed considering the two boundary conditions introduced in Section 3.1, namely the constant indentation volume condition ($V = \text{const}$) and the constant long-diagonal condition ($d_1 = \text{const}$).

All geometrical relationships are derived explicitly in order to identify where each equation comes from and what assumptions are behind the modelling procedure.

For the numerical application, a nominal reference state is first defined from a selected test force, prescribed reference hardness value and nominal indenter geometry. Then the

corresponding nominal long diagonal, short diagonal, penetration depth and indentation volume are calculated and used as the starting point for the parametric analysis.

Geometrical description of the Knoop indentation

The Knoop indenter generates a rhomboidal indentation characterised by two diagonals:

- Longest diagonal d_1
- Shortest diagonal d_2

Figure 3.4 shows the geometrical representation used in the model. The geometry of the indenter is defined by two edge angles, α and β, which are associated with the faces that control the formation of d_1 and d_2, respectively. The nominal values of these angles are 172.5° for α and 130° for β. The penetration depth of the indenter is denoted by h.

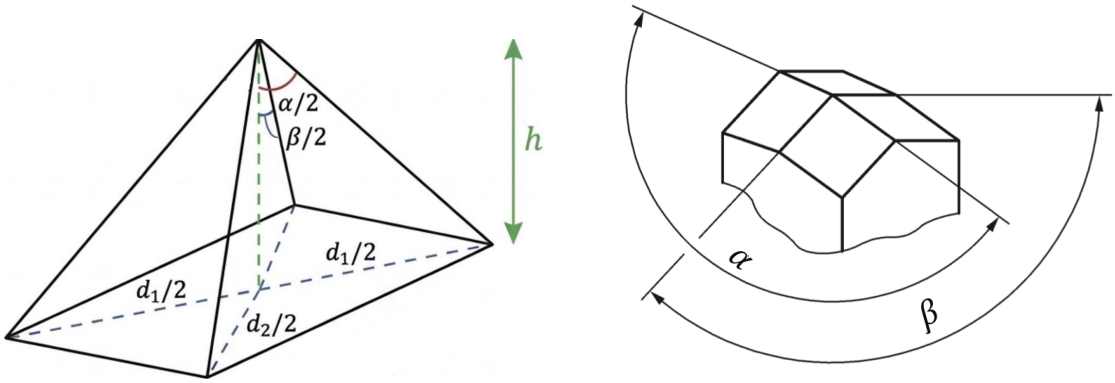

(a) 3D geometry of the Knoop indenter

(b) Angles between opposite edges α and β [20]

Figure 3.4: Geometrical construction adopted for the Knoop indentation model

Using trigonometry on each diagonal, the following relationships are obtained:

$$\tan\left(\frac{\alpha}{2}\right) = \frac{d_1/2}{h} \qquad \tan\left(\frac{\beta}{2}\right) = \frac{d_2/2}{h} \tag{3.61}$$

Which results in:

$$\boxed{d_1 = 2h\ \tan\left(\frac{\alpha}{2}\right) \qquad d_2 = 2h\ \tan\left(\frac{\beta}{2}\right)} \tag{3.62}$$

Projected area and indentation volume

The projected contact area is the rhomboid area [51]:

$$A_p = \frac{d_1 d_2}{2} \tag{3.63}$$

Replacing Eq. (3.62) into Eq. (3.63) gives:

$$A_p = \frac{1}{2}\left(2h\tan\frac{\alpha}{2}\right)\left(2h\tan\frac{\beta}{2}\right) = 2h^2\tan\left(\frac{\alpha}{2}\right)\tan\left(\frac{\beta}{2}\right) \tag{3.64}$$

These geometrical relations make it possible to describe the indentation volume depending on the indenter geometry and the penetration depth.

In this geometrical model based on volume conservation, the displaced volume is simply taken as the volume of a pyramid with projected area A_p and height h:

$$V = \frac{1}{3}A_p h \tag{3.65}$$

Using Equation (3.64), the volume becomes:

$$V = \frac{1}{3}\left[2h^2\tan\left(\frac{\alpha}{2}\right)\tan\left(\frac{\beta}{2}\right)\right]h \tag{3.66}$$

That is:

$$\boxed{V = \frac{2}{3}\,h^3\tan\left(\frac{\alpha}{2}\right)\tan\left(\frac{\beta}{2}\right)} \tag{3.67}$$

So this is basically the expression used for the indentation volume in the Knoop model.

Indenter constant c and Knoop hardness formula

From Equation (3.62), the ratio of diagonals is:

$$\frac{d_2}{d_1} = \frac{\tan(\beta/2)}{\tan(\alpha/2)} \qquad \Rightarrow \qquad d_2 = d_1 \, \frac{\tan(\beta/2)}{\tan(\alpha/2)} \tag{3.68}$$

Therefore, the projected area can be expressed as a function of d_1:

$$A_p = \frac{d_1 d_2}{2} = \frac{d_1^2}{2} \, \frac{\tan(\beta/2)}{\tan(\alpha/2)} = c(\alpha, \beta) \, d_1^2 \tag{3.69}$$

With the indenter constant c:

$$\boxed{c(\alpha, \beta) = \frac{\tan(\beta/2)}{2 \tan(\alpha/2)}} \tag{3.70}$$

In line with the ISO formulation [20], Knoop hardness is defined as force F divided by the projected contact area A_p:

$$HK = \frac{1}{g_n} \frac{F}{A_p} \tag{3.71}$$

Using Equation (3.69), the following expression is obtained (Equation (2.7)):

$$\boxed{HK(\alpha, \beta) = \frac{1}{g_n} \frac{F}{c(\alpha, \beta) \, d_1^2}} \tag{3.72}$$

This expression is the starting point for the two boundary-condition formulations presented below.

Nominal state and reference volume

The nominal angles are denoted as α_0 and β_0, with the corresponding constant given by $c_0 = c(\alpha_0, \beta_0)$. For the nominal condition (F, HK_{ref}), the long diagonal can be obtained

by inverting Eq. (3.72) in the nominal geometry.

$$\boxed{d_{1,0} = \sqrt{\frac{1}{g_n}\,\frac{F}{c_0\,H K_{\mathrm{ref}}}}} \tag{3.73}$$

From Equation (3.62), the nominal depth h_0 is:

$$\boxed{h_0 = \frac{d_{1,0}}{2\tan(\alpha_0/2)}} \tag{3.74}$$

The nominal short diagonal is:

$$\boxed{d_{2,0} = 2h_0 \tan\left(\frac{\beta_0}{2}\right)} \tag{3.75}$$

And the nominal volume used in the constant-volume formulation follows from Equation (3.67):

$$\boxed{V_0 = \frac{2}{3}\,h_0^3 \tan\left(\frac{\alpha_0}{2}\right)\tan\left(\frac{\beta_0}{2}\right)} \tag{3.76}$$

So this nominal state is the reference starting point used later in the parametric analysis.

Constant indentation volume condition ($V = \mathrm{const}$)

> *In this formulation it is assumed that the indentation volume remains equal to the reference value V_0.*

According to the constant indentation volume condition introduced in Section 3.1, the indentation volume is assumed to remain constant even when small variations occur in the indenter angles α and β.

$$\frac{2}{3}h^3 \tan\left(\frac{\alpha}{2}\right)\tan\left(\frac{\beta}{2}\right) = V_0 \tag{3.77}$$

Using the expression of the indentation volume, this condition can be written in terms of the indenter angles and the penetration depth.

$$h^3 = \frac{3V_0}{2\tan\left(\frac{\alpha}{2}\right)\tan\left(\frac{\beta}{2}\right)} \tag{3.78}$$

Solving this relation gives the penetration depth as a function of the indenter angles:

$$\boxed{h(\alpha,\beta) = \left[\frac{3V_0}{2\tan(\alpha/2)\tan(\beta/2)}\right]^{1/3}} \tag{3.79}$$

The corresponding projected diagonals are:

$$d_1(\alpha,\beta) = 2h(\alpha,\beta)\tan\left(\frac{\alpha}{2}\right) \qquad d_2(\alpha,\beta) = 2h(\alpha,\beta)\tan\left(\frac{\beta}{2}\right) \tag{3.80}$$

Once the projected diagonals are known, the Knoop hardness is evaluated according to Equations (3.63) and (3.71):

$$\boxed{HK_{V=\text{const}}(\alpha,\beta) = \frac{1}{g_n}\frac{F}{A_p(\alpha,\beta)} = \frac{1}{g_n}\frac{2F}{d_1(\alpha,\beta)\,d_2(\alpha,\beta)}} \tag{3.81}$$

Under the constant-volume condition, an increase in α or β modifies the penetration depth and the projected diagonals. Since hardness is inversely proportional to the projected area, the model predicts a negative slope of HK with respect to both angles. This tendency is clearly observed in Figures 4.22 and 4.23.

Constant measured long diagonal condition ($d_1 = \text{const}$)

> *In the ISO-based metrological formulation, the measured longest indentation diagonal is assumed to remain equal to the nominal value $d_{1,0}$.*

$$\boxed{d_1 = d_{1,0} = \text{const}} \tag{3.82}$$

According to this condition, variations in α and β do not modify the measured long diagonal.

Instead, the hardness value changes only through the dependence of the indenter constant $c(\alpha, \beta)$ on the indenter geometry.

Therefore, the geometrical dependence is introduced only through the analytical relation between applied force, indenter constant and hardness:

$$\boxed{HK_{d_1=\text{const}}(\alpha, \beta) = \frac{1}{g_n} \frac{F}{c(\alpha, \beta)\, d_{1,0}^2}} \tag{3.83}$$

In this formulation, hardness variations are governed only by the dependence of the indenter constant on the indenter angles. The resulting trend can be evaluated numerically from Equation (3.83).

Sensitivity coefficients to indenter angles

Similar to the Brinell and Vickers analyses, the influence of indenter angles is quantified using sensitivity coefficients. For each result of the model $HK(\alpha, \beta)$, the sensitivity coefficients are defined as:

$$\boxed{c_\alpha = \frac{\partial HK}{\partial \alpha} \qquad c_\beta = \frac{\partial HK}{\partial \beta}} \tag{3.84}$$

Because obtaining these derivatives analytically is not easy, the sensitivity coefficients are evaluated numerically using forward finite differences [48]:

$$\boxed{c_\alpha \approx \frac{HK(\alpha + \Delta\alpha, \beta) - HK(\alpha, \beta)}{\Delta\alpha}} \tag{3.85}$$

$$\boxed{c_\beta \approx \frac{HK(\alpha, \beta + \Delta\beta) - HK(\alpha, \beta)}{\Delta\beta}} \tag{3.86}$$

In the numerical implementation developed in MATLAB, these coefficients are evaluated

for different nominal hardness levels in order to quantify how sensitive the Knoop hardness result is to deviations in the indenter geometry.

Sensitivity to long-diagonal measurement error

In addition to the angular sensitivity coefficients c_α and c_β, the numerical implementation also includes a more general metrological study based on the sensitivity of the Knoop hardness value to the measured long diagonal d_1. This is useful because d_1 is the direct measurand used in the Knoop hardness test.

Starting from the nominal Knoop hardness expression used in the numerical implementation:

$$HK = \frac{C_{HK}\, F}{d_1^2} \tag{3.87}$$

where $C_{HK} \approx 1.451$ for F in N and d_1 in mm, the sensitivity coefficient with respect to the measured long diagonal is defined as:

$$\boxed{c_{d_1} = \frac{\partial HK}{\partial d_1}} \tag{3.88}$$

Differentiating with respect to d_1 gives:

$$\boxed{c_{d_1} = -\frac{2\, C_{HK}\, F}{d_1^3}} \tag{3.89}$$

This coefficient is evaluated in the numerical simulations for the complete set of ISO Knoop test forces considered in this work and for several nominal hardness levels.

In this way, it is possible to quantify the propagation of long-diagonal measurement errors to the final hardness value under different testing conditions.

Unlike the angular sensitivity coefficients c_α and c_β, which are linked to deviations in indenter geometry for a fixed reference configuration, the coefficient c_{d_1} provides a more direct metrological indicator associated with the measurement process itself. For this reason, it is particularly useful for global comparisons across different Knoop scales.

3.2 Numerical implementation and modelling methodology

A numerical code was implemented in MATLAB to analyse the influence of small deviations in the indenter geometry on the hardness values obtained in BVK tests. The models were based on the geometrical definitions of the corresponding hardness scales and on the nominal geometries of the indenters specified by the ISO standards [14, 17, 20].

For each scale, a nominal reference condition was first defined. Next, controlled variations were introduced into the geometrical parameter of interest in order to evaluate the corresponding change in calculated hardness. The disturbed parameters were the ball diameter D for Brinell hardness, the included face angle α for the Vickers indenter, and the two characteristic angles α and β for the Knoop indenter. In the local sensitivity analyses, the parameters were varied symmetrically around the nominal value, considering three increments and three decrements together with the reference configuration.

Two idealised modelling conditions were analysed. In the first case, it was assumed that the indentation volume remained constant ($V = \text{const}$). In the second case, it was assumed that the characteristic dimension measured from the indentation mark remained constant. This corresponds to the indentation diameter d for Brinell and Vickers tests, and to the long diagonal d_1 for Knoop tests.

For each disturbed configuration, the geometry of the indentation and the corresponding hardness value were recalculated. Then the sensitivity coefficients around the nominal condition were computed numerically using direct finite differences.

$$c_x \approx \frac{H(x_0 + \Delta x) - H(x_0)}{\Delta x} \tag{3.90}$$

Where x denotes the perturbed geometric parameter.

Table 3.1: Perturbed geometrical parameters considered in the numerical model

Hardness scale	Perturbed parameter(s)	Perturbation strategy
Brinell	Ball diameter D	$D_0 \pm n\Delta D$, $n = 1,2,3$
Vickers	Face angle α	$\alpha_0 \pm n\Delta\alpha$, $n = 1,2,3$
Knoop	Angles α, β	$\alpha_0 \pm n\Delta\alpha$, $\beta_0 \pm n\Delta\beta$, $n = 1,2,3$

3.3 Experimental measurements

The experimental study was designed to investigate the influence of sample orientation and surface misalignment on indentation hardness measurements and to experimentally evaluate the sensitivity coefficients associated with force misalignment.

In contrast to the geometrical models from Section 3.1, which study how the indenter geometry affects hardness values, the experimental investigation focuses on the effect of load misalignment (tilt). This effect cannot be fully described by the solid geometry model, since the deformation caused by the inclined force is not directly represented through geometrical volume boundary conditions.

Two geometrical factors are taken into account in the experimental plan.

In the experiments the main factor considered is the inclination of the sample surface relative to the horizontal plane, indicated by the angle θ. This inclination represents a misalignment between the indenter axis and the axis perpendicular to the sample surface, similar to the situation analysed in the modelling work. The tilted blocks used for the measurements were supplied by the Polish National Metrology Institute (GUM) [52].

- For Brinell, Vickers and Knoop tests:
  - $\theta = 0°$, $0.25°$, $0.5°$, $1°$, $2°$ and $5°$

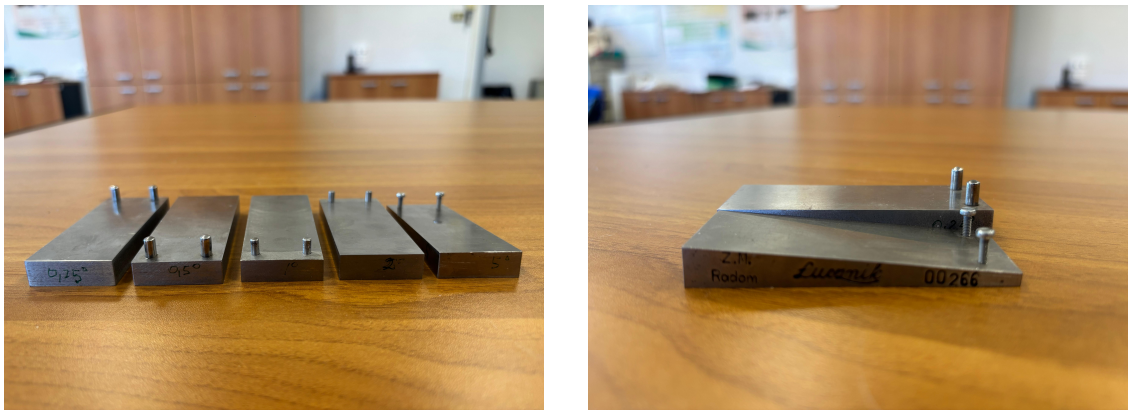

(a) All θ configurations (b) Difference between $\theta = 0.25°$ and $\theta = 5°$

Figure 3.5: Specimen inclination configurations used in the experimental study

A second geometrical factor is the rotation in the plane of the samples, referred to as

the angle ω, which represents the rotation of the hardness block around the vertical axis. The ω rotation is not the primary subject of the present study; however, it is included because, particularly in Vickers and Knoop tests, different sample orientations may lead to different measured hardness values even under nominally identical test conditions. The inclusion of ω therefore allows orientational effects to be accounted for and ensures that the influence attributed to θ is not biased by a specific specimen orientation.

The rotation angle ω only applies to Vickers and Knoop tests, as the spherical geometry of the Brinell indenter makes the measurement invariant to rotations in the plane.

- For Vickers tests:
  - $\omega = 0°$, $30°$, $60°$ and $90°$
- For Knoop tests:
  - $\omega = 0°$, $45°$, $90°$, $135°$ and $180°$
- For Brinell tests:
  - $\omega = 0°$

A graphical representation of the geometrical parameters ω and θ is shown in Figure 3.6.

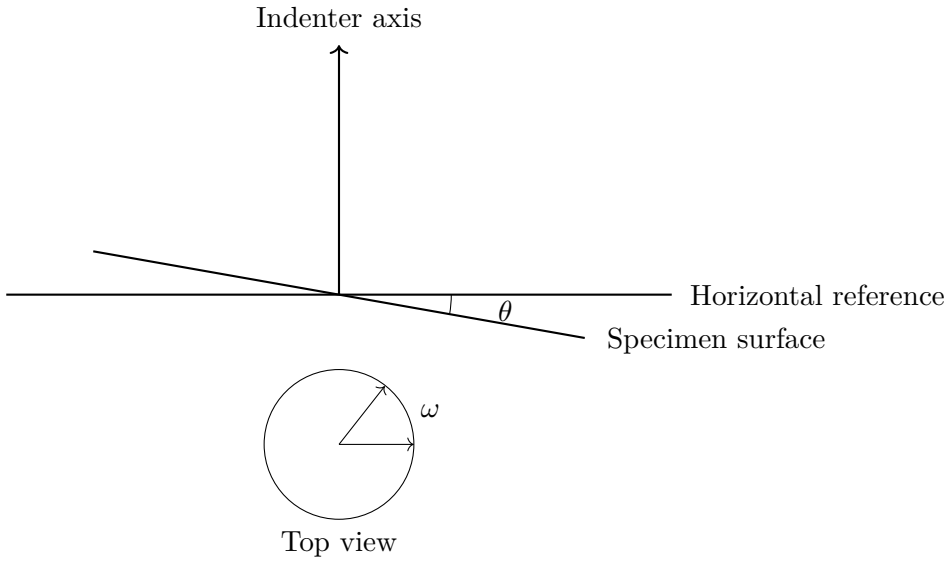

Figure 3.6: Rotation of the specimen around the indenter axis (ω) and inclination of the specimen surface with respect to the horizontal plane (θ)

Macro-hardness measurements were performed using the Brinell HBW 2.5/62.5 scale and

the Vickers HV 30 scale. Micro-hardness measurements were performed using the Vickers HV 1 and Knoop HK 2 scales.

Macro-hardness measurements (HBW 2.5/62.5 and HV 30) were performed using the PHS DW & PRIMARY (The Hardness Standardization Machine).

Micro-hardness measurements (HV 1 and HK 2) were performed with the MHSM (Micro Hardness Standardization Machine).

(a) PHS DW & PRIMARY machine

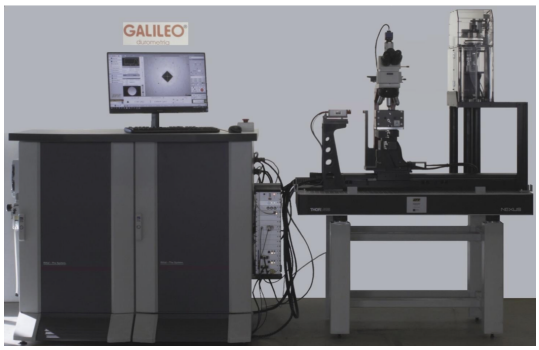

(b) MHSM machine

Figure 3.7: Hardness standardization machines used for macro- and micro-hardness measurements

In addition to the schematic representation of the setups, real views of the experimental arrangements are shown in Figures 3.8 and 3.9. The first figure shows the reference blocks mounted in the macro- and micro-hardness machines, while the second one shows the corresponding optical systems used during the measurement stage.

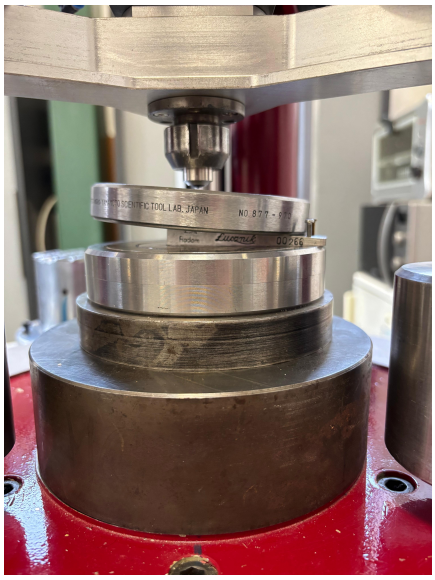

(a) Tilted block mounted in the macro-hardness machine

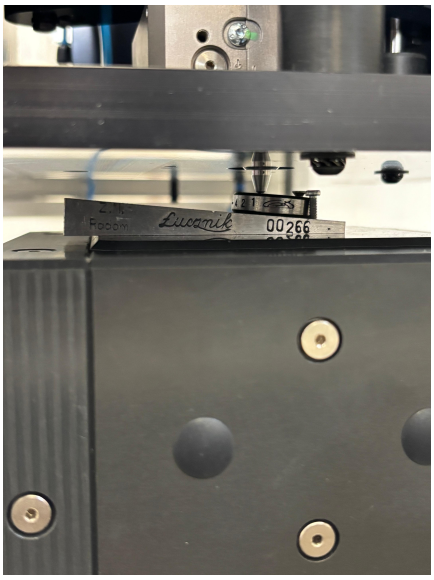

(b) Tilted block mounted in the micro-hardness machine

Figure 3.8: Tilted blocks mounted in the macro- and micro-hardness machines

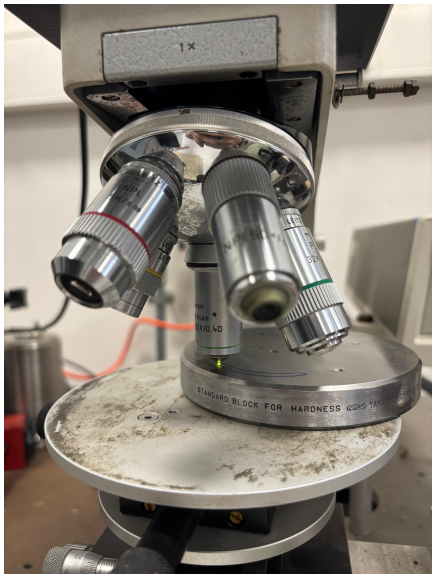

(a) Macro optical system

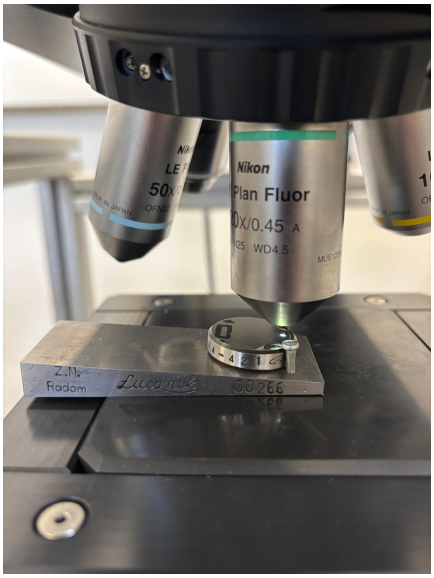

(b) Micro optical system

Figure 3.9: Optical systems used for macro- and micro-hardness measurements

The HBW 500 block was originally designed for Brinell measurements. However, once the tests were carried out it became clear that the indentation produced with the 2.5 mm

ball was extremely small due to the high hardness of the block. In practice, this caused difficulties during observation under the microscope. The boundaries of the projected sphere were not clearly visible, making it very difficult to take the d_1 and d_2 measurements. For this reason, the results of the HBW 500 block were not taken into account and only the HBW 200 block was included in the Brinell analysis.

The experimental blocks (hardness levels) selected for the tests are:

Macro Brinell (HBW 2.5/62.5)
- HBW 200 block

Micro Vickers (HV 1)
- HMV 200 block
- HMV 700 block

Macro Vickers (HV 30)
- HV 100 block
- HV 700 block

Micro Knoop (HK 2)
- HMV 200 block
- HMV 700 block

The certified reference blocks used in the experimental campaign are shown in Figure 3.10. From top to bottom, the figure includes the Brinell reference block, the macro-Vickers blocks and the micro-hardness blocks used for Vickers and Knoop measurements.

Figure 3.10: Certified reference blocks used in the experimental campaign. From top to bottom: Brinell block, macro-Vickers blocks and micro-hardness blocks used for Vickers and Knoop measurements

For Vickers and Knoop tests, full combinations of ω and θ were planned only for tilted

configurations ($\theta \neq 0°$). Only one measurement was taken for the nominal configuration ($\omega = 0°$, $\theta = 0°$). This avoids doing redundant measurements while still keeping a reference value for later comparison.

In the Brinell measurements only θ was varied, while ω was kept at 0°, since the spherical indenter is symmetric around its axis.

The resulting number of measurements is summarised in Table 3.2. For Knoop hardness, the ten measurements corresponding to $\theta = 5°$ were not retained because the resulting indentations were too irregular to be measured reliably.

Table 3.2: Experimental plan and number of hardness measurements

Hardness scale	**Regime**	**Blocks**	**Orientations**	**Measurements**
HV 30	Macro	HV 100, HV 700	4ω, 6θ	42
HV 1	Micro	HMV 200, HMV 700	4ω, 6θ	42
HK 2	Micro	HMV 200, HMV 700	5ω, θ up to 2°	42
HBW 2.5/62.5	Macro	HBW 200	1ω, 6θ	6
		Total number of experiments		**132**

3.3.1 Experimental workflow and measurement procedure

Although the objective was basically the same for all hardness scales, the way the measurements were done depended on the type of indentation and on the instrumentation available.

For Brinell measurements, the indentation diameters were evaluated manually using the measuring microscope. The operator first positioned the optical reference at one tangent point of the residual imprint and reset the displacement reading to zero. The microscope stage was then translated until the opposite tangent point was reached. The measured displacement directly provided the corresponding diameter. This procedure was repeated along two approximately orthogonal directions in order to obtain d_1 and d_2.

For macro-Vickers measurements, the indentations were produced in the macro-hardness machine and evaluated by combining the optical microscope with the LabVIEW-based acquisition and control software. The software allowed the indentation image to be captured and processed, and the diagonal lengths were obtained from the automatically detected indentation vertices. As a consequence, the measurement was less dependent on

direct manual tangent positioning than in the Brinell case.

For micro-Vickers and micro-Knoop measurements, the measurement stage was performed using the *GalVision* software environment associated with the micro-hardness standardization machine. In these cases, the images were acquired directly in the software and the indentation dimensions were obtained through the `Indirect Measure` mode. This mode allows the image to be analysed after indentation and provides a convenient framework for repeated measurements of the same imprint, including the corresponding statistical descriptors.

Representative views of the laboratory instrumentation are shown in Figures 3.11 and 3.12.

(a) Display at the beginning (b) Display at the end

Figure 3.11: Display of the microdurometer

(a) Micro-Vickers measurement in GalVision (b) Micro-Knoop measurement in GalVision

Figure 3.12: Examples of indentation measurement performed with the GalVision software using the `Indirect Measure` mode

Brinell tests

The experiments were performed on a certified HBW 200 reference block (HBW 2.5/62.5 level).

The indentations were made using tilt angles $\theta = 0°$, $0.25°$, $0.5°$, $1°$, $2°$ and $5°$.

For every angle, the diameters of the indentation (d_1 and d_2) were measured manually using the microscope. The optical reference was first placed on the left tangent point of the imprint and the reading was reset to zero. The microscope stage was then translated until the right tangent point was reached. The displacement obtained directly provided the diameter in millimetres. The same procedure was repeated in the orthogonal direction.

Finally, the mean diameter was calculated as

$$\bar{d} = \frac{d_1 + d_2}{2} \tag{3.91}$$

The Brinell hardness values were calculated using the indentation diameters measured on the specimen surface after the tests. The mean diameter obtained from the optical measurement was directly used in the ISO hardness equation, and the hardness values were determined following the standard Brinell formulation given in Equation (2.2).

A representative Brinell indentation observed through the microscope is shown in Figure 3.13. The manual procedure used for determining the indentation diameter is illustrated in Figure 3.14. The force–time and displacement–time curves related to the Brinell loading cycle are discussed later in Section 3.3.2.

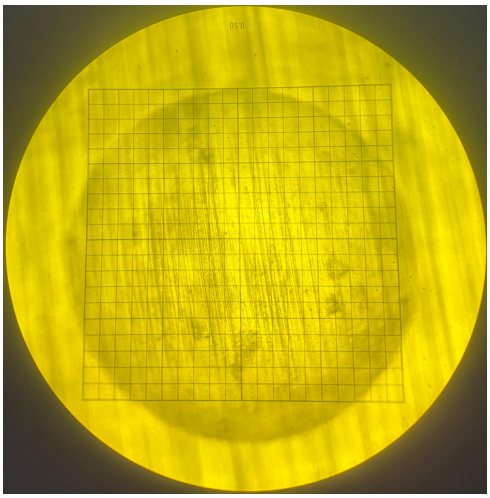

Figure 3.13: Example of Brinell indentation observed through the microscope

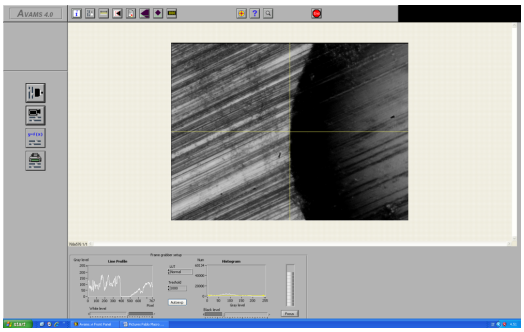

(a) Left tangent position

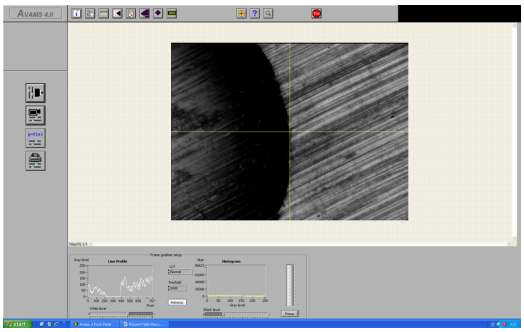

(b) Right tangent position

Figure 3.14: Manual determination of the Brinell indentation diameter using tangents placed on the two opposite edges of the imprint

Vickers tests

The experiments were done on certified Vickers reference blocks for macro- and micro-hardness measurements (HV 30 and HV 1).

The indentations were carried out using tilt angles $\theta = 0°$, $0.25°$, $0.5°$, $1°$, $2°$ and $5°$.

For each angle the diagonals of the indentation, d_1 and d_2, were measured and afterwards the mean diagonal was calculated as

$$\bar{d} = \frac{d_1 + d_2}{2} \tag{3.92}$$

The Vickers hardness values were obtained from the diagonals measured on the specimen surface after the tests. The mean diagonal from the optical measurement was used directly in the ISO hardness equation, and the hardness values were calculated using the standard Vickers formula given in Equation (2.6).

In the macro-Vickers measurements the diagonals were determined using the LabVIEW optical system. The software automatically detected the vertices of the indentation and directly gave the diagonal lengths. Because of this, the measurement was less dependent on manual positioning than in the Brinell measurements. Some examples of this procedure are shown in Figure 3.16.

For micro-Vickers measurements the images were analysed in the GalVision software using the indirect measurement mode after the indentation. Examples of these measurements are presented in Figures 3.17 and 3.18.

At higher tilt angles such as 2° and 5°, the imprints became more irregular and the corners were not always very clear. In these cases the appearance of the indentation also depended on the orientation of the imprint with respect to the surface texture.

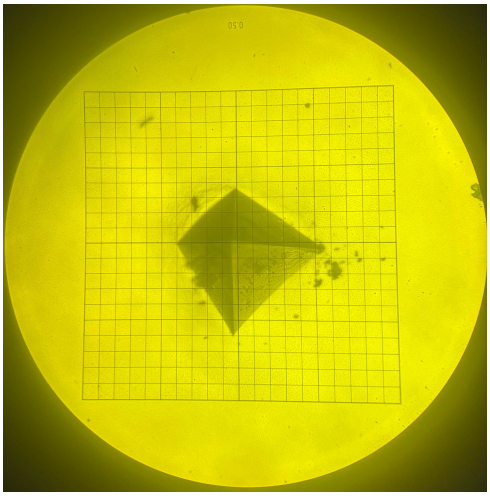

Figure 3.15: Vickers 5° indentation observed through the microscope

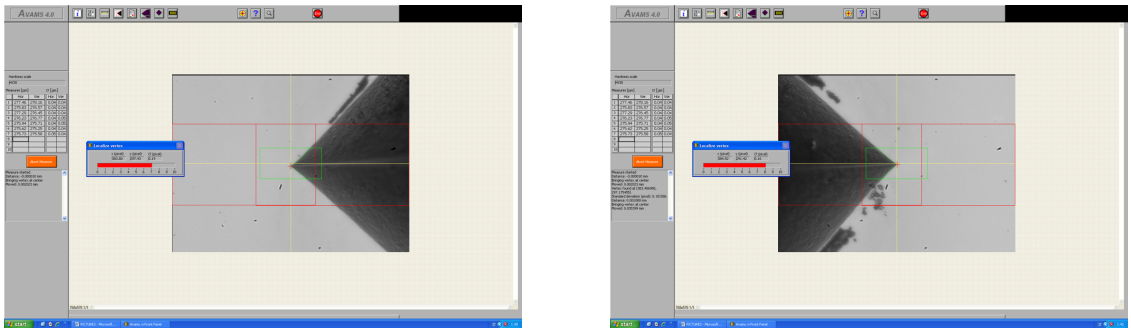

(a) Detection of one vertex

(b) Detection of the opposite vertex

Figure 3.16: Automatic vertex detection during macro-Vickers measurement

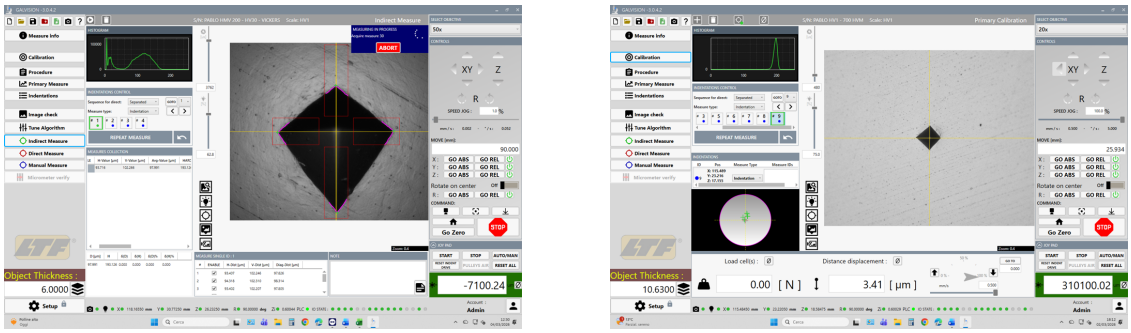

(a) Micro-Vickers indentation measurement with an inclination of 5°

(b) Example of a nominal micro-Vickers indentation

Figure 3.17: Examples of micro-Vickers measurements carried out using GalVision

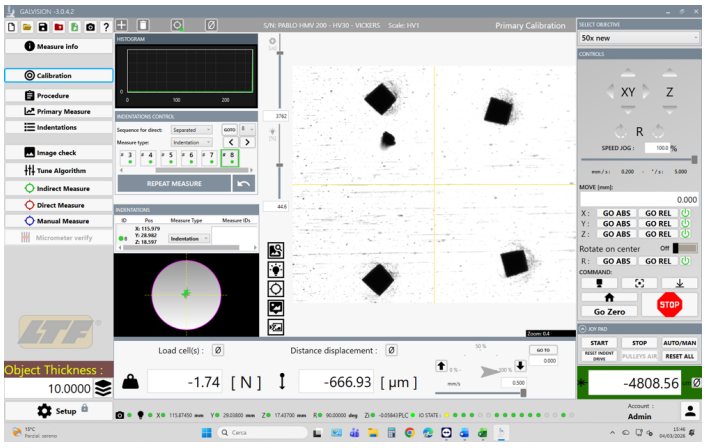

Figure 3.18: Micro-Vickers indentations for rotation angles $\omega = 0°, 30°, 60°$ and $90°$

Knoop tests

The experiments were performed on certified Knoop reference blocks (HK 2 level).

The indentations were made using tilt angles $\theta = 0°$, $0.25°$, $0.5°$, $1°$, $2°$ and $5°$. However, for $\theta = 5°$ the imprints became too irregular to be measured reliably, so those measurements were not included in the final dataset.

For every measurable angle, the two diagonals of the indentation (d_1 and d_2) were observed, but only the longest diagonal d_1 was used, as required by the ISO definition of Knoop hardness.

The Knoop hardness values were calculated from the longest diagonal measured on the specimen surface after the tests. This diagonal is the characteristic dimension used in the Knoop method, and the hardness values were obtained using the standard Knoop formulation given in Equation (2.9).

In the Knoop measurements the images were analysed in the GalVision software using the indirect measurement mode after the indentation. Some examples of these measurements are shown in Figure 3.19.

Because of the highly anisotropic geometry of the Knoop indentation, the imprint shape was much more sensitive to tilt and in-plane rotation than in the Brinell and Vickers measurements. At moderate tilt angles, the long diagonal could still be identified and measured with enough confidence. At $\theta = 5°$, however, several imprints were so distorted that no reliable measurement could be obtained.

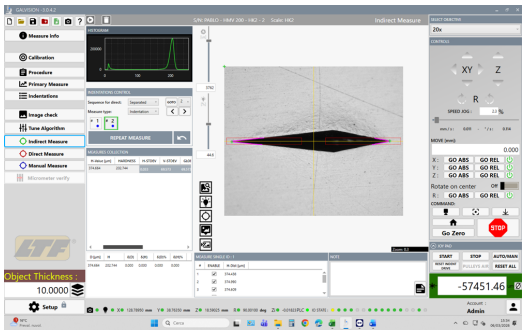

(a) Knoop indentation measurement with an inclination of 2°

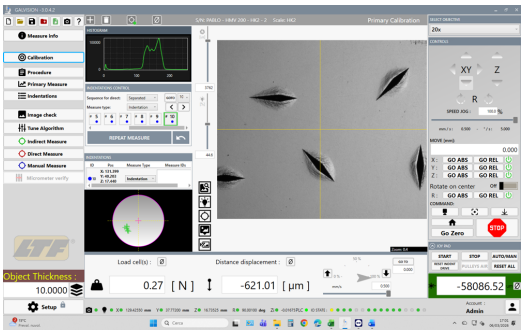

(b) Knoop indentations for rotation angles $\omega = 0°, 45°, 90°, 135°$ and $180°$

Figure 3.19: Knoop measurements performed with GalVision

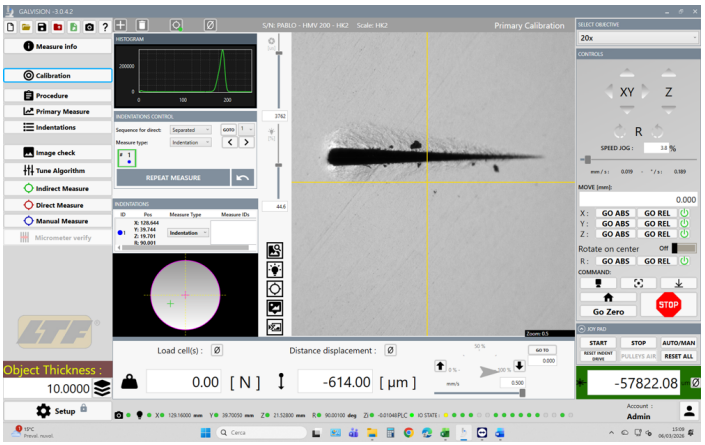

Figure 3.20: Example of a severely distorted Knoop indentation at $\theta = 5°$, which could not be measured reliably

3.3.2 Verification of test-cycle parameters

So apart from measuring the geometry of the residual imprints, the parameters describing the loading cycle of the indentation tests were also checked using the outputs provided by the software.

These records include parameters such as the load application time T_a, the full load dwell time T_{dl}, the approach velocity V_a and the final velocity during loading V_{fal}. They are useful because they allow to check how the real test cycle was performed and compare it with the standard conditions of the hardness tests.

In the Brinell and Vickers tests the software records how the force and displacement change with time. These curves make it possible to check if the loading cycle looks correct, with a progressive loading stage, a dwell period at full load and finally the unloading stage.

Examples of the force–time and displacement–time curves are shown in Figure 3.21. From the shape of the curves it can be seen that the loading sequence was carried out in controlled conditions and that the different stages of the cycle are easy to identify.

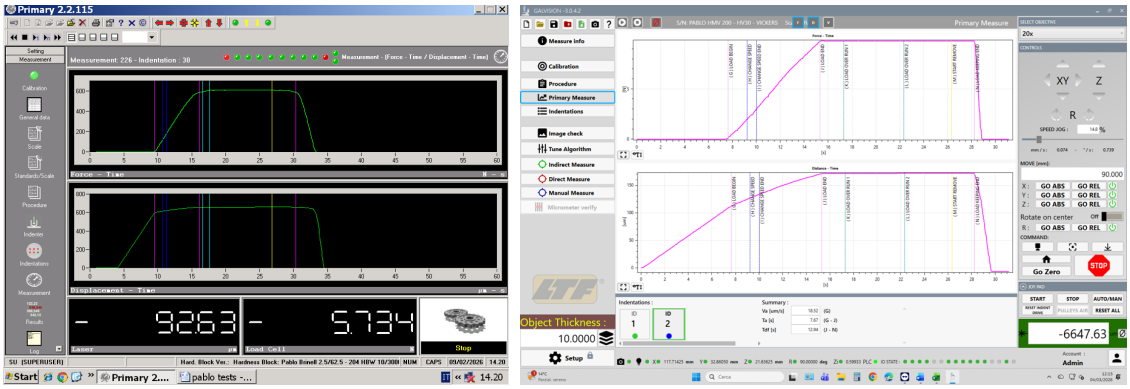

(a) Brinell test in Primary software (b) Vickers test in GalVision software

Figure 3.21: Examples of force–time and displacement–time curves recorded during Brinell and Vickers tests

In addition to the graphs, the software also keeps tables with the values of the main cycle parameters. In these tables the numerical values of T_a, T_{dl}, V_a and V_{fal} for each indentation are stored. Some examples of these records are shown in Figures 3.22 and 3.23.

VICKERS

Results

Indentation	Position	X	Ta	Tdl	Va	Vfal
30	30 Manual	☐	6,25	14,33	54,0	13,9
32	32 Manual	☐	6,75	14,30	53,7	13,4
34	34 Manual	☐	6,75	14,17	54,1	13,1
36	36 Manual	☐	6,83	14,19	53,5	13,2
38	38 Manual	☐	6,77	14,14	48,7	13,3
40	40 Manual	☐	7,81	14,33	53,7	13,4
42	42 Manual	☐	7,12	14,26	53,7	13,1
44	44 Manual	☐	7,06	14,27	54,2	13,1
46	46 Manual	☐	6,88	14,31	54,2	13,1

Figure 3.22: Example of recorded Vickers cycle parameters used to verify compliance of the test sequence

S/N: PABLO - HMV 200 - HK2 - 0.50.250 Scale: HK2

#	VA [UM / S]	TA [S]	TDF [S]
1	64.19	8.61	13.03
2	61.21	8.66	13.00
3	60.70	8.52	13.01
4	57.27	8.46	13.08
5	59.24	8.50	12.96
6	60.35	8.52	12.96
7	58.18	9.03	12.95
8	59.92	9.06	12.97
9	60.73	9.05	13.00
10	62.23	8.77	12.97
11	61.36	8.99	12.99
12	61.33	8.71	12.95

Figure 3.23: Example of recorded Knoop cycle parameters

Apart from the nominal values, these tables also show the repeatability of the recorded parameters for the different indentations. The values of T_a, T_{dl}, V_a and V_{fal} remain quite stable during the measurement sequence and only small differences appear from one indentation to another. This indicates that the loading procedure was applied consistently during the experimental work.

So basically the software records give another internal check of the experimental conditions. The hardness values are obtained from the residual imprint dimensions, as discussed before in Figures 3.17 and 3.18. Since the cycle parameters remain quite repeatable, this shows that the indentation process was carried out under controlled and reproducible loading conditions.

Chapter 4

Results, comparison and discussion

4.1 Indenter geometry models

4.1.1 Brinell hardness

The Brinell model was used in order to evaluate the influence of small changes in the ball diameter D on the hardness results. The reference condition considered here is HBW 2.5/62.5, corresponding to $D = 2.5\,\text{mm}$ and $F = 612.9\,\text{N}$, taking a nominal reference hardness of $HBW = 200$.

Reverse relation and reference sweep

First the inverse ISO relation was used to calculate the indentation diameter d as a function of hardness and applied force. Figure 4.1 shows the inverse map $d(F, HBW)$ for the Brinell geometry considered.

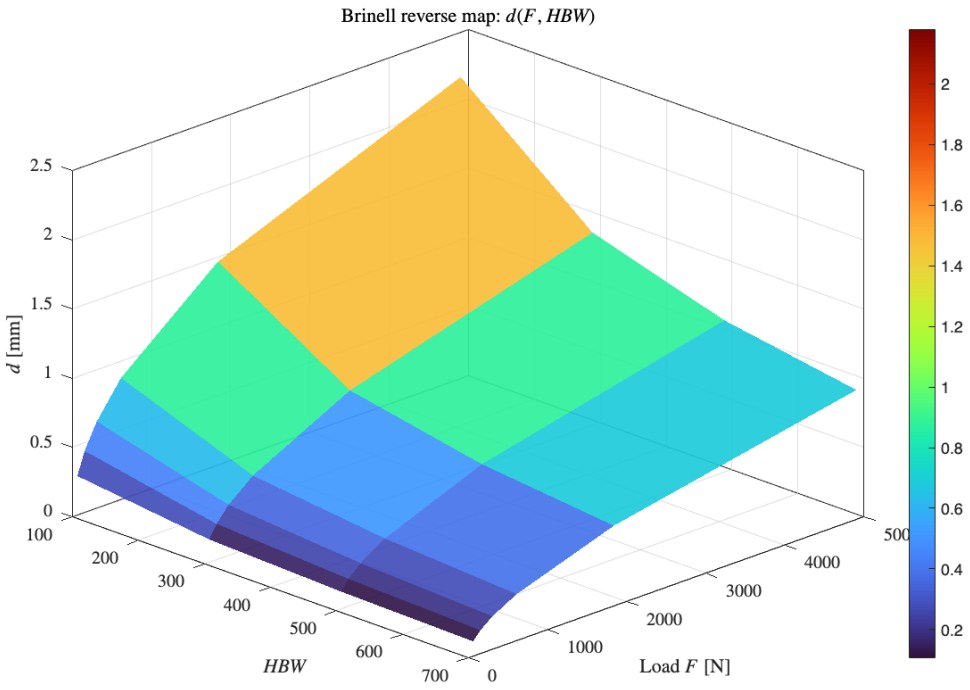

Figure 4.1: Brinell reverse-map surface $d(F, HBW)$

As expected, the map shows that keeping the force constant makes the indentation diameter smaller as hardness increases. On the other hand, if the hardness stays the same, increasing the force makes the diameter larger.

Then, a local sweep was performed around $D = 2.5\,\text{mm}$ at $HBW = 200$ under the constraint $V = \text{const}$. Figure 4.2 shows the corresponding evolution of d, h, A, and HBW.

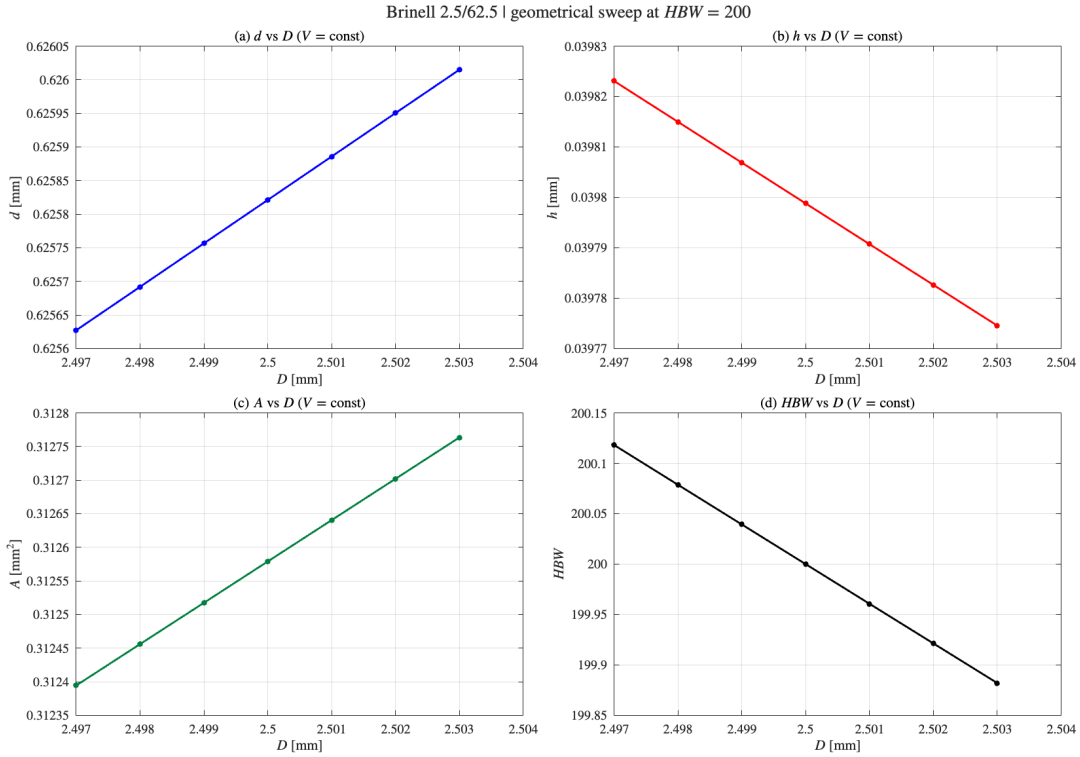

Figure 4.2: Brinell geometrical sweep around the nominal condition at $HBW = 200$ assuming $V = \text{const}$

The numerical values associated with the local sweep are summarized in Table 4.1.

Table 4.1: Brinell sweep around the nominal condition at $HBW = 200$

D (mm)	h (mm)	d (mm)	A (mm^2)	HBW ($V = \text{const}$)	HBW ($d = \text{const}$)
2.497	0.039823	0.62563	0.31239	200.12	199.99
2.498	0.039815	0.62569	0.31246	200.08	199.99
2.499	0.039807	0.62576	0.31252	200.04	200.00
2.500	0.039799	0.62582	0.31258	200.00	200.00
2.501	0.039791	0.62589	0.31264	199.96	200.00
2.502	0.039783	0.62595	0.31270	199.92	200.01
2.503	0.039775	0.62601	0.31276	199.88	200.01

The local sweep shows that with $V = \text{const}$, increasing the ball diameter makes the indentation a little wider and shallower, so the calculated hardness decreases slightly.

In contrast, when the alternative condition $d = \text{const}$ is considered, the hardness value

remains almost unchanged. This difference can already be seen in Table 4.1 and is related to the fact that Brinell hardness is normally calculated from the measured indentation diameter and not from the actual indentation volume.

Sensitivity to ball diameter

Figure 4.3 shows the fitted linear response around the nominal condition, while Figure 4.4 shows the isolated reference-case comparison between both modelling assumptions.

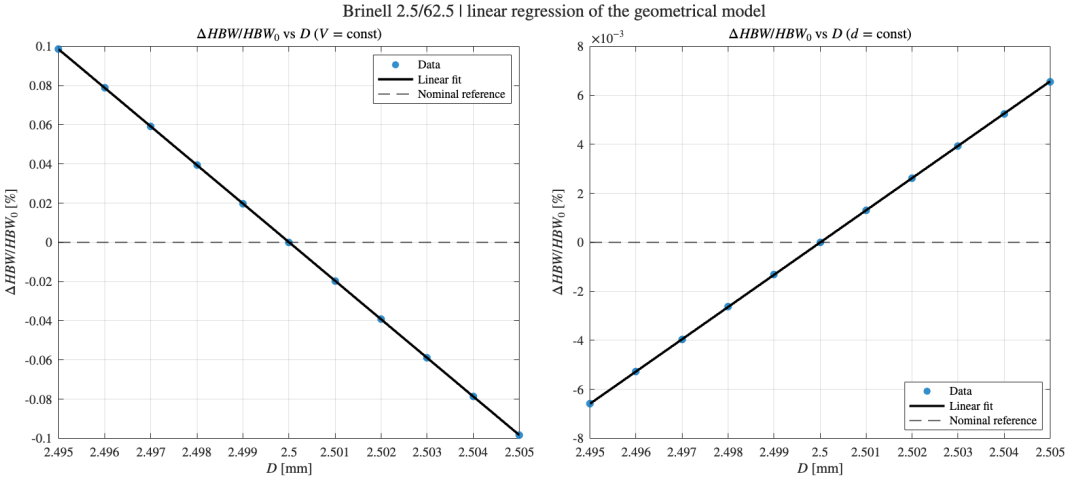

Figure 4.3: Linear regression of the relative Brinell response with respect to ball diameter around the nominal condition

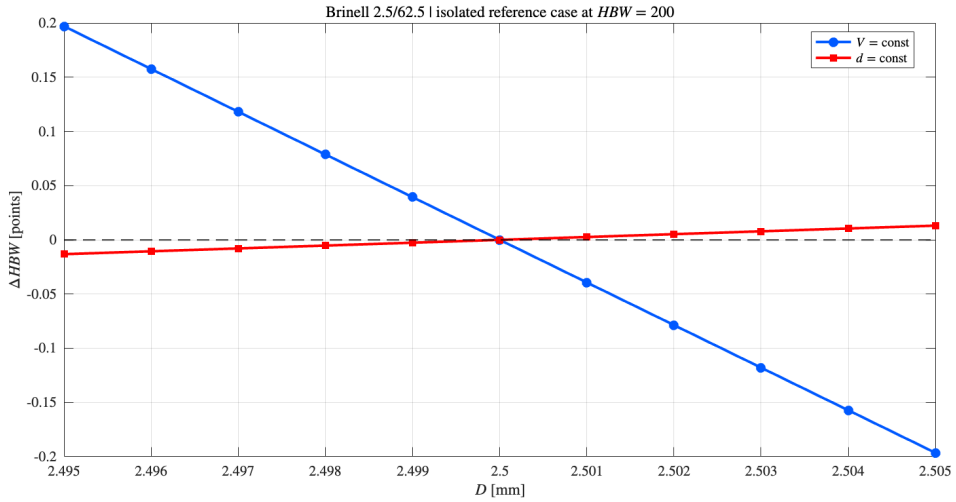

Figure 4.4: Isolated Brinell reference case at HBW = 200 comparing the $V = \text{const}$ and $d = \text{const}$ assumptions

The fitted linear models are reported in Table 4.2. For the case $V = \text{const}$, increasing the ball diameter makes the calculated hardness decrease. In the case $d = \text{const}$ the effect is much smaller and the sign goes in the opposite direction.

Table 4.2: Linear regression results for the Brinell relative response around the nominal diameter.

The regression results basically show that the two modelling assumptions give very different results. For $V = \text{const}$ the slope is around -19.7 HBW/mm, so increasing the ball diameter makes the hardness decrease. For $d = \text{const}$ the slope is only about $+1.3$ HBW/mm, which is much smaller, almost one order of magnitude less.

In Figure 4.5 the variation of hardness ΔHBW is shown as a function of D for some selected nominal values. Figure 4.6 presents the corresponding sensitivity coefficients.

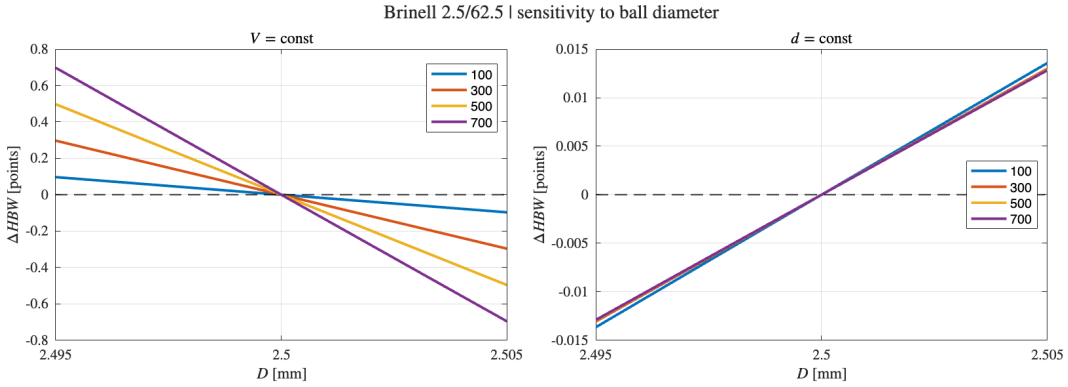

Figure 4.5: Brinell hardness variation due to deviations in ball diameter for selected nominal HBW levels under the two model assumptions

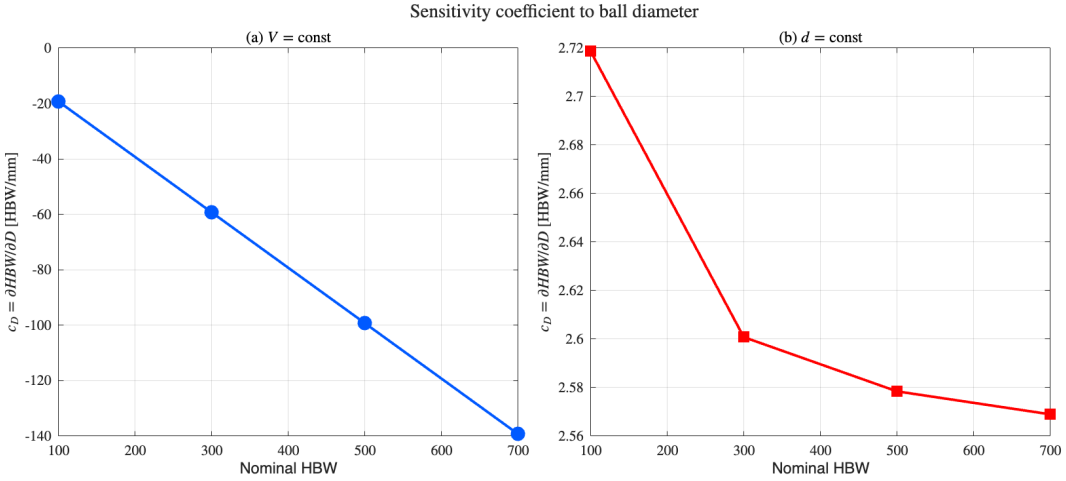

Figure 4.6: Sensitivity coefficients of Brinell hardness with respect to ball diameter for selected nominal hardness levels

The numerical values of the sensitivity coefficients are reported in Table 4.3.

Table 4.3: Sensitivity coefficients of Brinell hardness with respect to ball diameter for selected nominal hardness levels

Basically the results depend quite a lot on the nominal hardness level. For $V = \text{const}$ the value of c_D increases strongly with hardness, from about -19 HBW/mm at HBW 100 to about -139 HBW/mm at HBW 700. This is because when the hardness is higher the indentation is smaller, so the same geometrical deviation ends up having a much larger effect.

For $d = \text{const}$ the coefficient stays basically the same, around 2.6–2.7 HBW/mm.

In general, the Brinell results show that if the indentation process is interpreted only from a geometrical point of view, the sensitivity to the indenter diameter becomes much larger than in the usual ISO-based metrological approach. This difference is important when analysing the tolerances of indenters in practical hardness measurements.

4.1.2 Vickers hardness

The Vickers model was used in order to evaluate the influence of small changes in the face angle α on the hardness results. The reference condition considered here corresponds to the HV30 scale at $HV = 100$, with nominal face angle $\alpha_0 = 136°$.

Reverse relation and local angular sweep

First the inverse ISO relation was used to calculate the diagonal d as a function of hardness and applied force. Figure 4.7 shows the inverse map $d(F, HV)$ for the Vickers geometry considered.

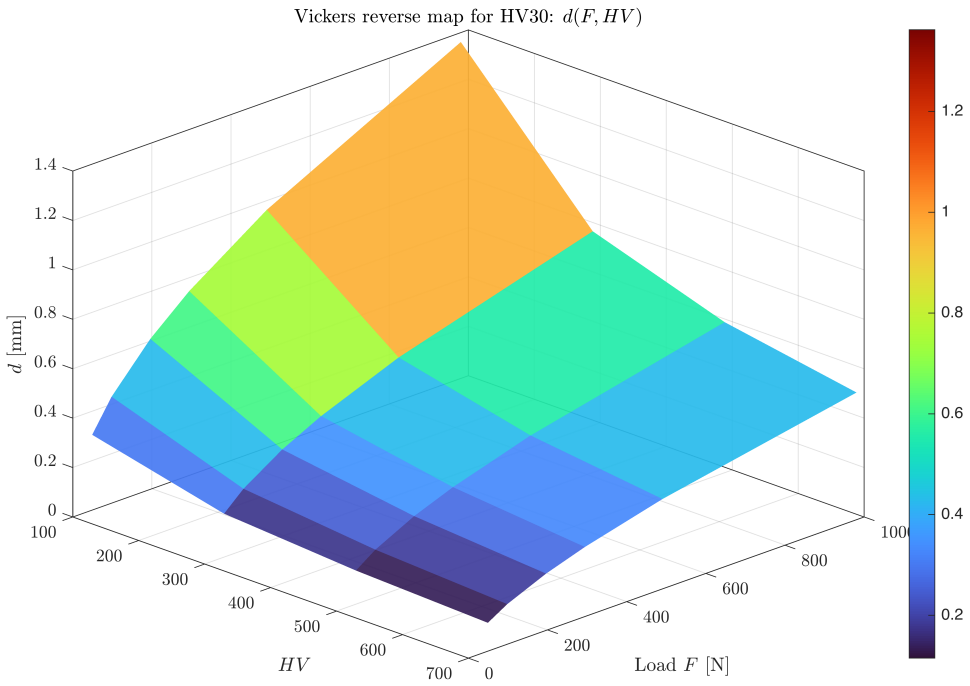

Figure 4.7: Vickers reverse-map surface $d(F, HV)$

As expected, the map shows that keeping the force constant makes the indentation diagonal smaller as hardness increases. On the other hand, if the hardness stays the same, increasing the force makes the diagonal larger.

Then, a local sweep was performed around the nominal face angle at $HV = 100$ for the HV30 scale under the constraint $V = \text{const}$. Figure 4.8 shows the corresponding evolution of d, h, A, and HV.

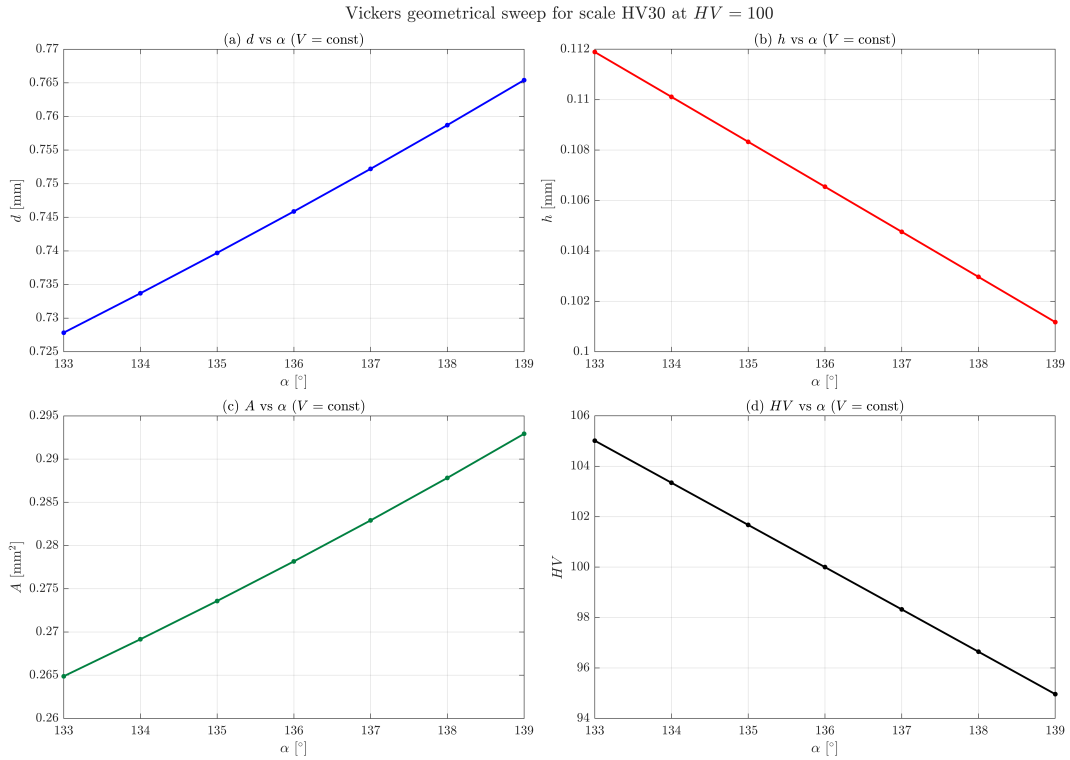

Figure 4.8: Vickers geometrical sweep for the HV30 scale around the nominal face angle at $HV = 100$ assuming $V = \text{const}$

The numerical values associated with the local sweep are summarized in Table 4.4.

Table 4.4: Vickers sweep for the HV30 scale around the nominal condition at $HV = 100$

α (deg)	$\tan(\alpha/2)$	h (mm)	d (mm)	A (mm^2)	HV ($V = \text{const}$)	HV ($d = \text{const}$)
133	2.2998	0.11189	0.72784	0.26488	105.02	98.904
134	2.3559	0.11011	0.73370	0.26916	103.35	99.276
135	2.4142	0.10833	0.73971	0.27359	101.67	99.640
136	2.4751	0.10654	0.74588	0.27817	100.00	99.996
137	2.5386	0.10476	0.75221	0.28291	98.324	100.34
138	2.6051	0.10297	0.75871	0.28782	96.645	100.69
139	2.6746	0.10118	0.76540	0.29292	94.962	101.02

The local sweep shows that with $V = \text{const}$, increasing the face angle makes the indentation a little wider and shallower, so the calculated hardness decreases.

In contrast, when the alternative condition $d = \text{const}$ is considered, the hardness value

changes much less and the sign goes in the opposite direction. This difference can already be seen in Table 4.4 and is related to the fact that Vickers hardness is normally calculated from the measured diagonal and not from the actual indentation volume.

Sensitivity to face angle

Figure 4.9 shows the fitted linear response around the nominal condition, while Figure 4.10 shows the isolated reference-case comparison between both modelling assumptions.

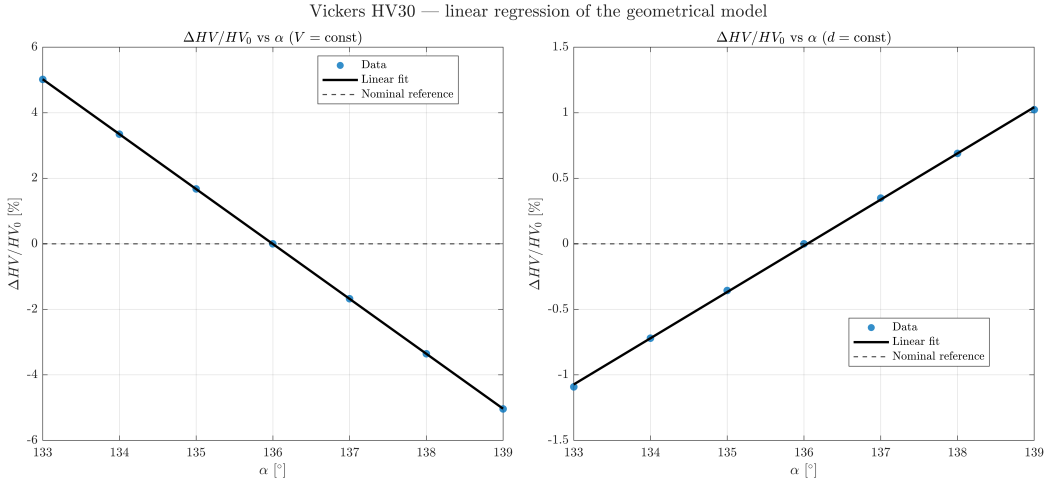

Figure 4.9: Linear regression of the relative Vickers response with respect to face angle α around the nominal condition

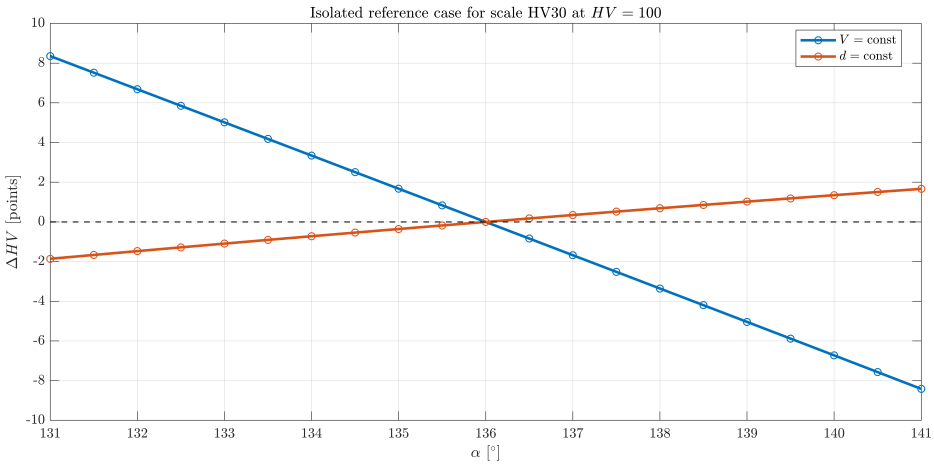

Figure 4.10: Isolated Vickers reference case at $HV = 100$ comparing the $V = \text{const}$ and $d = \text{const}$ assumptions

The fitted linear models are reported in Table 4.5. For the case $V = \text{const}$, increasing the face angle makes the calculated hardness decrease. In the case $d = \text{const}$ the effect is much smaller and the sign goes in the opposite direction.

Table 4.5: Linear regression results for the Vickers relative response around the nominal face angle.

Model assumption	Intercept	SE(intercept)	Slope	SE(slope)
$V = \text{const}$	-0.004449	0.001741	-1.67565	0.00087
$d = \text{const}$	-0.015230	0.005899	0.352548	0.00295

The regression results basically show that the two modelling assumptions give very different results. For $V = \text{const}$ the slope is around -1.68 %/deg, so increasing the face angle makes the hardness decrease. For $d = \text{const}$ the slope is only about $+0.35$ %/deg, which is much smaller.

In Figure 4.11 the variation of hardness ΔHV is shown as a function of α for some selected nominal values. Figure 4.12 presents the corresponding sensitivity coefficients.

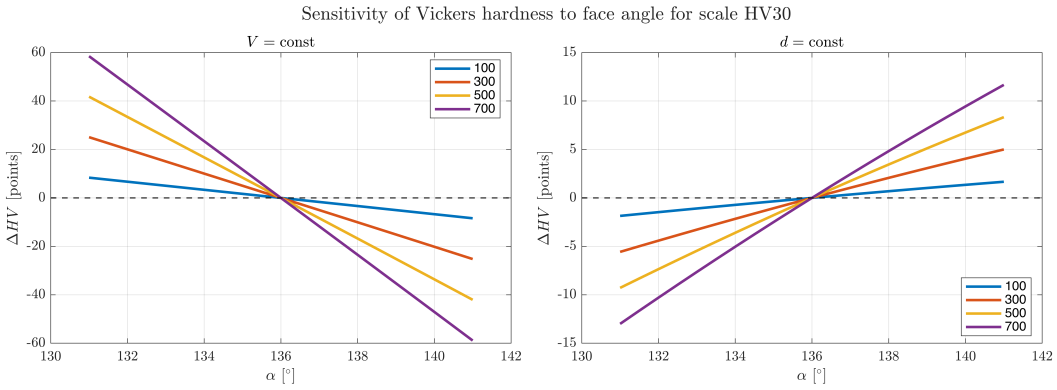

Figure 4.11: Vickers hardness variation due to deviations in face angle for selected nominal HV levels under the two model assumptions

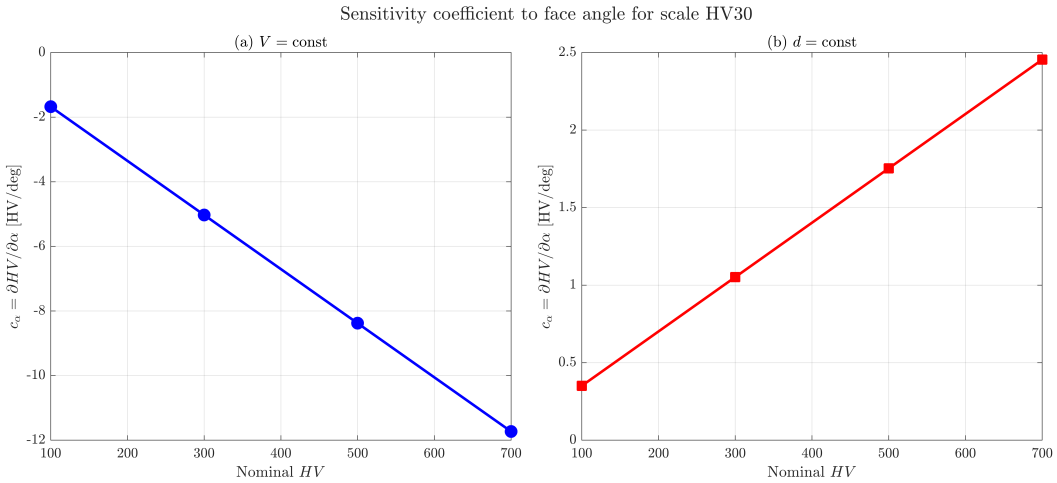

Figure 4.12: Sensitivity coefficients of Vickers hardness with respect to face angle for selected nominal hardness levels

The numerical values of the sensitivity coefficients are reported in Table 4.6.

Table 4.6: Sensitivity coefficients of Vickers hardness with respect to face angle for selected nominal hardness levels

HV	d_0 (mm)	V_0 (mm^3)	c_α [d = const] (HV/°)	c_α [V = const] (HV/°)
100	0.74588	0.0098790	0.35066	-1.6756
300	0.43063	0.0019012	1.0520	-5.0267
500	0.33357	0.0008836	1.7533	-8.3779
700	0.28191	0.0005334	2.4546	-11.729

Basically the results depend quite a lot on the nominal hardness level. For $V = \text{const}$ the value of c_α increases strongly with hardness, from about -1.68 HV/° at HV 100 to about -11.73 HV/° at HV 700. This is because when the hardness is higher the indentation is smaller, so the same geometrical deviation ends up having a much larger effect.

For $d = \text{const}$ the coefficient is much smaller, although it still increases from about 0.35 HV/° to about 2.45 HV/° in the same interval.

In general, the Vickers results show that if the indentation process is interpreted only from a geometrical point of view, the sensitivity to the indenter geometry becomes much larger than in the usual ISO-based metrological approach. This difference is important when analysing the tolerances of indenters in practical hardness measurements.

4.1.3 Knoop hardness

The Knoop model was used in order to evaluate the influence of changes in the edge angles α and β on the hardness results. The reference condition considered here corresponds to the HK2 scale at $HK = 200$, with nominal angles $\alpha_0 = 172.5°$ and $\beta_0 = 130°$.

Reverse relation and angular response

First the inverse ISO relation was used to calculate the long diagonal d_1 as a function of hardness and applied force. Figure 4.13 shows the inverse map $d_1(F, HK)$ for the Knoop geometry considered.

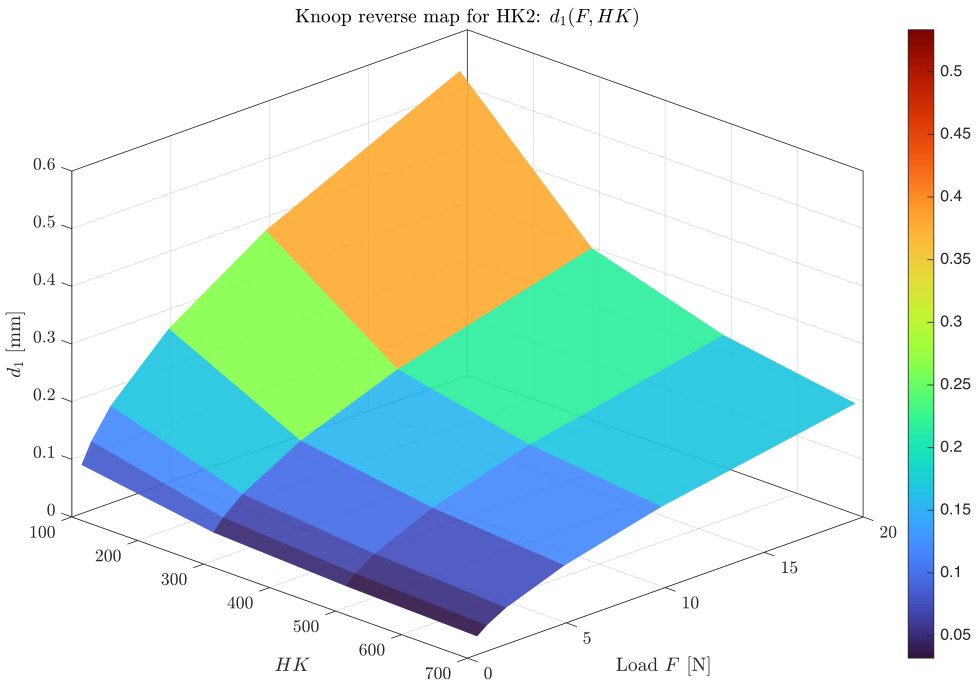

Figure 4.13: Knoop reverse-map surface $d_1(F, HK)$

As expected, the map shows that keeping the force constant makes the long diagonal smaller as hardness increases. On the other hand, if the hardness stays the same, increasing the force makes the long diagonal larger.

Then, the relative hardness variation was studied as a function of the edge angles. Figures 4.14 and 4.15 show the fitted response versus α and β, respectively. The global surface representation is shown in Figure 4.16.

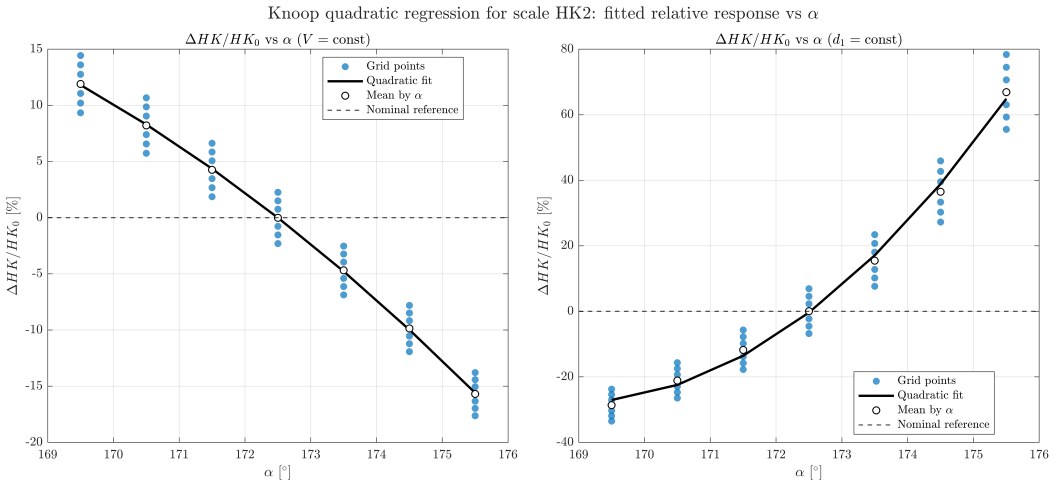

Figure 4.14: Quadratic regression of the relative Knoop hardness response as a function of α for the two model assumptions and for the HK2 scale

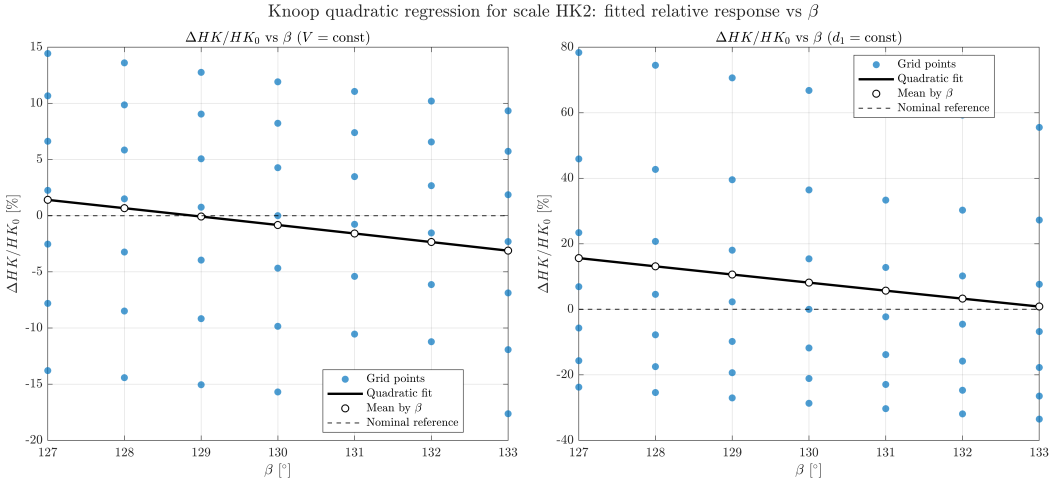

Figure 4.15: Quadratic regression of the relative Knoop hardness response as a function of β for the two model assumptions and for the HK2 scale

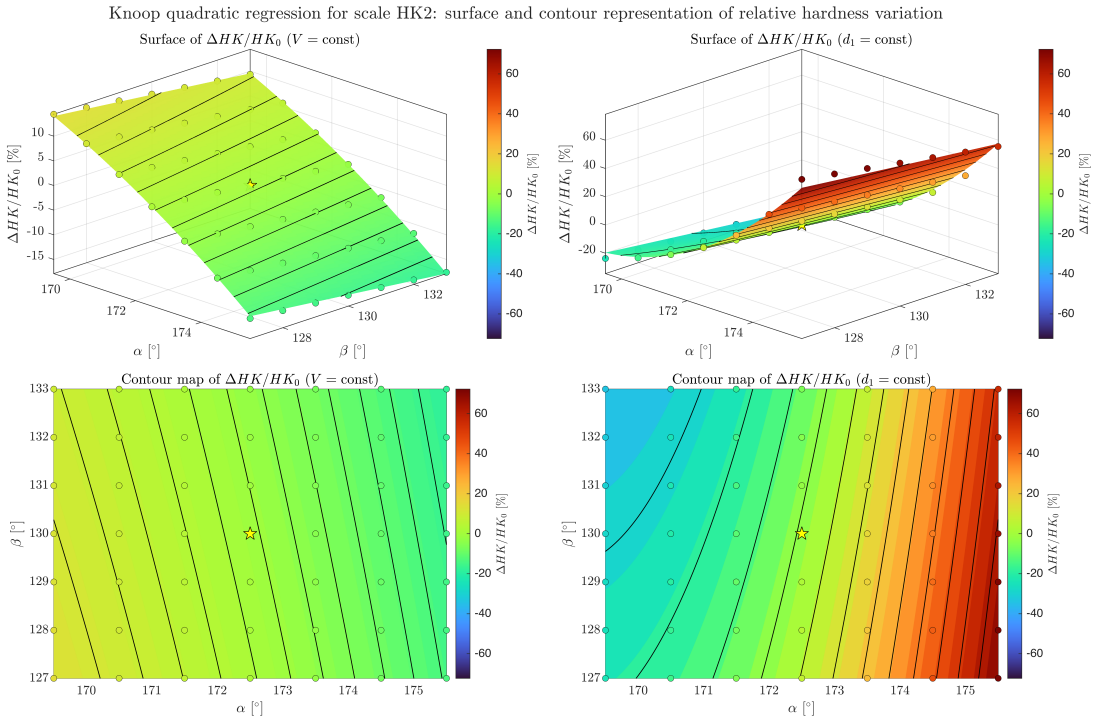

Figure 4.16: Surface and contour representation of the Knoop quadratic response around the nominal geometry for the HK2 scale

The fitted equations are summarized in Table 4.7.

Table 4.7: Quadratic regression models for the Knoop response around the nominal geometry for the HK2 scale

Model assumption	Fitted equation
$V = \text{const}$	$HK = 200.07896 - 9.13659\,d\alpha - 1.50756\,d\beta - 0.419744\,d\alpha^2 - 0.0053229\,d\beta^2$
$d_1 = \text{const}$	$HK = 199.22791 + 30.65043\,d\alpha - 4.93113\,d\beta + 4.28533\,d\alpha^2 + 0.0200733\,d\beta^2$

The fitted results show that the Knoop response is more complex than in Brinell and Vickers. It can also be seen that the effect of α is clearly larger than the effect of β. This is reasonable because α mainly controls the elongated shape of the indentation and therefore also the long diagonal.

Sensitivity to edge angles

Separate sweeps were carried out versus α at fixed $\beta = 130°$ and versus β at fixed $\alpha = 172.5°$. Figures 4.17 and 4.18 show the variation of the main geometrical variables and the corresponding hardness values.

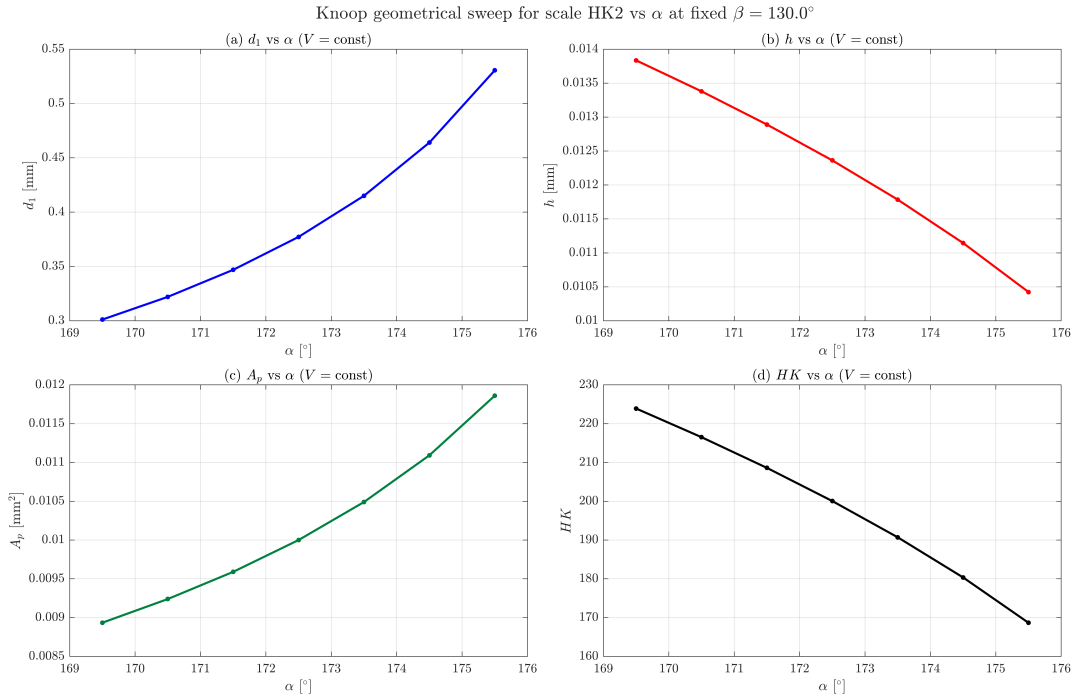

Figure 4.17: Knoop sweep for the HK2 scale versus α at fixed $\beta = 130°$ for the reference condition $HK = 200$

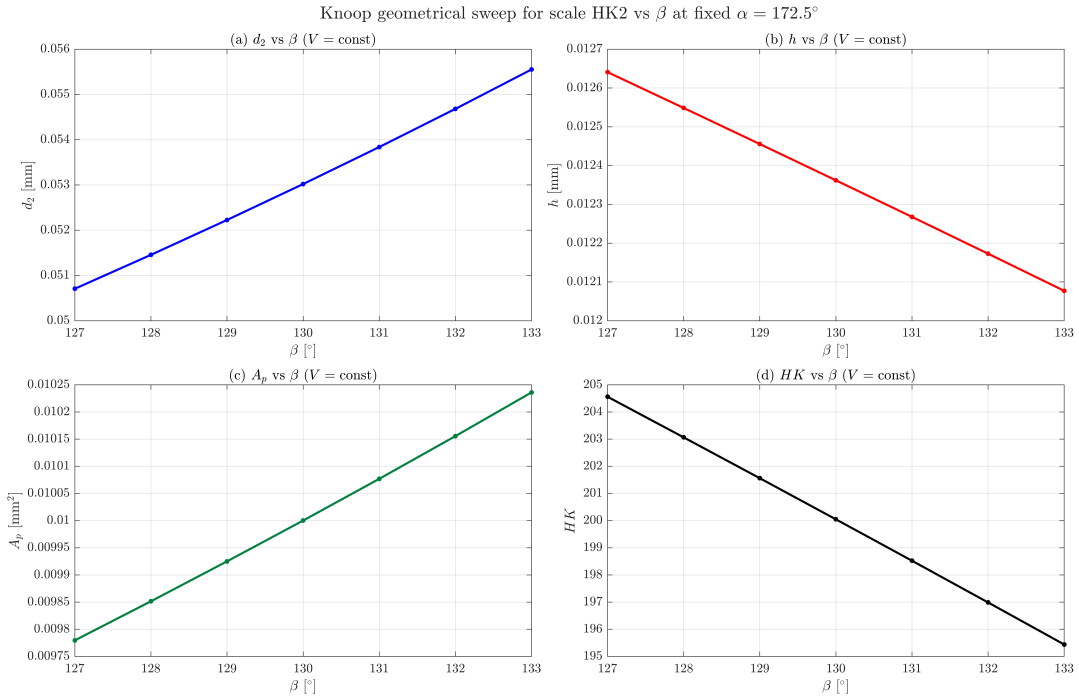

Figure 4.18: Knoop sweep for the HK2 scale versus β at fixed $\alpha = 172.5°$ for the reference condition $HK = 200$

The numerical values associated with the sweeps are summarized in Tables 4.8 and 4.9.

Table 4.8: Knoop sweep for the HK2 scale versus α at fixed $\beta = 130°$ for the reference condition $HK = 200$

α (deg)	d_1 (mm)	d_2 (mm)	h (mm)	A_p (mm^2)	HK (V = const)	HK (d_1 = const)
169.5	0.30114	0.059341	0.013836	0.0089351	223.89	142.70
170.5	0.32203	0.057384	0.013379	0.0092398	216.51	157.80
171.5	0.34692	0.055287	0.012890	0.0095903	208.60	176.44
172.5	0.37722	0.053021	0.012362	0.0100000	200.05	200.05
173.5	0.41507	0.050545	0.011785	0.0104900	190.71	230.91
174.5	0.46407	0.047803	0.011145	0.0110920	180.36	272.97
175.5	0.53058	0.044706	0.010423	0.0118600	168.68	333.72

Table 4.9: Knoop sweep for the HK2 scale versus β at fixed $\alpha = 172.5°$ for the reference condition $HK = 200$

β (deg)	d_1 (mm)	d_2 (mm)	h (mm)	A_p (mm^2)	HK (V = const)	HK (d_1 = const)
127	0.38573	0.050707	0.012641	0.0097796	204.56	213.89
128	0.38291	0.051457	0.012549	0.0098516	203.07	209.24
129	0.38007	0.052227	0.012456	0.0099251	201.56	204.63
130	0.37722	0.053021	0.012362	0.0100000	200.05	200.05
131	0.37434	0.053839	0.012268	0.0100770	198.52	195.51
132	0.37144	0.054682	0.012173	0.0101560	196.99	191.01
133	0.36853	0.055551	0.012077	0.0102360	195.44	186.54

The sweeps show clearly that the Knoop response is anisotropic. Changing α produces large changes in the long diagonal and therefore also in hardness, especially when the condition $d_1 = \text{const}$ is used. Changing β also affects the result, but the effect is much smaller. This means that the geometry associated with α has the main influence on Knoop hardness.

Figures 4.19 and 4.20 show isolated reference-case comparisons for deviations in α and β, respectively.

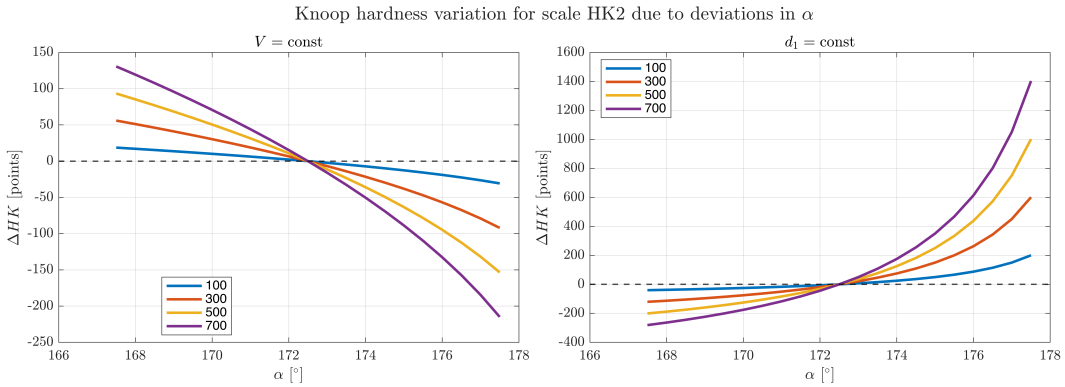

Figure 4.19: Isolated Knoop reference case at $HK = 200$: ΔHK versus α

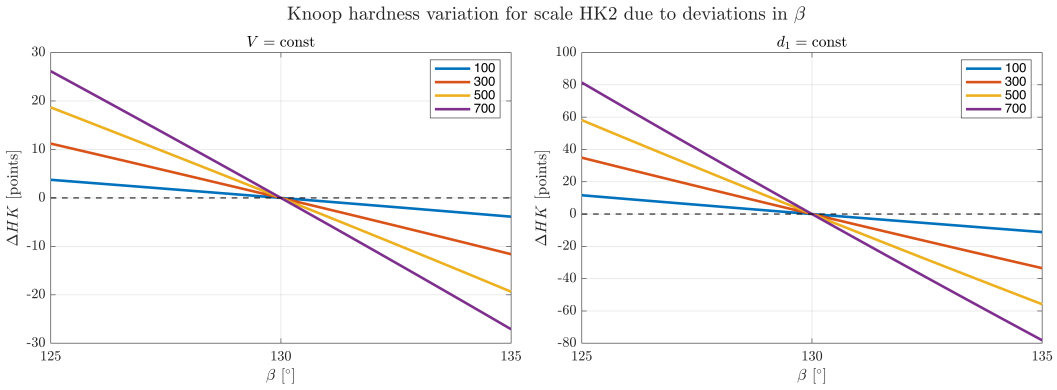

Figure 4.20: Isolated Knoop reference case at $HK = 200$: ΔHK versus β

In Figures 4.22 and 4.23 the variation of hardness is shown for some selected nominal HK values. Figure 4.21 shows the corresponding sensitivity coefficients.

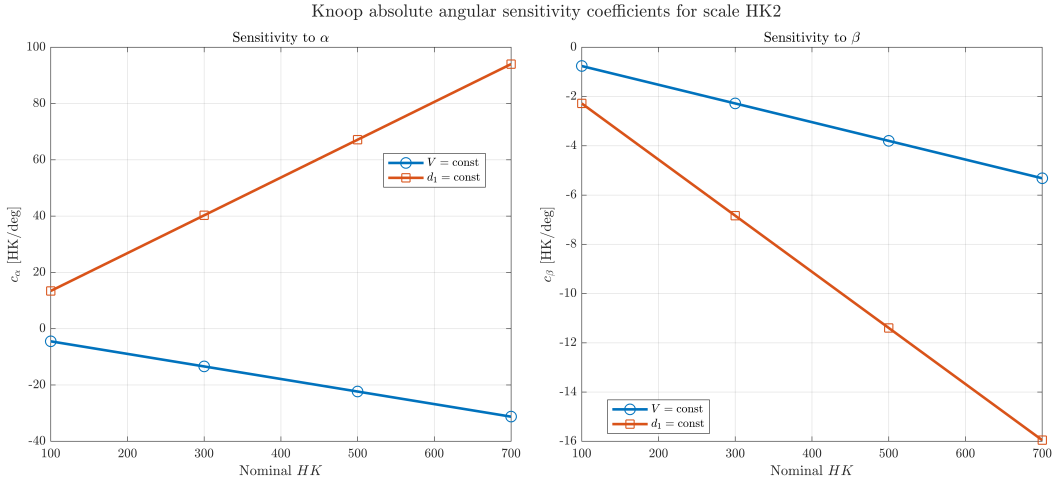

Figure 4.21: Absolute first-order angular sensitivity coefficients of Knoop hardness with respect to α and β for selected nominal hardness levels

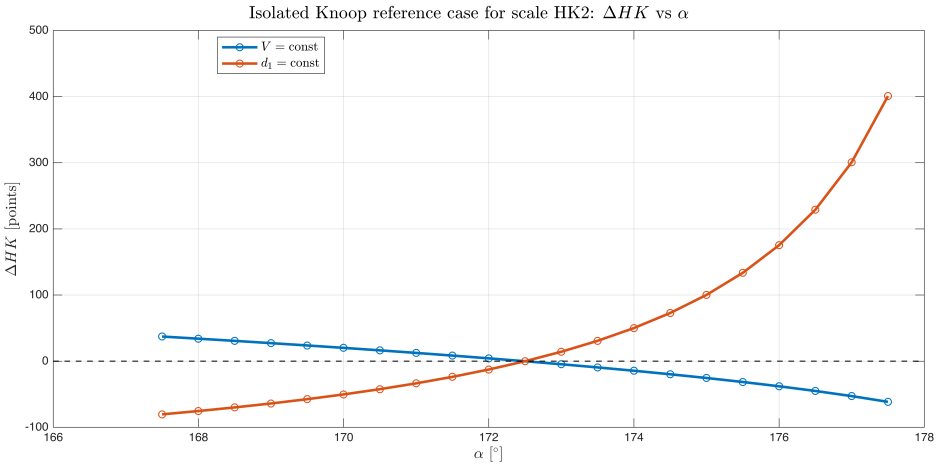

Figure 4.22: Knoop hardness variation due to deviations in α for selected nominal HK levels under the two model assumptions

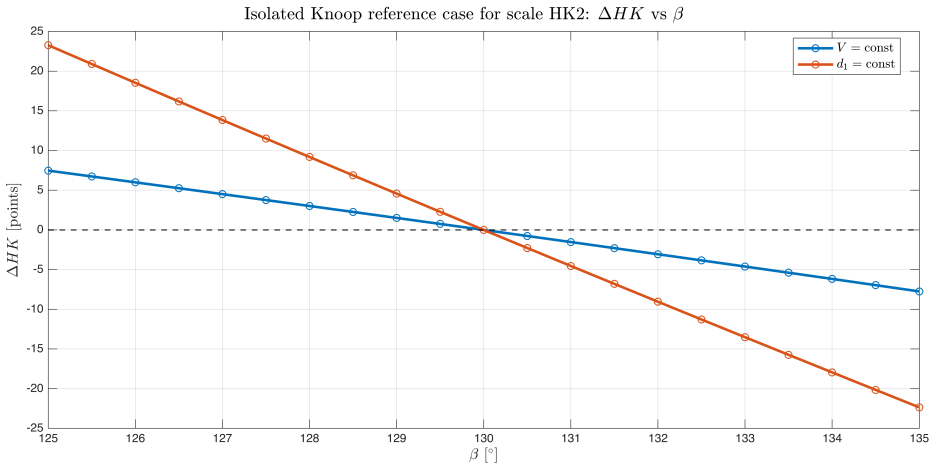

Figure 4.23: Knoop hardness variation due to deviations in β for selected nominal HK levels under the two model assumptions

The numerical values of the sensitivity coefficients are reported in Table 4.10.

Table 4.10: Angular sensitivity coefficients of Knoop hardness for selected nominal hardness levels

HK	$d_{1,0}$ (mm)	V_0 (mm^3)	c_α (HK/°)		c_β (HK/°)		$c_{\alpha\alpha}$ (HK/°^{2})		$c_{\beta\beta}$ (HK/°^{2})	
			$V = \text{const}$	$d_1 = \text{const}$	$V = \text{const}$	$d_1 = \text{const}$	$V = \text{const}$	$d_1 = \text{const}$	$V = \text{const}$	$d_1 = \text{const}$
100	0.53346	1.1655×10^{-4}	-4.5602	14.329	-0.7610	-2.2743	-0.4197	4.2853	-0.00532	0.02007
300	0.30800	2.2431×10^{-5}	-13.6805	42.986	-2.2830	-6.8229	-0.4197	4.2853	-0.00532	0.02007
500	0.23857	1.0425×10^{-5}	-22.8008	71.644	-3.8050	-11.3715	-0.4197	4.2853	-0.00532	0.02007
700	0.20163	6.2933×10^{-6}	-31.9211	100.301	-5.3270	-15.9202	-0.4197	4.2853	-0.00532	0.02007

Basically the results show that α has a much stronger effect than β. At every hardness level, the value of $|c_\alpha|$ is larger than $|c_\beta|$. The strongest effect appears for the $d_1 = \text{const}$ condition, where the sensitivity to α becomes larger than 100 HK/° at HK 700. Even under $V = \text{const}$, the sensitivity to α is still important. The second-order coefficients are also useful because they show the curvature of the response, especially for the dependence on α.

In general, the Knoop results show that this method is the most sensitive to deviations in indenter geometry among the three hardness tests studied here. This is mainly due to the anisotropic shape of the indenter and to the fact that the hardness value depends on only one geometrical quantity, the long diagonal, which is especially affected by changes in α.

4.1.4 Comparative discussion of Brinell, Vickers and Knoop models

In general the results for the three indentation methods look quite similar. The effect of the indenter geometry does not only depend on the indenter shape, but also on how the indentation process is modelled.

There is quite a clear difference between the purely geometrical interpretation of the indentation, which is represented here by $V = \text{const}$, and the usual metrological interpretation used in hardness standards. In this second case the hardness value is calculated from a measured value, which is the indentation diameter in Brinell, the diagonal in Vickers and the long diagonal in Knoop.

If the assumption $V = \text{const}$ is used, the calculated hardness depends quite a lot on the indenter geometry. Small deviations in the indenter parameters change the indentation geometry and this directly affects the hardness value. However, when the usual metrological definition is used, the effect is much smaller, since the hardness is calculated only

from one measured dimension of the indentation.

Out of the three methods analysed, Brinell is the one with the lowest sensitivity to the indenter geometry. The indentation produced by the ball is quite large, so small deviations in the ball diameter do not affect the result as much.

The Vickers method shows a kind of intermediate behaviour. The face angle α affects the indentation geometry more directly than the ball diameter in Brinell. So when hardness increases the sensitivity also increases, because the indentation becomes smaller. However, when the hardness is calculated using the diagonal length, the effect of the angle looks smaller than what would be expected if only the geometry was considered.

The Knoop method appears to be the most sensitive to the geometry of the indenter. This is mainly because the indenter has a very anisotropic shape and also because the hardness value is calculated using only one characteristic dimension, which is the long diagonal d_1. When the angle α changes, which mostly controls the elongated shape of the indentation, the hardness value can change quite a lot. This effect becomes even more noticeable when the hardness level is higher.

Basically, the comparison shows that the effect of indenter geometry on hardness measurements cannot be understood only from geometry. It also depends on how the hardness scale is defined and on which parameter is used to calculate the hardness value. Because of that, the sensitivity is different for each method: Knoop is the most sensitive, Vickers is somewhere in the middle, and Brinell is the least sensitive.

4.2 Experimental results: Force misalignment

The experimental study was performed to check how force misalignment affects Brinell, Vickers and Knoop hardness measurements. In all cases the change in hardness was evaluated with respect to the aligned configuration and analysed using first-order regression models. To not repeat the same information many times, the uncertainty framework and the statistical treatment are presented first, and after that the results for each hardness scale are discussed.

4.2.1 Common uncertainty and statistical treatment

For all the datasets the inclination angle θ was considered the main independent variable. For Vickers and Knoop measurements another parameter ω was also introduced to account for the relative orientation between the indentation geometry and the tilt direction.

The uncertainty associated with the inclination angle was evaluated by assuming a rectangular distribution corresponding to the mechanical tolerance of the tilt stage:

$$u^2(\theta) = \frac{a_\theta^2}{3}, \qquad u(\theta) = \frac{0.1^\circ}{\sqrt{3}} \tag{4.1}$$

With $a_\theta = 0.1^\circ$. For Vickers and Knoop, the in-plane rotation angle was treated in the same way:

$$u^2(\omega) = \frac{a_\omega^2}{3}, \qquad u(\omega) = \frac{5^\circ}{\sqrt{3}} \tag{4.2}$$

The uncertainty of the hardness value was derived from calibration and measurement capability expressions following the CMC framework available in the BIPM KCDB [53,54]. In this work the same approach as in Luigi's thesis [6] was also used.

For Brinell, the relative standard uncertainty was written as:

$$u_{\mathrm{rel}}(HBW) = \frac{1}{2}\left(1 + \frac{240}{d_\mu}\right) \times 10^{-2} \tag{4.3}$$

In this case d_μ corresponds to the mean indentation diameter measured in µm. For the macro-Vickers HV30 measurements, the corresponding expression was:

$$u_{\mathrm{rel}}(HV30) = \frac{1}{2}\left(1 + \frac{43}{d_\mu}\right) \times 10^{-2} \tag{4.4}$$

For micro-Vickers HV1 and Knoop HK2, a conservative constant relative standard uncertainty was adopted:

$$u_{\mathrm{rel}}(H) = \frac{1.5}{200} \tag{4.5}$$

In all cases, the standard uncertainty associated with the hardness value was written as:

$$u(H_i) = u_{\mathrm{rel}}(H_i)\, H_i \tag{4.6}$$

The effect of force misalignment was described through first-order regression models. For Brinell, a linear dependence on θ was assumed:

$$H = H_0 + c_\theta\, \theta \tag{4.7}$$

Whereas for Vickers and Knoop a first-order plane was adopted:

$$H = H_0 + c_\theta\, \theta + c_\omega\, \omega \tag{4.8}$$

Since both the independent variables and the hardness values are affected by uncertainty, the model parameters were estimated by weighted total least squares (WTLS) using the CCC software in the two-variable case and an equivalent dedicated implementation for the planar case.

For the linear model, the effective variance of the i-th point was written as:

$$\sigma^2_{\mathrm{eff},i} = u^2(H_i) + c^2_\theta\, u^2(\theta_i) \tag{4.9}$$

While for the planar model it became:

$$\sigma^2_{\mathrm{eff},i} = u^2(H_i) + c^2_\theta\, u^2(\theta_i) + c^2_\omega\, u^2(\omega_i) \tag{4.10}$$

With corresponding weights:

$$w_i = \frac{1}{\sigma^2_{\mathrm{eff},i}} \tag{4.11}$$

The residuals were defined as:

$$r_i = H_i - \widehat{H}_i \tag{4.12}$$

Two complementary statistical criteria were used afterwards. The first one corresponds to the reduced chi-square statistic:

$$\chi^2_\nu = \frac{1}{\nu}\sum_{i=1}^{n}\frac{r_i^2}{\sigma^2_{\text{eff},i}} \tag{4.13}$$

With $\nu = n - 2$ for the Brinell linear model and $\nu = n - 3$ for the Vickers and Knoop plane models. The fit was regarded as consistent with the adopted uncertainty model when:

$$\chi^2_\nu < \chi^2_{\nu,\text{crit}} \tag{4.14}$$

The second criterion was based on a Fisher-type comparison between the residual variance:

$$s^2_{\text{res}} = \frac{1}{\nu}\sum_{i=1}^{n} r_i^2 \tag{4.15}$$

And the non-uniformity variance of the block, s^2_{nu}, through:

$$F = \frac{s^2_{\text{nu}}}{s^2_{\text{res}}} \tag{4.16}$$

The fitted trend was considered significant with respect to the intrinsic block variability only when:

$$F > F_{\text{crit}} \tag{4.17}$$

In this case, χ^2_ν is used to verify if the fit is consistent with the uncertainty model that was adopted, whereas F is used to evaluate whether the fitted trend is sufficiently strong

compared to the baseline variability related to block non-uniformity.

4.2.2 Macrohardness tests

Brinell hardness tests

The influence of force misalignment on Brinell hardness measurements was investigated by using a certified reference block.

· **Brinell hardness 200 block**

The indentations were performed using the inclination angles:

$$\theta = \{0^\circ, 0.25^\circ, 0.5^\circ, 1^\circ, 2^\circ, 5^\circ\} \tag{4.18}$$

For every condition, the two diameters of the indentation were measured and afterwards the average value was calculated as:

$$\bar{d} = \frac{d_1 + d_2}{2} \tag{4.19}$$

The corresponding Brinell hardness for the HBW 2.5/62.5 scale was calculated as:

$$HBW = 0.102 \, \frac{2F}{\pi D \left(D - \sqrt{D^2 - \bar{d}^2} \right)} \tag{4.20}$$

with $F = 612.9\,\mathrm{N}$ and $D = 2.5\,\mathrm{mm}$.

The effect of the force misalignment was evaluated taking the aligned condition ($\theta = 0^\circ$) as reference. The absolute and relative variations of hardness were defined as:

$$\Delta HBW = HBW(\theta) - HBW_{\mathrm{ref}}, \qquad HBW_{\mathrm{ref}} = HBW(\theta = 0^\circ) \tag{4.21}$$

And:

$$\delta H(\%) = \frac{HBW(\theta) - HBW_{\mathrm{ref}}}{HBW_{\mathrm{ref}}} \times 100 \tag{4.22}$$

Under a first-order approximation, the response was described by:

$$HBW = HBW_0 + c_\theta\,\theta \tag{4.23}$$

Or, in relative form:

$$\delta H = c_{\theta,\mathrm{rel}}\,\theta \tag{4.24}$$

The measured values are reported in Table 4.11.

Table 4.11: Mean indentation diameter, hardness value, and hardness variation measured on the Brinell hardness 200 block

θ (°)	$\bar{d}$ (mm)	HBW	ΔHBW	δH (%)
0.00	0.64520	187.842	0.000	0.000
0.25	0.64420	188.455	0.613	0.326
0.50	0.64445	188.304	0.462	0.246
1.00	0.64365	188.791	0.949	0.505
2.00	0.64555	187.627	-0.215	-0.114
5.00	0.65555	181.861	-5.981	-3.184

Figure 4.24 shows the relative variation of Brinell hardness as a function of inclination angle.

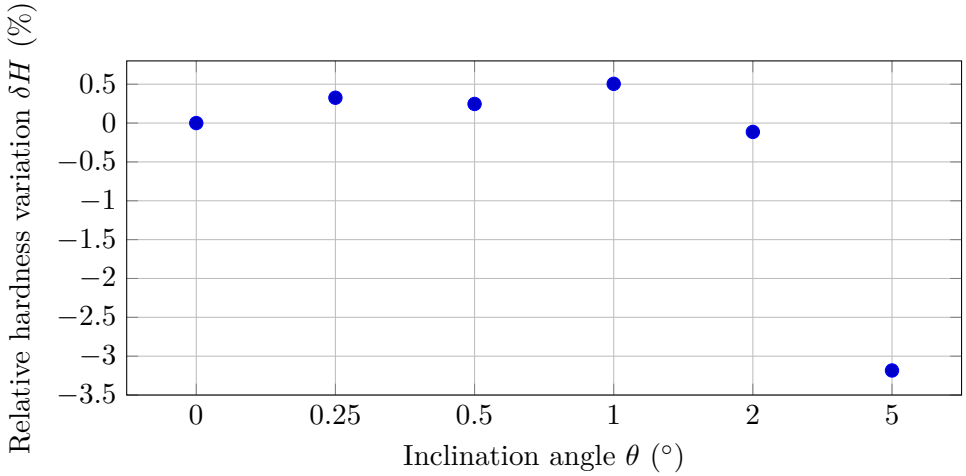

Figure 4.24: Relative variation of Brinell hardness, δH, as a function of the inclination angle θ for the Brinell hardness 200 block

Up to 2° the variations are quite small, but at 5° a clearer decrease can be observed. This indicates that misalignment has an effect, although over most of the range the influence is still limited.

To evaluate the internal variability of the reference block, five additional indentations were performed under nominal alignment conditions. The results are reported in Table 4.12.

Table 4.12: Mean indentation diameter and hardness value for the non-uniformity study on the Brinell hardness 200 block

Indent number	$\bar{d}$ (mm)	HBW
1	0.639150	191.6112
2	0.639800	191.2146
3	0.644300	188.5064
4	0.641950	189.9137
5	0.641850	190.0498

The mean hardness value obtained from the five indentations is:

$$\overline{HBW} = 190.259 \tag{4.25}$$

With a sample standard deviation:

$$s(HBW) = 1.222 \tag{4.26}$$

This dispersion represents the combined effect of repeatability and local block non-uniformity.

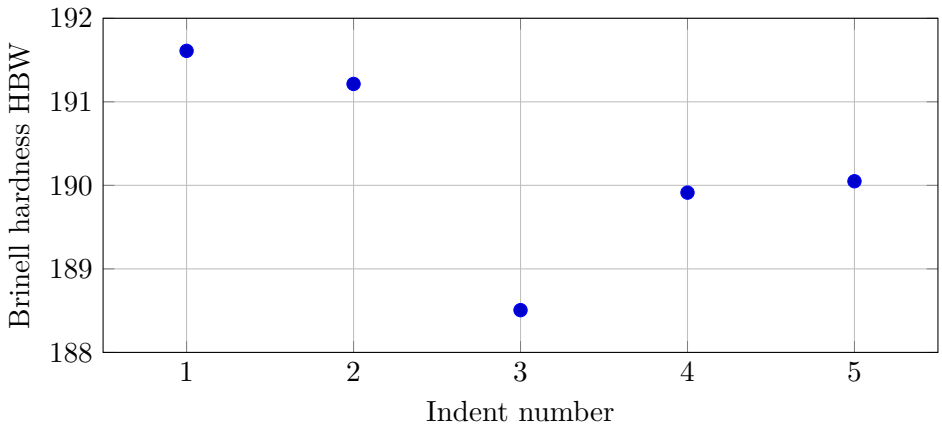

Figure 4.25: Non-uniformity study: HBW of five separate indentations in the Brinell hardness 200 block

The Brinell misalignment data were fitted using the linear WTLS model of Eq. (4.23). The numerical results are summarised in Table 4.13.

Table 4.13: Statistical results of the WTLS regression analysis for the Brinell misalignment experiment

Range of θ	$\hat{H}_0$	$u(\hat{H}_0)$	$\hat{c}_\theta$	$u(\hat{c}_\theta)$	χ^2_ν	$\chi^2_{\nu,\mathrm{crit}}$	F	F_{crit}
0°–5°	189.173	0.693	−1.314	0.301	0.674	1.497	1.335	2.483

The reduced chi-square criterion is satisfied since $\chi^2_\nu < \chi^2_{\nu,\mathrm{crit}}$, but Fisher's criterion is not satisfied because $F < F_{\mathrm{crit}}$. This indicates that the fitted line is consistent with the adopted uncertainty model, although the trend cannot be considered statistically significant compared with the intrinsic non-uniformity of the block. Therefore, the Brinell regression should mainly be interpreted as a first-order descriptive model.

The corresponding WTLS fit in absolute and relative form is shown in Figure 4.26.

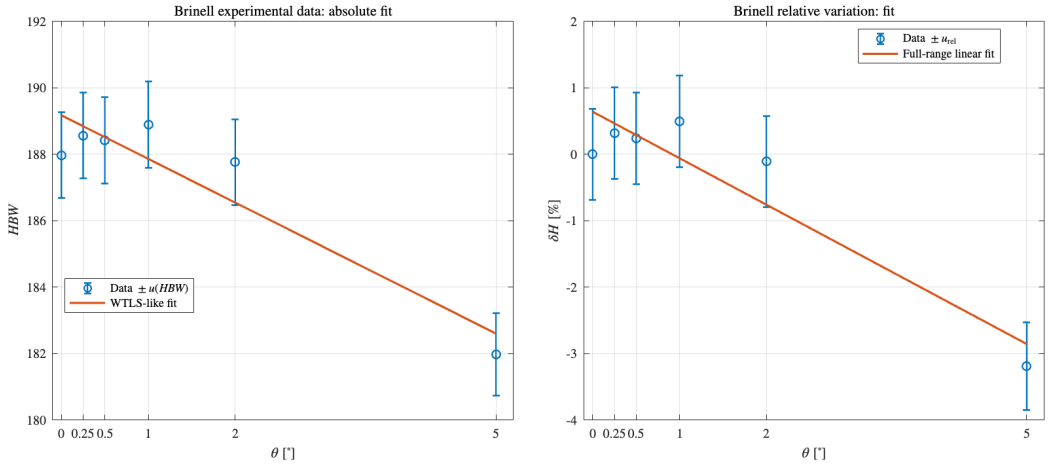

Figure 4.26: WTLS fit of the Brinell experimental data in absolute and relative terms

As an additional metrological check, the Brinell regression was also processed using the CCC software, which is commonly used at INRIM for calibration problems with n data pairs (x, y) and uncertainties in both variables [55]. The values obtained with CCC are consistent with the Matlab results, within small numerical rounding differences, both for the intercept $\hat{H}_0$ and the sensitivity coefficient $\hat{c}_\theta$, as well as for the associated uncertainties.

A screenshot of the CCC elaboration for the Brinell full-range dataset is reported in Figure 4.27.

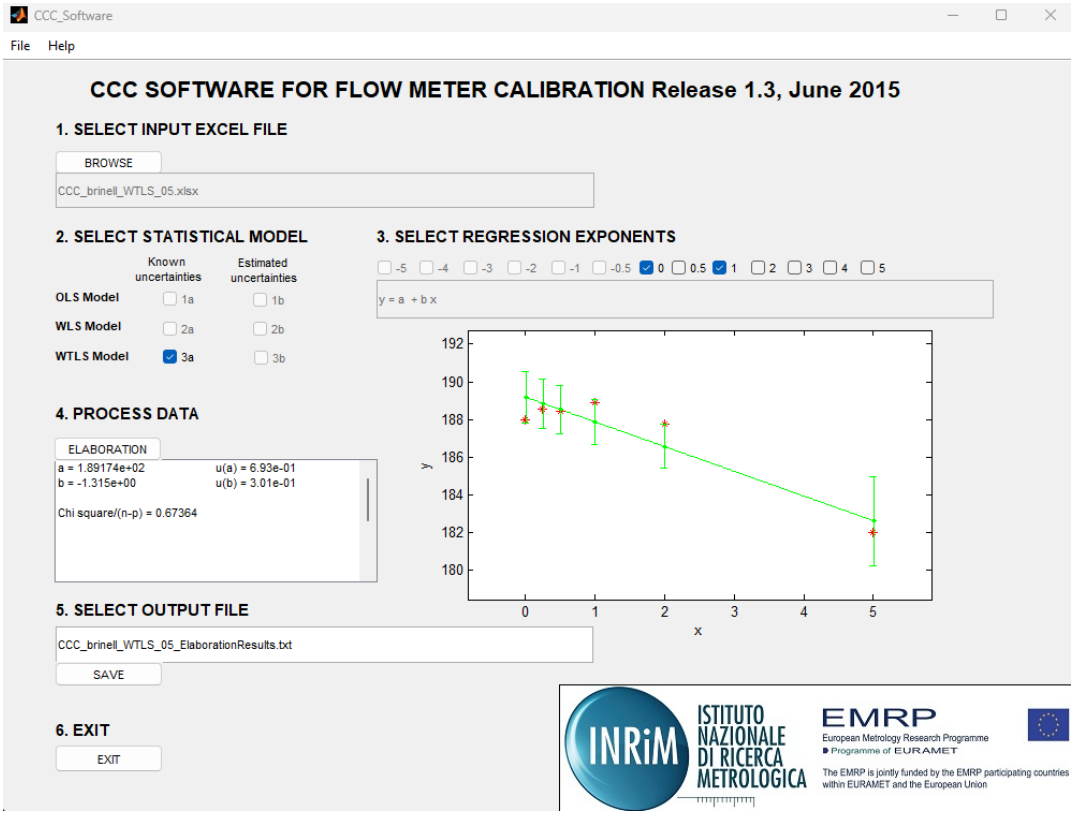

Figure 4.27: WTLS regression of the Brinell force-misalignment dataset carried out with the CCC software used at INRIM [55]

Unlike the Brinell case, the Vickers and Knoop analyses were not processed with CCC because the adopted models include three variables, namely hardness, the tilt angle θ, and the in-plane rotation angle ω. Therefore, the regression analysis for these datasets was performed directly in MATLAB using the dedicated WTLS plane implementation.

Vickers hardness tests

The influence of force misalignment on macro-Vickers hardness was investigated using two certified reference blocks.

The indentations were performed using tilt angles $\theta = \{0°, 0.25°, 0.5°, 1°, 2°, 5°\}$, and for each inclination angle the indentation was measured at four in-plane rotation angles $\omega = \{0°, 30°, 60°, 90°\}$.

For macro-Vickers HV30, the standard uncertainty of each hardness value was evaluated

using the CMC-type expression of Eq. (4.4), with d_μ expressed in µm.

Figure 4.28 shows how the relative hardness changes with the inclination angle for the four in-plane orientations.

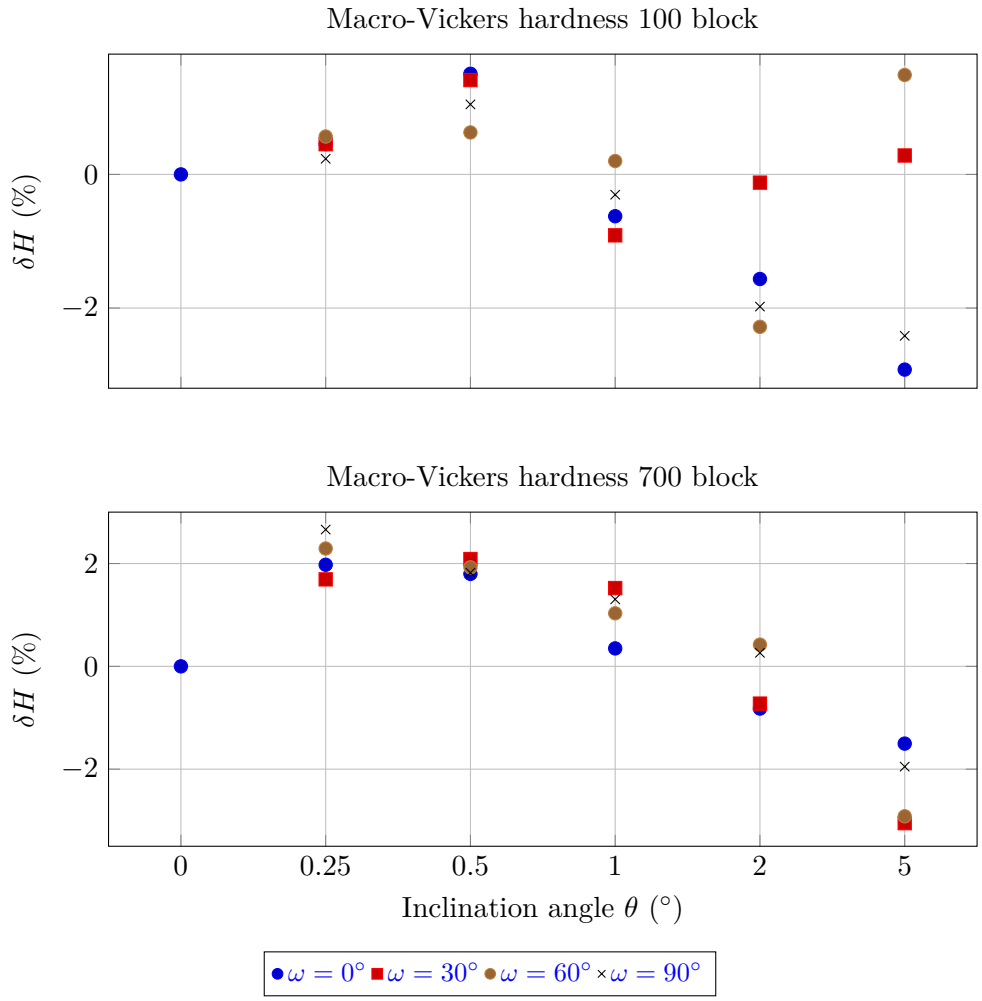

Figure 4.28: Relative variation of macro-Vickers hardness with inclination angle for the hardness 100 and 700 blocks, considering different in-plane rotation angles as parameter

For the hardness 100 block, the variations are not very large at small tilt angles, and they become more irregular mainly at the largest inclinations. For the hardness 700 block, the effect can already be seen more clearly even at small tilt angles. This means that the harder block is more sensitive to the misalignment.

The macro-Vickers datasets were fitted using the WTLS plane of Eq. (4.8). The results are reported in Table 4.14. For these data, the critical values are $\chi^2_{\nu,\text{crit}} = 1.264$ and

$F_{\text{crit}} = 1.497$.

Table 4.14: WTLS-plane regression parameters for the macro-Vickers force-misalignment experiments

Block	$\hat{H}_0$	$u(\hat{H}_0)$	$\hat{c}_\theta$	$u(\hat{c}_\theta)$	$\hat{c}_\omega$	$u(\hat{c}_\omega)$	$\hat{c}_{\theta,\text{rel}}$	$\hat{c}_{\omega,\text{rel}}$	χ^2_ν	F
HV30 hardness 100	101.718	0.215	-0.343	0.067	-0.000	0.003	-0.338	-0.00023	5.647	0.365
HV30 hardness 700	729.779	1.680	-6.410	0.520	0.062	0.027	-0.892	0.00862	1.382	1.257

For both macro-Vickers datasets, neither the reduced chi-square criterion nor the Fisher criterion is satisfied. This means that the fitted planes cannot really be taken as statistically validated models over the whole range that was studied. Even so, they are still useful as first-order descriptive representations of the average trend with θ and ω, especially if the idea is to compare the relative sensitivity of the two hardness levels.

For the harder macro-Vickers block, the corresponding WTLS-plane visualization and the absolute/relative fit are shown in Figures 4.29 and 4.30. These figures make it easier to see the combined effect of θ and ω.

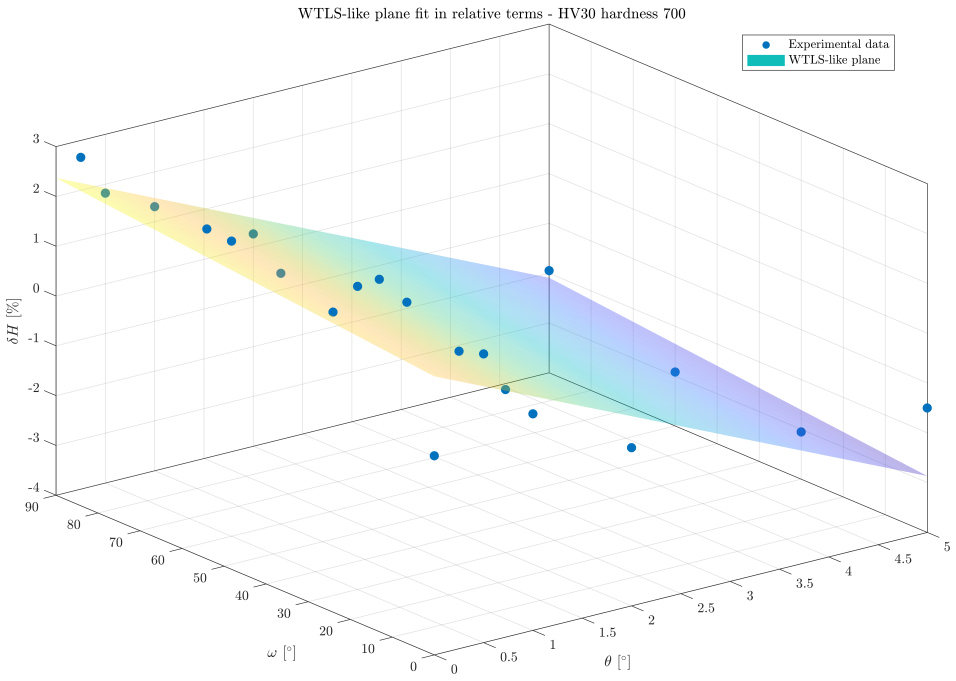

Figure 4.29: WTLS-like plane fit in relative terms for the macro-Vickers HV30 hardness 700 block

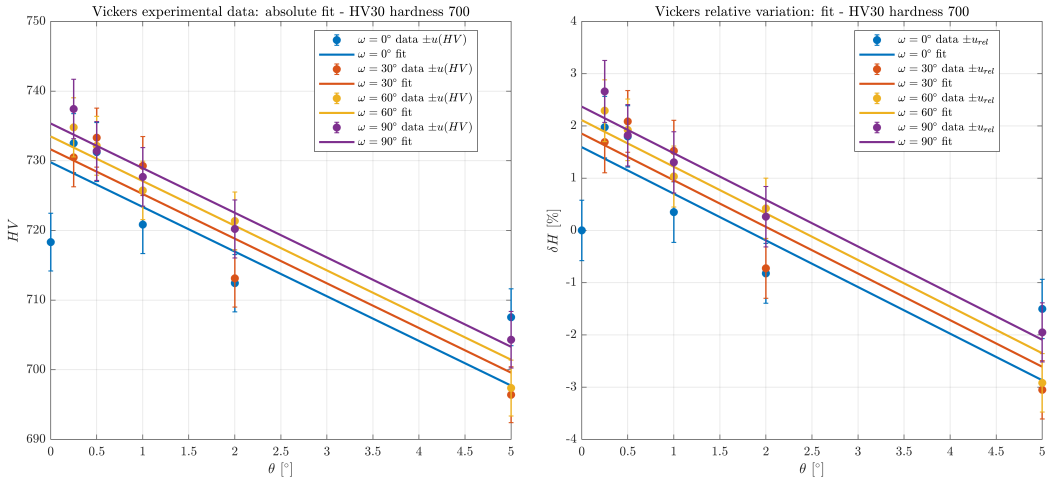

Figure 4.30: Absolute and relative WTLS fits for the macro-Vickers HV30 hardness 700 block

4.2.3 Microhardness tests

Vickers hardness tests

The micro-Vickers experiments were carried out on hardness 200 and 700 blocks. In this case, the uncertainty of the hardness values was evaluated using the constant relative standard uncertainty given in Eq. (4.5).

Figure 4.31 shows how the relative hardness changes with the inclination angle for the different in-plane orientations.

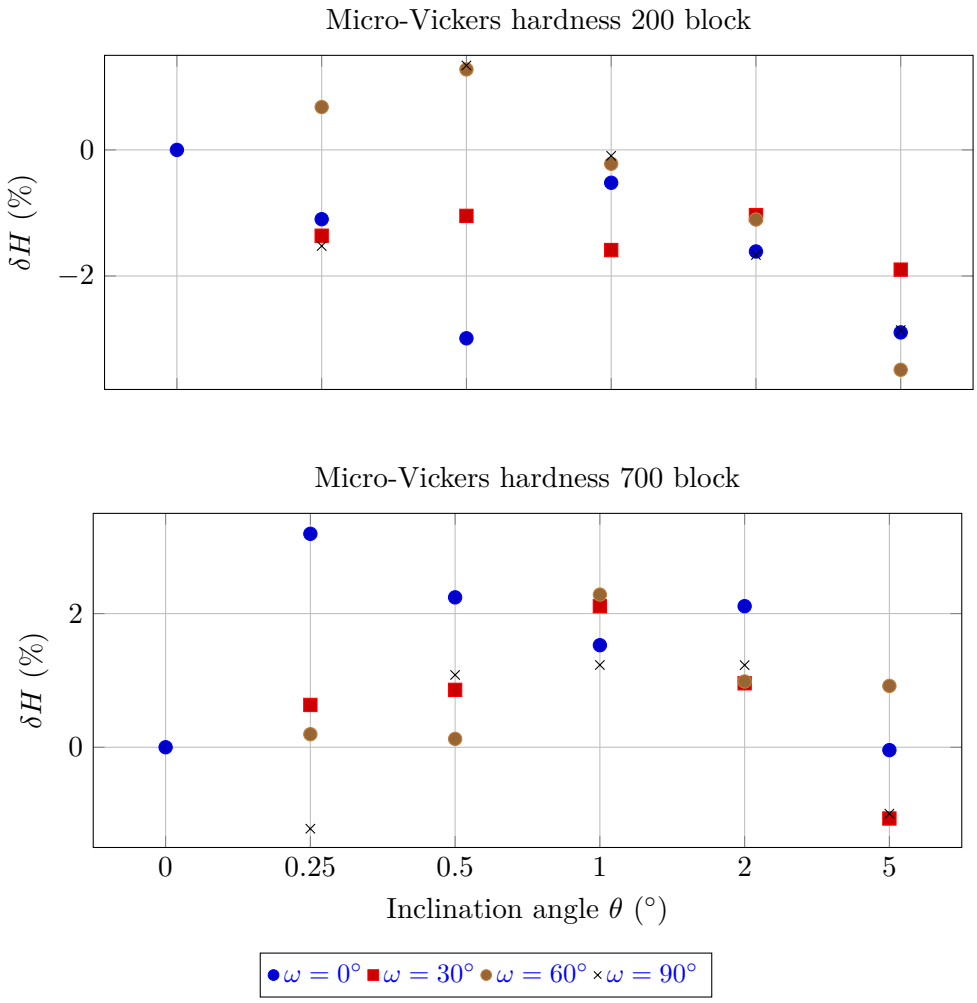

Figure 4.31: Relative variation of micro-Vickers hardness as a function of inclination angle for the hardness 200 and 700 blocks, with in-plane rotation angle as parameter

For the hardness 200 block, the variations are not very large and most of them are negative. The values remain within a moderate range even when the inclination increases.

For the hardness 700 block, the behaviour is a bit more irregular. In this case both positive and negative deviations appear depending on the in-plane orientation. This suggests that the harder block is more sensitive to the misalignment.

The micro-Vickers datasets were fitted using the WTLS plane of Eq. (4.8). The results are reported in Table 4.15. For these data, the critical values are $\chi^2_{\nu,\mathrm{crit}} = 1.264$ and $F_{\mathrm{crit}} = 1.497$.

Table 4.15: WTLS-plane regression parameters for the micro-Vickers force-misalignment experiments

Block	$\hat{H}_0$	$u(\hat{H}_0)$	$\hat{c}_\theta$	$u(\hat{c}_\theta)$	$\hat{c}_\omega$	$u(\hat{c}_\omega)$	$\hat{c}_{\theta,\mathrm{rel}}$	$\hat{c}_{\omega,\mathrm{rel}}$	χ^2_ν	F
HV1 hardness 200	198.926	0.479	-1.001	0.150	0.019	0.008	-0.499	0.00970	2.751	2.232
HV1 hardness 700	742.888	2.076	-1.744	0.645	-0.082	0.033	-0.239	-0.01119	2.267	2.033

For both micro-Vickers datasets, the Fisher criterion is satisfied, while the reduced chi-square criterion is not satisfied. This means that the fitted planes describe a variation that is larger than the intrinsic non-uniformity of the block, but they do not reproduce the whole experimental dispersion when the adopted uncertainty model is considered.

For this reason, the fitted coefficients can mainly be interpreted as first-order sensitivity indicators, while the complete plane representation should still be considered approximate.

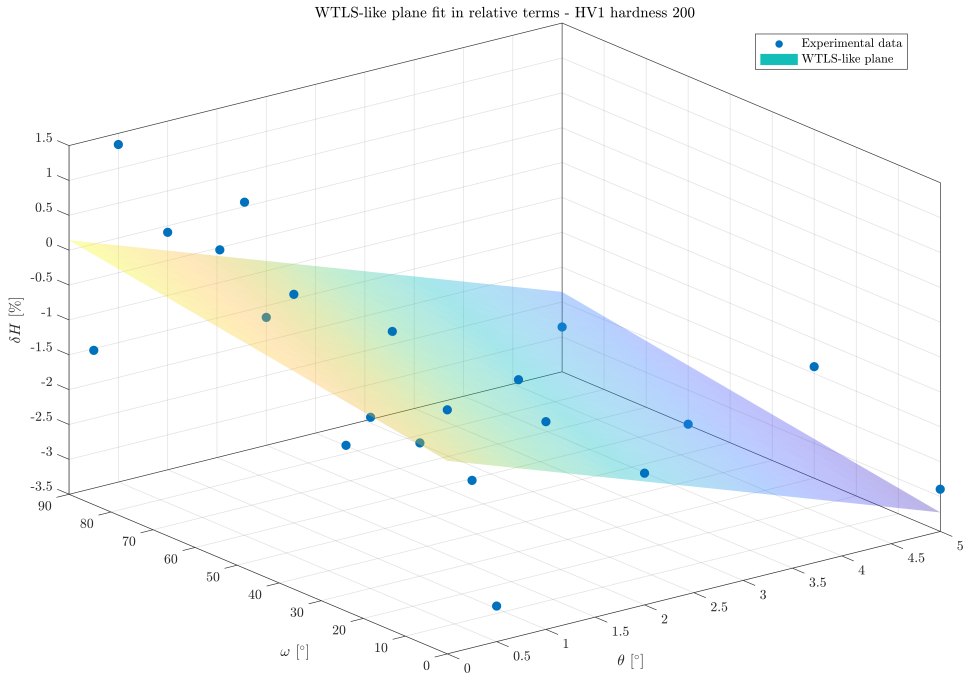

Figure 4.32: WTLS-like plane fit in relative terms for the micro-Vickers HV1 hardness 200 block

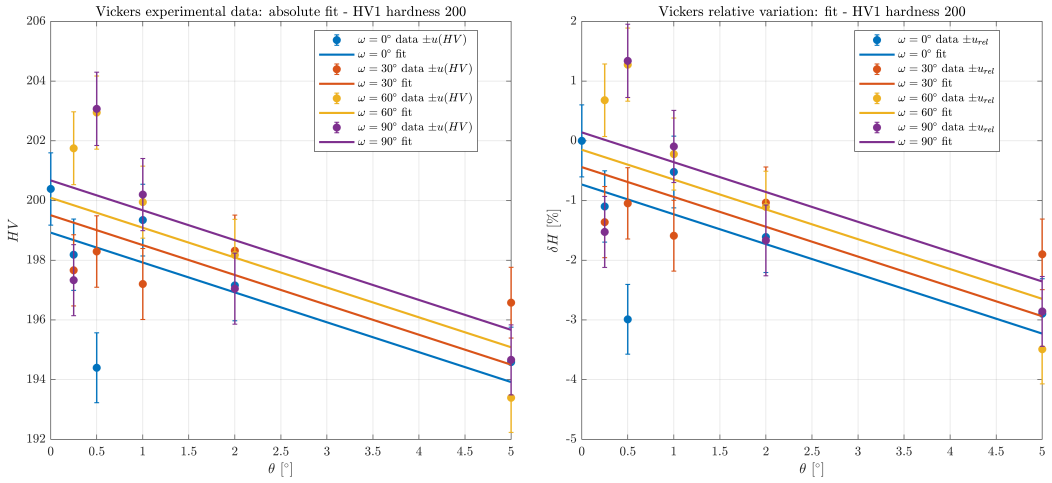

Figure 4.33: Absolute and relative WTLS fits for the micro-Vickers HV1 hardness 200 block

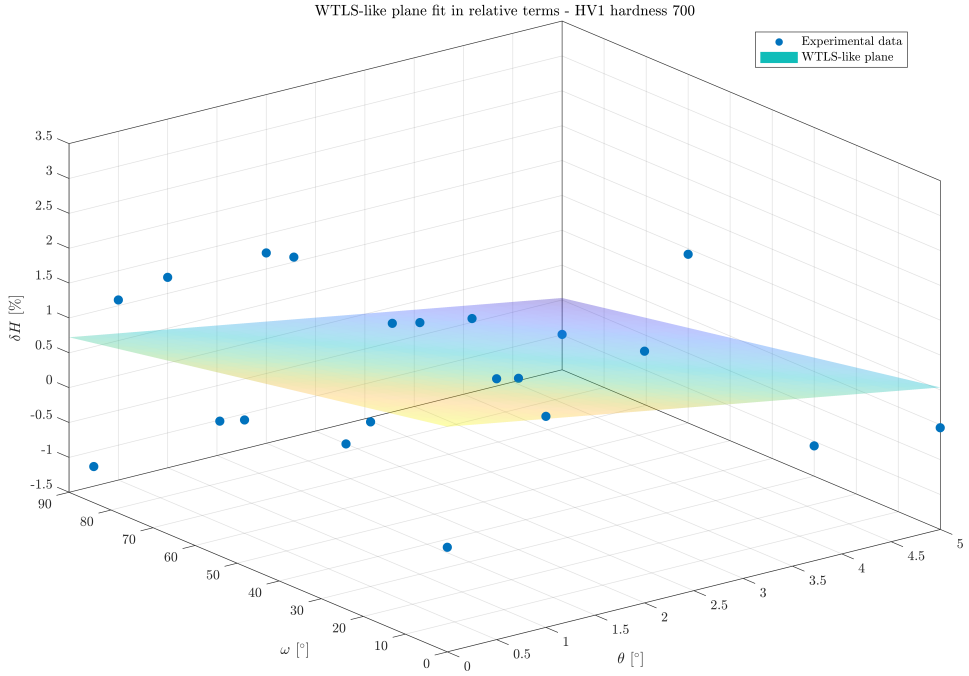

Figure 4.34: WTLS-like plane fit in relative terms for the micro-Vickers HV1 hardness 700 block

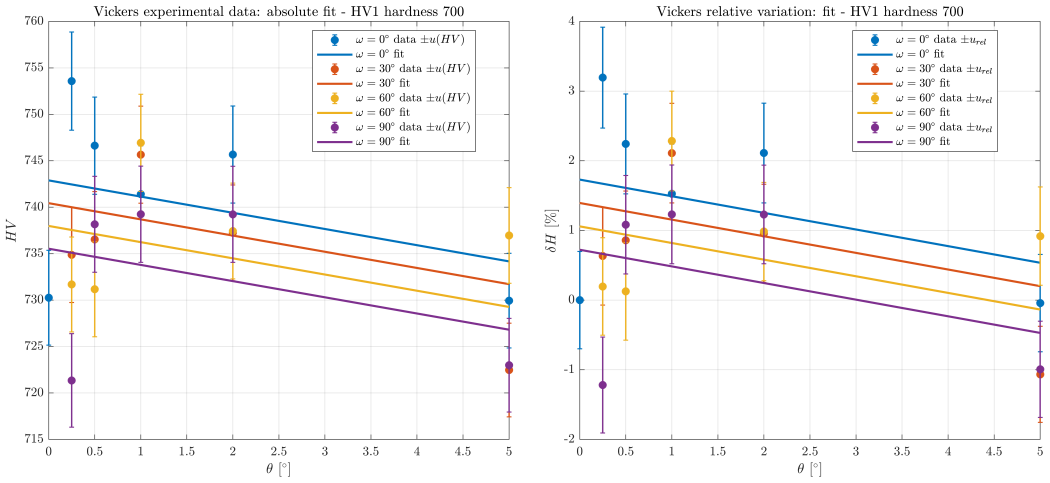

Figure 4.35: Absolute and relative WTLS fits for the micro-Vickers HV1 hardness 700 block

Knoop hardness tests

The Knoop force-misalignment experiments were carried out on reference blocks of nominal hardness 200 and 700.

Because of the anisotropic shape of the Knoop indentation, the measured response depends quite a lot on both the tilt angle and the in-plane orientation.

For the Knoop HK2 datasets, the hardness uncertainty was also evaluated using the constant relative standard uncertainty given in Eq. (4.5).

Figure 4.36 shows how the relative hardness changes for both blocks. Even at small inclination angles the dependence on the in-plane orientation can already be seen, especially for the harder block.

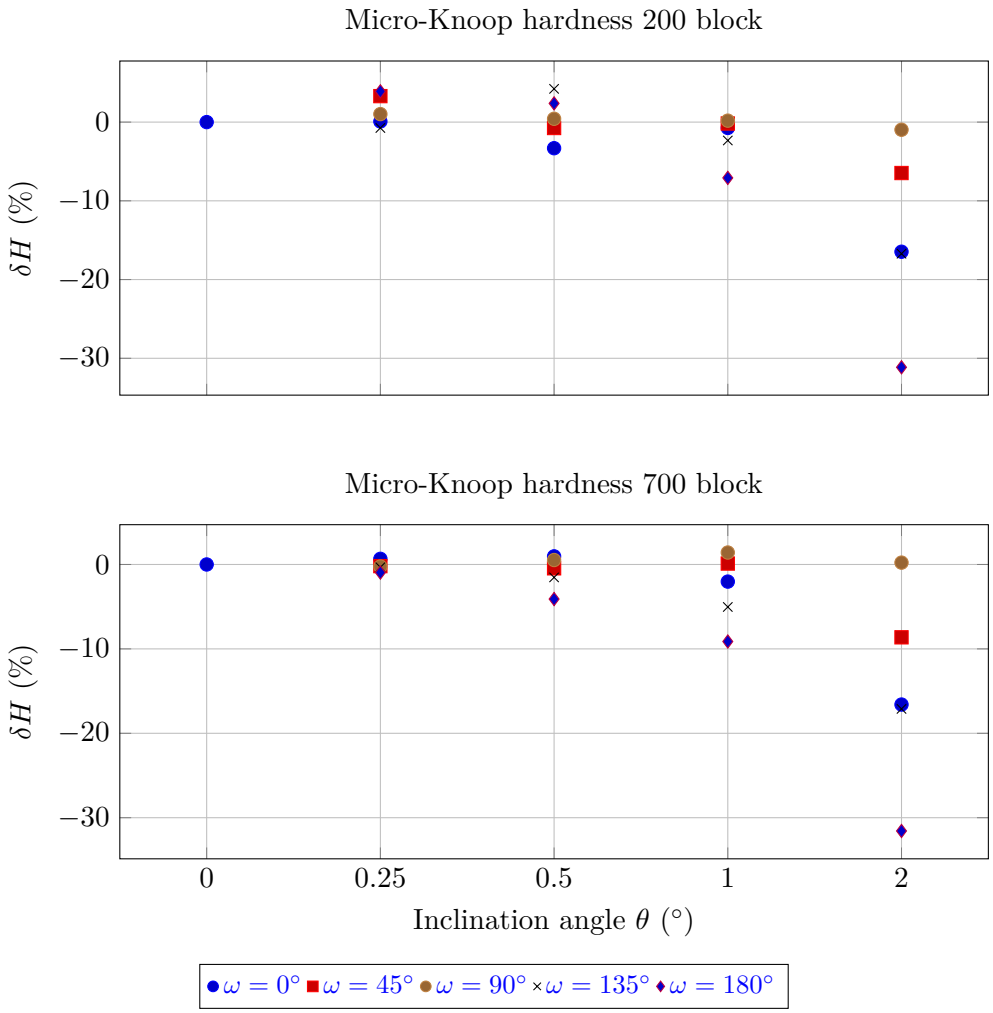

Figure 4.36: Relative variation of Knoop hardness as a function of inclination angle for the hardness 200 and 700 blocks, with in-plane rotation angle as parameter

The Knoop datasets were fitted using the WTLS plane of Eq. (4.8). The results are in Table 4.16. For these data, the critical values are $\chi^2_{\nu,\text{crit}} = 1.264$ and $F_{\text{crit}} = 1.497$.

Table 4.16: WTLS-plane regression parameters for the Knoop force-misalignment experiments

Block	$\hat{H}_0$	$u(\hat{H}_0)$	$\hat{c}_\theta$	$u(\hat{c}_\theta)$	$\hat{c}_\omega$	$u(\hat{c}_\omega)$	$\hat{c}_{\theta,\text{rel}}$	$\hat{c}_{\omega,\text{rel}}$	χ^2_ν	F
HK2 hardness 200	228.067	0.868	-20.418	0.605	-0.044	0.006	-9.528	-0.02031	51.276	0.056
HK2 hardness 700	749.216	2.795	-62.186	1.932	-0.280	0.021	-8.835	-0.03981	47.267	0.061

For both Knoop datasets, neither the reduced chi-square criterion nor the Fisher criterion is satisfied. This means that the fitted plane is not enough to represent the whole experimental response.

Even so, the plots are still useful because they show quite clearly the strong directional dependence of Knoop hardness under force misalignment. This is basically the main qualitative result of this experimental series.

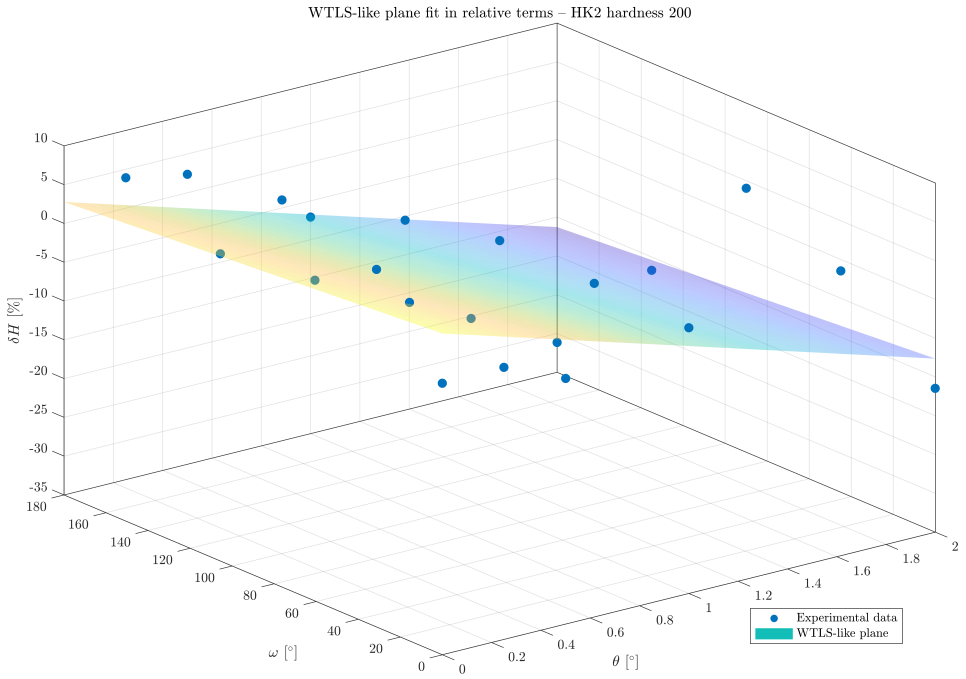

Figure 4.37: WTLS-like plane fit in relative terms for the Knoop hardness 200 block

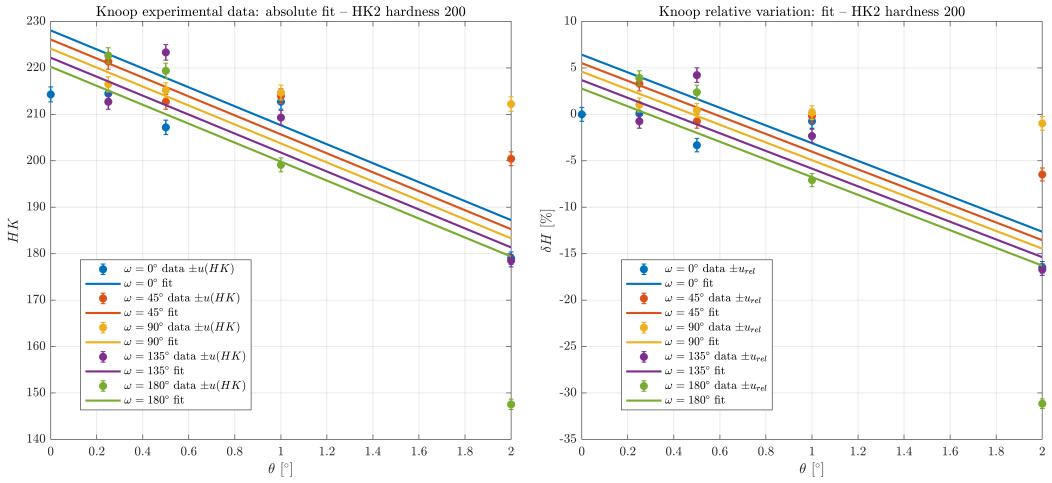

Figure 4.38: Absolute and relative WTLS fits for the Knoop hardness 200 block

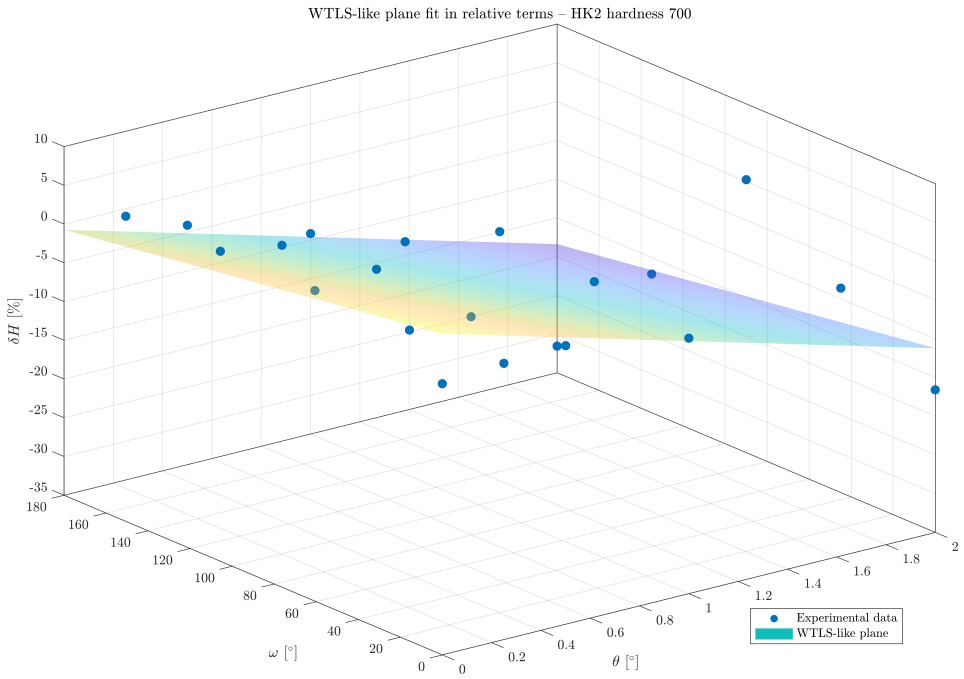

Figure 4.39: WTLS-like plane fit in relative terms for the Knoop hardness 700 block

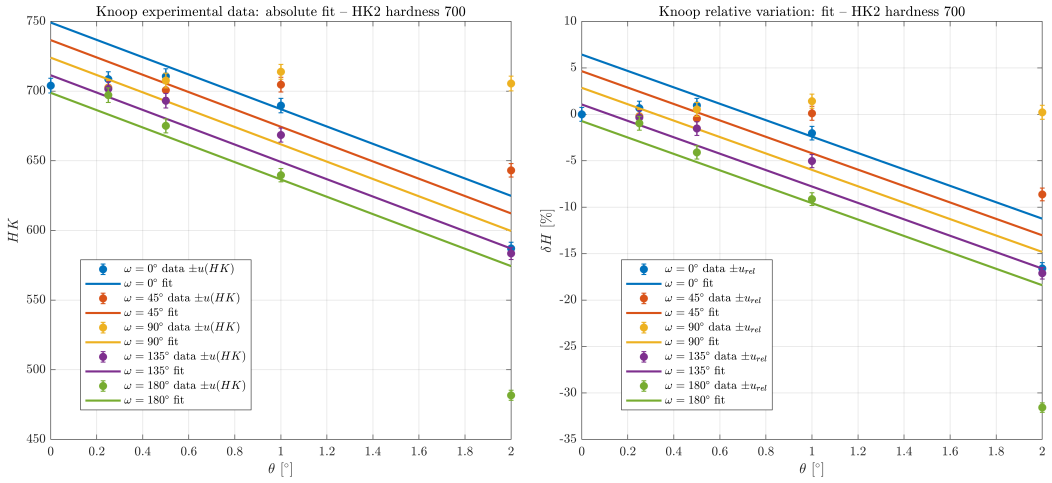

Figure 4.40: Absolute and relative WTLS fits for the Knoop hardness 700 block

The three indentation methods behave differently when geometrical deviations are present or when the applied force is not perfectly aligned.

For Brinell, the main geometrical parameter is the ball diameter and the behaviour remains quite smooth. The two modelling assumptions behave very differently, since the $V = \text{const}$ condition produces a much stronger sensitivity than the $d = \text{const}$ condition. In the experiments the decrease in hardness is only clearly observed at the largest tilt angle. From the statistical analysis, the fitted line is compatible with the uncertainty model, but the trend is not statistically significant due to the natural non-uniformity of the block.

In the Vickers method the hardness is affected by the face angle α, and the sensitivity increases as the hardness becomes higher. The experiments also indicate that force misalignment interacts with the in-plane orientation of the diagonals, particularly for harder blocks and in microhardness tests. From the statistical analysis, the macro-Vickers fits do not satisfy the required criteria, while the micro-Vickers fits satisfy only the Fisher criterion. For this reason, the fitted coefficients should mainly be interpreted as first-order sensitivity indicators.

Knoop is clearly the most anisotropic of the three methods. The response is much more sensitive to α than to β, and the experiments show a strong dependence on the relative orientation between the long diagonal and the tilt direction. This makes Knoop the most direction-sensitive method among those analysed here. However, the very large values of χ^2_ν and the failure of the Fisher criterion indicate that a simple WTLS plane is not

sufficient to fully describe the Knoop behaviour over the explored range.

From a metrological perspective, the WTLS analysis shows that the measured response does not depend only on geometrical trends. It is also necessary to consider the fitted sensitivity, the associated uncertainty, the non-uniformity of the block and the directional effects in order to determine whether the observed variations are statistically meaningful. For this reason, the combination of geometrical modelling and uncertainty-weighted regression provides a useful framework to analyse force misalignment, although simple first-order models still present some limitations.

The comparison therefore shows that geometrical imperfections and force misalignment cannot be described by a single universal trend. The magnitude of the effect, and in some cases even its sign, depends on several factors such as the indentation geometry, the adopted modelling condition, the hardness level and the orientation of the imprint relative to the perturbation direction.

Chapter 5

Conclusions and Future Work

5.1 Conclusions

In this study the influence of geometrical deviations of the indenter and also the effect of force misalignment on Brinell, Vickers and Knoop hardness measurements was analysed. For doing this, geometrical modelling and experimental observations were used together.

The results show that hardness is not only depending on the material itself but also on the geometrical and metrological conditions of the test. Small variations in the Brinell ball diameter, or in the characteristic angles of the Vickers and Knoop indenters, change the geometry of the indentation and therefore modify the hardness value obtained. Also if the test axis is not perfectly aligned with the surface, the imprint is not symmetric anymore and differences in the hardness measurement can appear.

Basically the geometrical modelling done in this work was used to see how much the hardness changes depending on the geometry of the indenter. Two modelling conditions were used: one with $V = const$ and another with $d = const$, which is the parameter used in the ISO hardness definitions. When comparing these two cases it becomes quite obvious that the predicted influence of the indenter geometry changes a lot depending on which quantity is assumed to stay constant during the indentation process.

Among the three hardness methods analysed in this work, Brinell shows the smallest sensitivity to geometrical deviations, Vickers shows an intermediate behaviour and Knoop

the largest sensitivity. As it can be seen before, this difference is related to the geometry of the indenters and also to the way the hardness value is defined in each hardness scale. In the case of Knoop the sensitivity is larger because the indenter has an anisotropic geometry and the hardness depends a lot on the long diagonal.

Another thing observed in the study is that when the hardness level increases the geometry of the indenter becomes more important. Basically, when hardness is higher the indentation is smaller, so the same geometrical deviation affects more the hardness you measure. This behaviour can be seen in the modelling results and also in the experimental measurements.

The magnitude of the hardness variations predicted by the modelling is similar to the deviations observed experimentally, especially for higher hardness levels. However, the experiments also show that the effect of force misalignment cannot be explained only using a simple geometrical condition like $V = const.$ The effect depends not only on the tilt angle but also, in the case of Vickers and especially Knoop, on the in-plane orientation of the indentation with respect to the perturbation direction.

The weighted total least squares analysis provides a framework based on uncertainty for interpreting the experimental results. In the Brinell case the fitted trend is compatible with the uncertainty model adopted, although it is not statistically significant when compared with the intrinsic non-uniformity of the reference block. For Vickers the fitted coefficients seem to be more representative in microhardness conditions than in macrohardness conditions. In the Knoop case the experiments show the strongest directional behaviour, but they also indicate that a simple first-order plane is not sufficient to represent the complete response in the analysed range.

Basically the results show that the uncertainty in hardness measurements depends on several things like the geometry of the indenter and the alignment of the test. This becomes quite important in high level metrology where traceability and reproducibility of hardness values must be ensured. Because of this the hardness measurement cannot be interpreted only from the material behaviour. The geometry of the indenter, the alignment conditions and also the metrological framework used to calculate the hardness value must be considered.

In conclusion, this study compares geometrical modelling with experimental observations for conventional hardness tests. The results show that the effect of geometrical deviations and alignment errors cannot be explained by one universal trend. The magnitude of the

effect changes depending on several factors such as the hardness scale used, the hardness level, the modelling condition assumed ($V = const$ or $d = const$) and also the orientation of the indentation with respect to the perturbation direction.

5.2 Future Work

The work presented in this thesis is part of a broader research activity carried out within the framework of the project, where several factors that can influence indentation hardness measurements are being investigated. Among these factors there are effects such as creep, temperature, indenter geometry and also the alignment of the applied force.

Within this context, the study of force misalignment developed in this thesis represents only one part of a larger experimental campaign. Additional measurements have already been carried out at INRiM together with other partners of the project, extending the investigation of the inclined plate methodology to other hardness scales and experimental conditions. In particular, measurements have been performed on additional scales such as HBW 2.5/31.25, HBW 2.5/187.5, HV 0.2 and HK 0.2, considering different materials and different hardness levels. These additional datasets should allow a more complete evaluation of the influence of alignment under different testing situations.

Basically, more measurements and simulations are planned in the project to study better the influence of indenter geometry, temperature and creep on hardness measurements. The geometrical modelling framework developed in this thesis can also be used to estimate sensitivity coefficients related to the geometry of the indenter. Also FEM simulations with controlled geometrical and loading conditions can help to support the experimental observations and to separate purely geometrical effects from effects related to the mechanical behaviour of the material.

The results of these ongoing activities are expected to contribute to future scientific publications and also to provide a more complete metrological evaluation of the different factors that influence Brinell, Vickers and Knoop hardness measurements.

Bibliography

[1] G. Barbato, G. Genta, and A. Germak, *Misurare per Decidere*, 3 2014. [Online]. Available: https://doi.org/10.15651/978-88-748-8704-0

[2] P. De Bièvre, "The 2007 International Vocabulary of Metrology (VIM), JCGM 200:2008 [ISO/IEC Guide 99]: Meeting the need for intercontinentally understood concepts and their associated intercontinentally agreed terms," *Clinical Biochemistry*, vol. 42, no. 4-5, pp. 246–248, 3 2009. [Online]. Available: https://doi.org/10.1016/j.clinbiochem.2008.09.007

[3] "About us | INRIM." [Online]. Available: https://www.inrim.it/en/about-us

[4] C. Kuzu, "Home - TRACIND BVK-H Project," 4 2024. [Online]. Available: https://tracind-bvk-h.org/

[5] C. Merolli *et al.*, "Analisi dell'effetto di creep nelle misure di durezza brinell, vickers e knoop," Master's thesis, Politecnico di Torino, Torino, Italy, 2025.

[6] L. Panarese, "Analysis of the effect of temperature on vickers, brinell, and knoop hardness measurements," Master's thesis, Politecnico di Torino, Torino, Italy, 2025.

[7] B. D. B. Hibbert, "Evaluation of Measurement Data: The Role of Measurement Uncertainty in Conformity Assessment," *Chemistry International*, vol. 35, no. 2, 1 2013. [Online]. Available: https://doi.org/10.1515/ci.2013.35.2.22

[8] International Organization for Standardization, *Metallic materials — Instrumented indentation test for hardness and materials parameters — Part 1: Test method*, International Organization for Standardization Standard ISO 14 577-1:2015, 2015.

[9] F. Mohs, *Grund Riss der Mineralogie, von Friedrich Mohs: 1: Terminologie, Systematik, Nomenklatur, Charakteristik von Friederich Mohs.* In der Arnoldischen buchhandlung, 1822.

[10] M. Marghany, "Chapter 1 - an introduction to minerals, rocks, and mineral deposits," in *Advanced Algorithms for Mineral and Hydrocarbon Exploration Using Synthetic Aperture Radar*, M. Marghany, Ed. Elsevier, 2022, pp. 1–30. [Online]. Available:

https://www.sciencedirect.com/science/article/pii/B9780128217962000148

[11] J. A. Brinell, "Ein verfahren zur härtebestimmung nebst einigen anwendungen desselben," *Baumaterialienkunde*, vol. 5, pp. 276–280, 294–297, 317–320, 364–367, 392–394, 412–416, 1900.

[12] S. M. Walley, "Historical origins of indentation hardness testing," *Materials Science and Technology*, vol. 28, no. 9-10, pp. 1028–1044, 2 2012. [Online]. Available: https://doi.org/10.1179/1743284711y.0000000127

[13] E. Broitman, "Indentation Hardness Measurements at Macro-, Micro-, and Nanoscale: A Critical Overview," *Tribology Letters*, vol. 65, no. 1, 12 2016. [Online]. Available: https://doi.org/10.1007/s11249-016-0805-5

[14] ISO 6506-1:2014, *Metallic materials — Brinell hardness test — Part 1: Test method*, International Organization for Standardization Std. ISO 6506-1, 2014.

[15] ISO 6506-2:2014, *Metallic materials — Brinell hardness test — Part 2: Verification and calibration of testing machines*, International Organization for Standardization Std. ISO 6506-2, 2014.

[16] ISO 6506-3:2014, *Metallic materials — Brinell hardness test — Part 3: Calibration of reference blocks*, International Organization for Standardization Std. ISO 6506-3, 2014.

[17] ISO 6507-1:2018, *Metallic materials — Vickers hardness test — Part 1: Test method*, International Organization for Standardization Std. ISO 6507-1, 2018.

[18] ISO 6507-2:2018, *Metallic materials — Vickers hardness test — Part 2: Verification and calibration of testing machines*, International Organization for Standardization Std. ISO 6507-2, 2018.

[19] ISO 6507-3:2018, *Metallic materials — Vickers hardness test — Part 3: Calibration of reference blocks*, International Organization for Standardization Std. ISO 6507-3, 2018.

[20] ISO 4545-1:2017, *Metallic materials — Knoop hardness test — Part 1: Test method*, International Organization for Standardization Std. ISO 4545-1, 2017.

[21] ISO 4545-2:2017, *Metallic materials — Knoop hardness test — Part 2: Verification and calibration of testing machines*, International Organization for Standardization Std. ISO 4545-2, 2017.

[22] ISO 4545-3:2017, *Metallic materials — Knoop hardness test — Part 3: Calibration of reference blocks*, International Organization for Standardization Std. ISO 4545-3, 2017.

[23] W. D. Callister and D. G. Rethwisch, *Materials Science and Engineering: An Introduction*, 10th ed. Hoboken: Wiley, 2018, original Date: 2000.

[24] Centro Español de Metrología, "Metrología abreviada," https://www.cem.es/sites/

default/files/metrologia20abreviada.pdf, 2020, accessed: 2026-02-16.

[25] "Istituto Nazionale di Ricerca Metrologica - INRIM - bioPmed," 3 2025. [Online]. Available: https://biopmed.eu/en/partner/istituto-nazionale-di-ricerca-metrologica-inrim/#:~:text=The%20National%20Institute%20for%20Metrological,EURAMET

[26] M. Sega, "Il mondo delle misure: la metrologia e il nuovo si," in *I modelli nelle Scienze*, ser. Quaderni di Ricerca in Didattica, M. A. Floriano and M. Russo, Eds. SPAIS, University of Palermo, 2020, no. Numero speciale 6, pp. 162–174. [Online]. Available: https://iris.inrim.it/retrieve/handle/11696/67030/dd2573c2-d6fb-e71c-e053-d805fe0ad5dc/QRD_2020_NumSpec_6_MSega.pdf

[27] Centro Español de Metrología, "Infraestructura metrológica española," 2024, accessed: 17 February 2026. [Online]. Available: https://www.cem.es/es/cem/metrologia/infraestructura-metrologica-espanola

[28] "Servizi di metrologia | INRIM." [Online]. Available: https://www.inrim.it/it/servizi/servizi-di-metrologia

[29] T. B.-H. Poroject, "Project Summary - TRACIND BVK-H Poroject," 4 2024. [Online]. Available: https://tracind-bvk-h.org/project-summary

[30] Institute of Metrology of Bosnia and Herzegovina. (2023) The kick-off meeting of 22rpt01 tracind bvk-h project was held. Accessed: 2026-02-20. [Online]. Available: https://www.met.gov.ba/en/news/1272/the-kick-off-meeting-of-22rpt01-tracind-bvk-h-project-was-held

[31] T. B.-H. Poroject, "Work Packages - TRACIND BVK-H Poroject," 4 2024. [Online]. Available: https://tracind-bvk-h.org/work-packages/

[32] C. Kuzu, A. Germak, F. Menelao, A. Stibler, G. Genta, M. Loewit, J. Borovsky, G. Maculotti, M. Hiti, A. Prato, E. Pelit, J. Fidelus, T. Apostol, v. Alibegović, B. Fakić, P. Reinstadt, F. Turotti, R. Affri, B. Muminovic, and A. Alibegović, "Traceability for indentation measurements in brinell–vickers–knoop hardness," *Measurement Sensors*, Dec. 2024.

[33] IMEKO TC6, "Traceability and reliability of bvk hardness measurements," in *Proceedings of the IMEKO TC6 International Conference on Metrology and Properties of Engineering Surfaces*, 2025. [Online]. Available: https://www.imeko.info/publications/tc6-2025/IMEKO-TC6-2025-021.pdf

[34] EURAMET, "Guidelines on the estimation of uncertainty in hardness measurements," 2011, eURAMET cg-16, Version 2.0.

[35] J. D. Fidelus, D. Bejma, A. Prato, and A. Germak, "Alignment tilt and force transducer creep effects on hardness in conventional hardness tests," in *IMEKO TC3, TC5, TC16 and TC22 International Conference*, 2022.

[36] N. Ilie, T. Hilton, S. Heintze, R. Hickel, D. Watts, N. Silikas, J. Stansbury, M. Cadenaro, and J. Ferracane, "Academy of dental materials guidance,Äîresin composites: Part i,Äîmechanical properties," *Dental Materials*, vol. 33, 05 2017.

[37] M. El-Sherbiny, R. Hegazy, M. Ibrahim, and A. Abuelezz, "The influence of geometrical tolerances of vickers indenter on the accuracy of measured hardness," *International Journal of Metrology and Quality Engineering*, vol. 3, pp. 1–6, 2012.

[38] G. Barbato, M. Galetto, and A. Germak, "Influence of the indenter shape in rockwell hardness test," *Measurement*, vol. 24, pp. 123–134, 1998.

[39] S. Yamamoto, "Influence of indenter geometry on rockwell hardness," *Journal of Testing and Evaluation*, 1969.

[40] R. Hegazy, M. Ibrahim, A. Abuelezz, and M. El-Sherbiny, "The effect of indenter geometrical errors on the accuracy and uncertainty of brinell hardness," in *14th International Conference on Applied Mechanics and Mechanical Engineering*, 2010.

[41] *ASTM E384: Standard Test Method for Microindentation Hardness of Materials*, ASTM International Std., 2022.

[42] G. Barbato, S. Desogus, and R. Levi, "The meaning of the geometry of rockwell indenters," 1978, p. 4.

[43] OIML, "Factors influencing hardness measurement: A systematic survey of research results," International Organization of Legal Metrology, Tech. Rep., 1983, p. 32.

[44] X. Hernot, O. Bartier, G. Mauvoisin, and J.-M. Collin, "A universal formulation for indentation whatever the indenter geometry," *Mechanics of Materials*, vol. 81, pp. 101–109, 2015. [Online]. Available: https://www.sciencedirect.com/science/article/pii/S0167663614002117

[45] R. D. Morrison, "Chapter 16 - forensic applications of subsurface contaminant transport models," in *Introduction to Environmental Forensics (Third Edition)*, third edition ed., B. L. Murphy and R. D. Morrison, Eds. San Diego: Academic Press, 2015, pp. 555–591. [Online]. Available: https://www.sciencedirect.com/science/article/pii/B9780124046962000163

[46] D. Kunar and B. Bhattacharyya, "Experimental investigation into surface structuring by electrochemical micromachining," p. 2016, 02 2022.

[47] S. Shelbey, Ed., *CRC Standard Mathematical Tables*. Boca Raton, FL, USA: CRC Press, 1975.

[48] S. Rao, "Finite difference methods," in *Encyclopedia of Vibration*, S. Braun, Ed. Oxford: Elsevier, 2001, pp. 520–530. [Online]. Available: https://www.sciencedirect.com/science/article/pii/B0122270851000023

[49] M. Saikia, "The pythagoras' theorem," 09 2013.

[50] M. ROELENS, "The volume of a pyramid through the ages."

[51] T. Puttaswamy, "10 - aryabhata ii and sripati," in *Mathematical Achievements of Pre-Modern Indian Mathematicians*, T. Puttaswamy, Ed. Oxford: Elsevier, 2012, pp. 317–330. [Online]. Available: https://www.sciencedirect.com/science/article/pii/B9780123979131000107

[52] C. O. of Measures, "Central Office of Measures." [Online]. Available: https://www.gum.gov.pl/en

[53] BIPM, "The kcdb – the bipm key comparison database," 2026, accessed: 2026-03-11.

[54] BIPM , "Cipm mra and calibration and measurement capabilities (cmcs)," 2026, accessed: 2026-03-11.

[55] "CCC Software | INRIM." [Online]. Available: https://www.inrim.it/en/services/software-and-databases/ccc-software

Chapter A

Mathematical derivations and model details

A.1 Inversion of the ISO Brinell hardness formula

Starting from the following expression (Eq. (3.18)):

$$HBW = \frac{0.204\,F}{\pi D\left(D - \sqrt{D^2 - d^2}\right)} \tag{A.1}$$

The denominator is first removed, resulting in:

$$\pi D\,HBW\left(D - \sqrt{D^2 - d^2}\right) = 0.204\,F \tag{A.2}$$

Dividing both sides by $\pi D\,HBW$ gives:

$$D - \sqrt{D^2 - d^2} = \frac{0.204\,F}{\pi D\,HBW} \tag{A.3}$$

For compactness, an auxiliary variable X:

$$X \equiv \frac{0.204\,F}{\pi D\,HBW} \tag{A.4}$$

Is introduced, so that:

$$\sqrt{D^2 - d^2} = D - X \tag{A.5}$$

Squaring both sides leads to:

$$D^2 - d^2 = (D - X)^2 = D^2 - 2DX + X^2 \tag{A.6}$$

From which:

$$d^2 = 2DX - X^2 \tag{A.7}$$

Finally, the indentation diameter d is obtained as:

$$d = \sqrt{2DX - X^2} \tag{A.8}$$

And by introducing the auxiliary variable X into Equation (A.8), the final expression for the Brinell indentation diameter d is derived:

$$\boxed{d = \sqrt{2D\left(\frac{0.204\,F}{\pi D\,HBW}\right) - \left(\frac{0.204\,F}{\pi D\,HBW}\right)^2}} \tag{A.9}$$

A.2 Solution of the constant-volume condition for the Brinell model

Starting from the spherical-cap volume expression (Eq. (3.23)):

$$V(R_1, h_1) = \frac{\pi h_1^2 (3R_1 - h_1)}{3} \tag{A.10}$$

The constant-volume condition $V(R_1, h_1) = V_0$ leads to:

$$h_1^3 - 3R_1 h_1^2 + \frac{3V_0}{\pi} = 0 \tag{A.11}$$

Introducing the change of variable:

$$h_1 = y + R_1 \tag{A.12}$$

The equation is reduced to the depressed cubic form:

$$y^3 + py + q = 0 \tag{A.13}$$

With:

$$p = -3R_1^2, \qquad q = -2R_1^3 + \frac{3V_0}{\pi} \tag{A.14}$$

As the discriminant is negative, three real roots exist. The solution is therefore obtained using the trigonometric Cardano–Viète method.

$$y_k = 2\sqrt{-\frac{p}{3}} \cos\left[\frac{1}{3} \arccos\left(\frac{3q}{2p}\sqrt{-\frac{3}{p}}\right) - \frac{2\pi k}{3}\right], \qquad k = 0,1,2 \tag{A.15}$$

Among the three solutions, only the root satisfying:

$$0 < h_1 < 2R_1 \tag{A.16}$$

Is physically admissible. This corresponds to $k = 1$, what results in:

$$\boxed{h_1 = R_1 + 2R_1 \cos\left[\frac{1}{3}\arccos\left(1 - \frac{3V_0}{2\pi R_1^3}\right) - \frac{2\pi}{3}\right]} \tag{A.17}$$

Chapter B

Supplementary geometrical results

B.1 Brinell supplementary figures

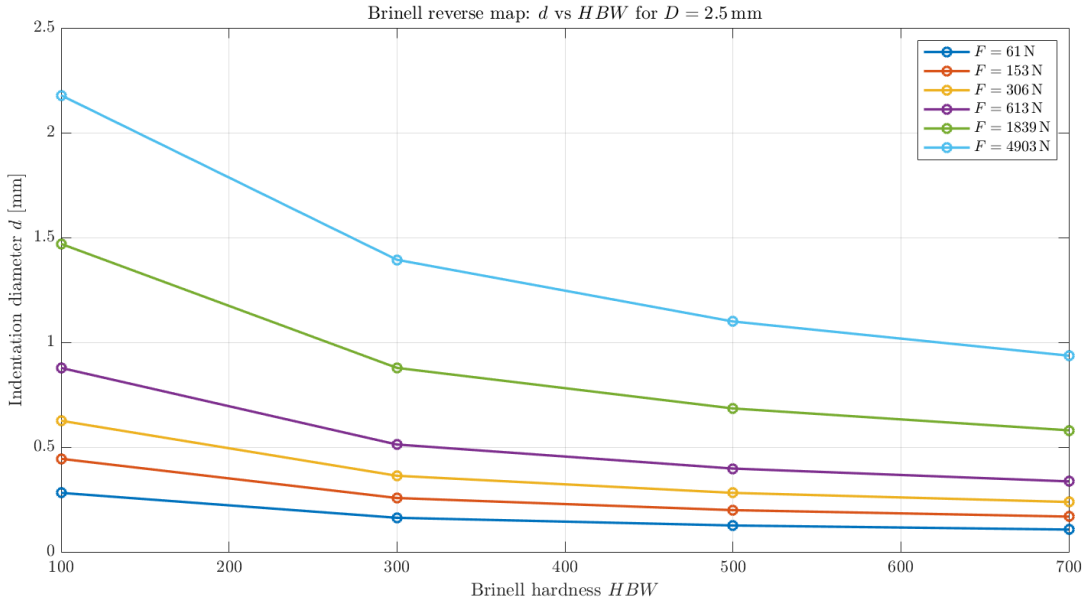

Figure B.1: Brinell reverse map: indentation diameter d as a function of Brinell hardness and applied force for $D = 2.5\,\mathrm{mm}$

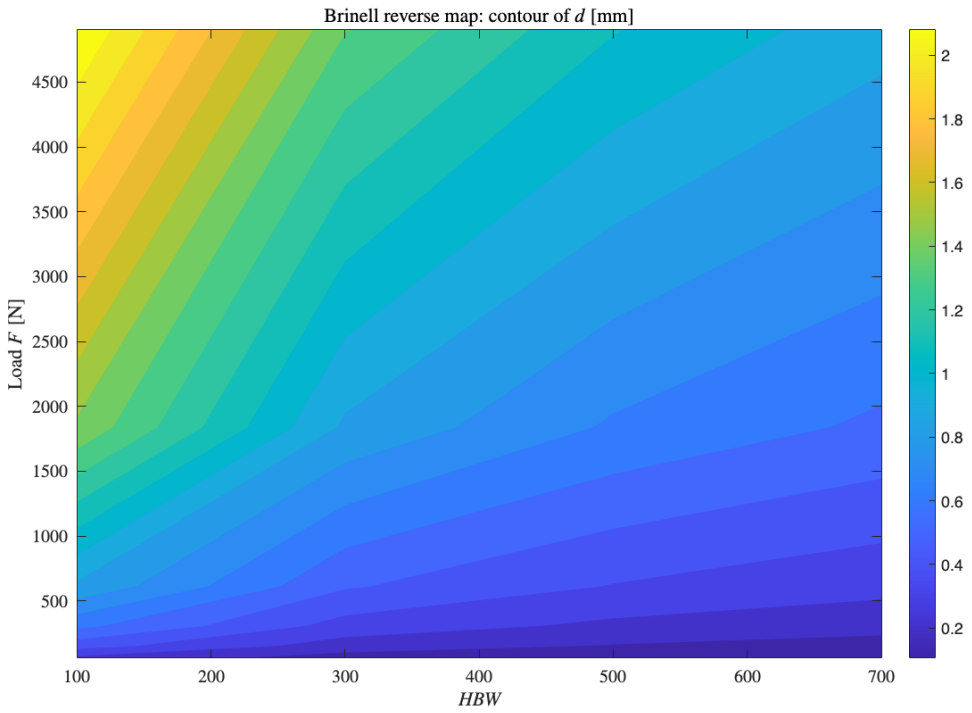

Figure B.2: Brinell reverse-map contour representation

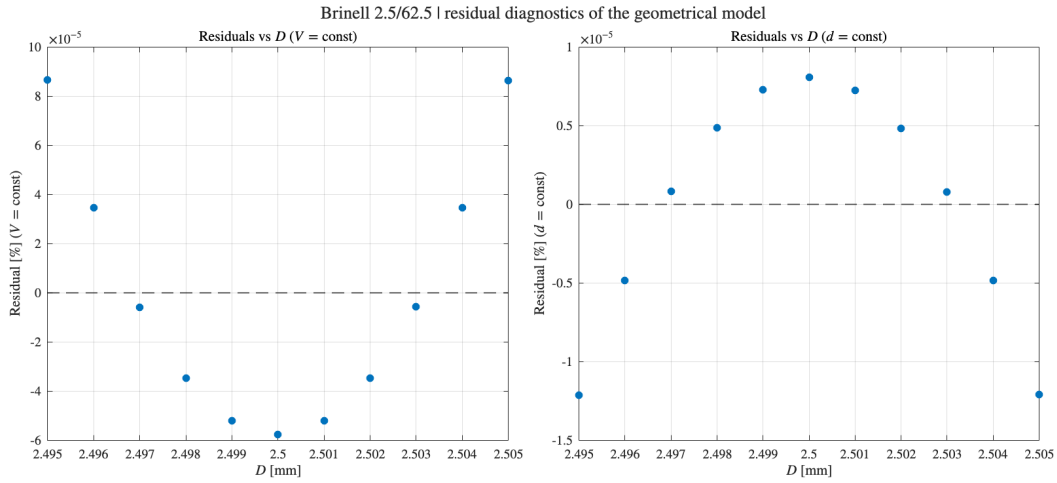

Figure B.3: Residual diagnostics of the Brinell geometrical model

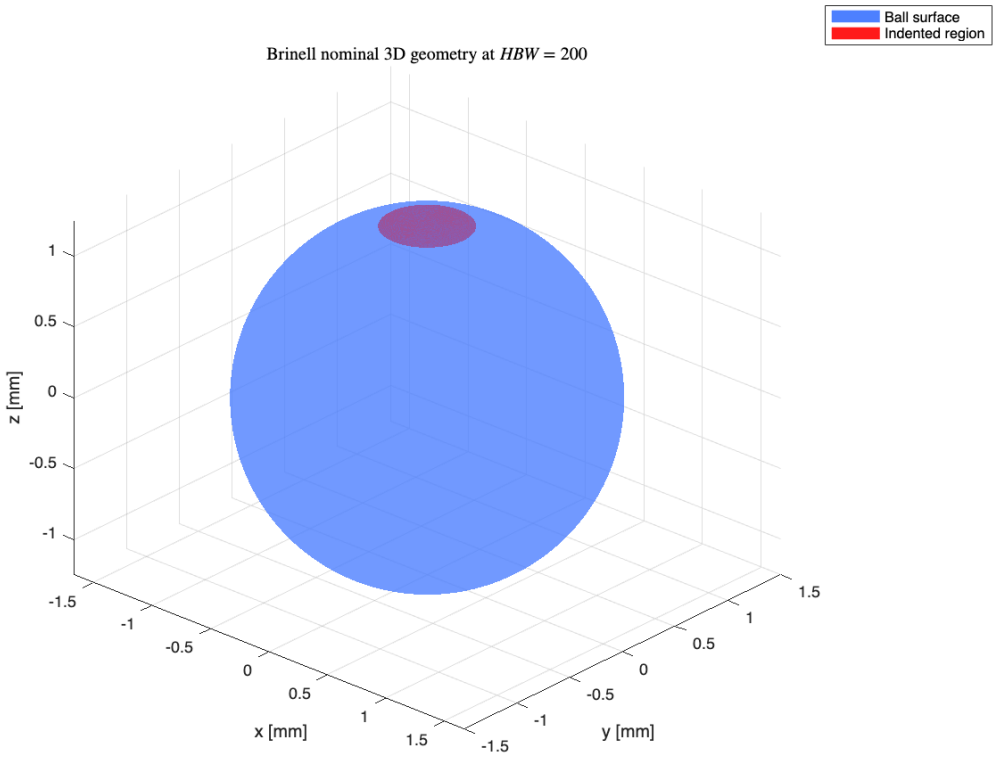

Figure B.4: Nominal Brinell 3D geometry at HBW = 200

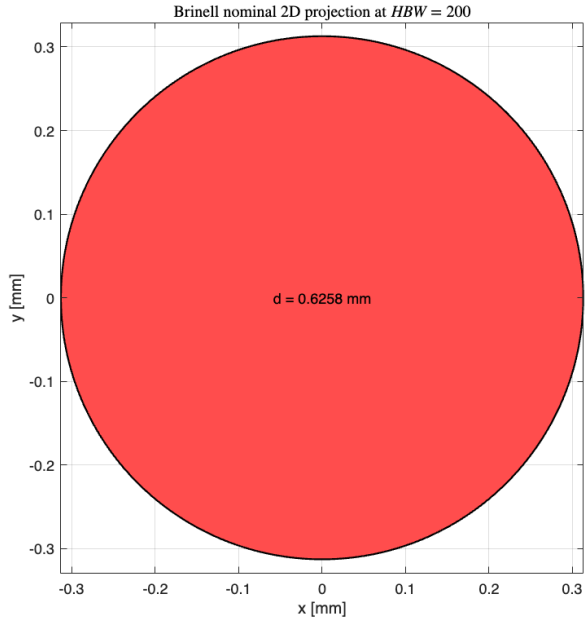

Figure B.5: Nominal Brinell projected indentation at HBW = 200

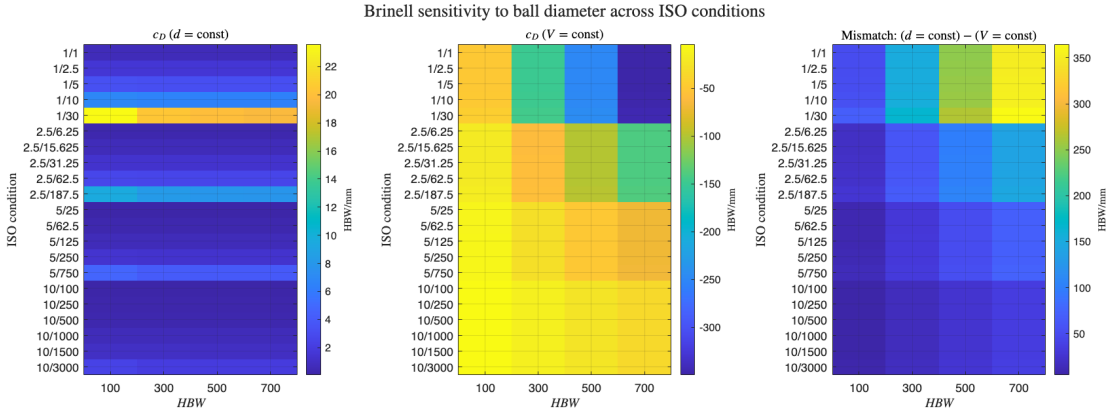

Figure B.6: Brinell sensitivity to ball diameter across ISO conditions

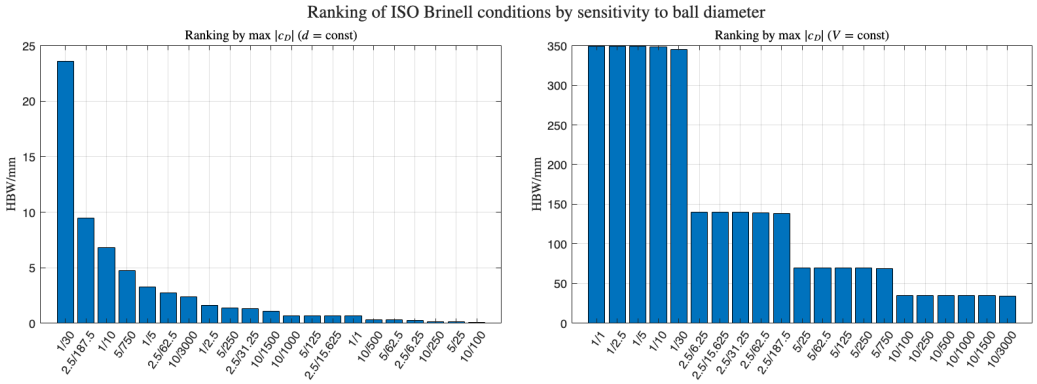

Figure B.7: Ranking of ISO Brinell conditions by sensitivity to ball diameter

B.2 Brinell supplementary tables

Table B.1: Nominal indentation diameter d_0 [mm] for the selected Brinell ISO conditions and nominal hardness levels

Condition	HBW100	HBW300	HBW500	HBW700
10/3000	5.8786	3.5115	2.7378	2.3203
10/1500	4.2652	2.5033	1.9453	1.6464
10/1000	3.5115	2.0495	1.5909	1.3458
10/500	2.5032	1.4530	1.1267	0.95267
10/250	1.7774	1.0289	0.79741	0.67409
10/100	1.1268	0.65123	0.50454	0.42646
5/750	2.9393	1.7557	1.3689	1.1601
5/250	1.7559	1.0248	0.79551	0.67294
5/125	1.2517	0.72658	0.56341	0.47638
5/62.5	0.88862	0.51441	0.39867	0.33702
5/25	0.56341	0.32563	0.25229	0.21324
2.5/187.5	1.4697	0.87793	0.68450	0.58011
2.5/62.5	0.87786	0.51236	0.39772	0.33644
2.5/31.25	0.62587	0.36329	0.28170	0.23819
2.5/15.625	0.44427	0.25719	0.19932	0.16850
2.5/6.25	0.28168	0.16280	0.12613	0.10661
1/30	0.58786	0.35115	0.27378	0.23203
1/10	0.35115	0.20495	0.15909	0.13458
1/5	0.25032	0.14530	0.11267	0.095267
1/2.5	0.17774	0.10289	0.079741	0.067409
1/1	0.11268	0.065123	0.050454	0.042646

Table B.2: Sensitivity coefficient c_D [HBW/mm] for the selected Brinell ISO conditions under $V = \text{const}$

Condition	HBW100	HBW300	HBW500	HBW700
10/3000	-4.4717	-14.506	-24.511	-34.513
10/1500	-4.7489	-14.756	-24.757	-34.757
10/1000	-4.8352	-14.838	-24.838	-34.837
10/500	-4.9188	-14.919	-24.918	-34.918
10/250	-4.9595	-14.959	-24.958	-34.958
10/100	-4.9837	-14.983	-24.982	-34.981
5/750	-8.9428	-29.009	-49.019	-69.021
5/250	-9.6697	-29.674	-49.672	-69.670
5/125	-9.8368	-29.835	-49.833	-69.830
5/62.5	-9.9183	-29.916	-49.913	-69.910
5/25	-9.9666	-29.964	-49.961	-69.958
2.5/187.5	-17.883	-58.010	-98.024	-138.02
2.5/62.5	-19.337	-59.339	-99.330	-139.32
2.5/31.25	-19.671	-59.662	-99.651	-139.64
2.5/15.625	-19.834	-59.823	-99.811	-139.80
2.5/6.25	-19.930	-59.918	-99.906	-139.89
1/30	-44.692	-144.96	-244.95	-344.90
1/10	-48.321	-148.28	-248.21	-348.14
1/5	-49.155	-149.09	-249.02	-348.94
1/2.5	-49.562	-149.49	-249.41	-349.34
1/1	-49.803	-149.73	-249.65	-349.58

Table B.3: Sensitivity coefficient c_D [HBW/mm] for the selected Brinell ISO conditions under $d = \text{const}$

Condition	HBW100	HBW300	HBW500	HBW700
10/3000	2.3611	2.0400	1.9860	1.9637
10/1500	1.0559	0.98646	0.97365	0.96827
10/1000	0.68003	0.65053	0.64494	0.64257
10/500	0.32880	0.32174	0.32037	0.31978
10/250	0.16177	0.16005	0.15971	0.15956
10/100	0.06408	0.063808	0.063754	0.06373
5/750	4.7214	4.0794	3.9713	3.9268
5/250	1.3600	1.3010	1.2898	1.2851
5/125	0.65763	0.64352	0.64077	0.63960
5/62.5	0.32344	0.31999	0.31931	0.31902
5/25	0.12815	0.12761	0.12750	0.12745
2.5/187.5	9.4411	8.1573	7.9414	7.8523
2.5/62.5	2.7186	2.6008	2.5784	2.5690
2.5/31.25	1.3149	1.2867	1.2812	1.2788
2.5/15.625	0.64658	0.63969	0.63833	0.63774
2.5/6.25	0.25619	0.25510	0.25488	0.25479
1/30	23.574	20.371	19.832	19.610
1/10	6.7907	6.4964	6.4406	6.4170
1/5	3.2834	3.2131	3.1994	3.1935
1/2.5	1.6155	1.5983	1.5949	1.5934
1/1	0.63994	0.63722	0.63668	0.63644

B.3 Vickers supplementary figures

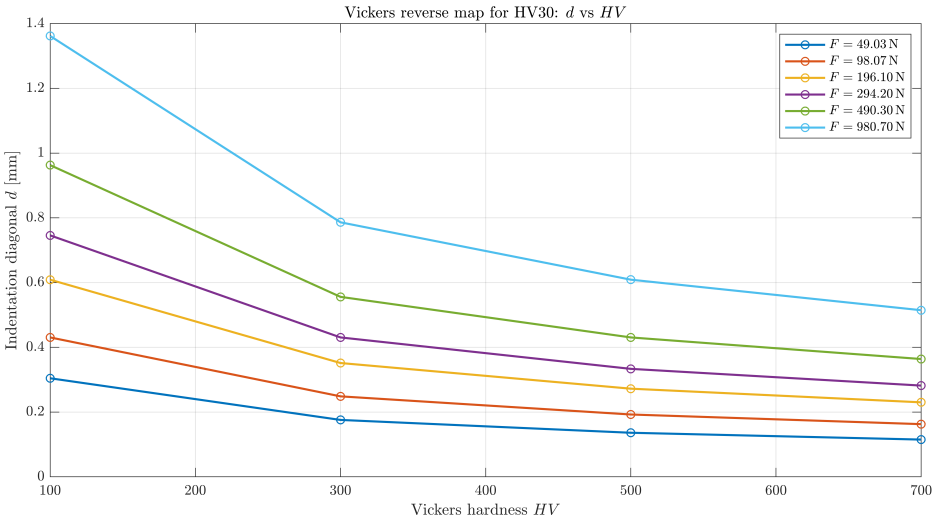

Figure B.8: Vickers reverse map for the HV30 scale: indentation diagonal d as a function of Vickers hardness and applied force

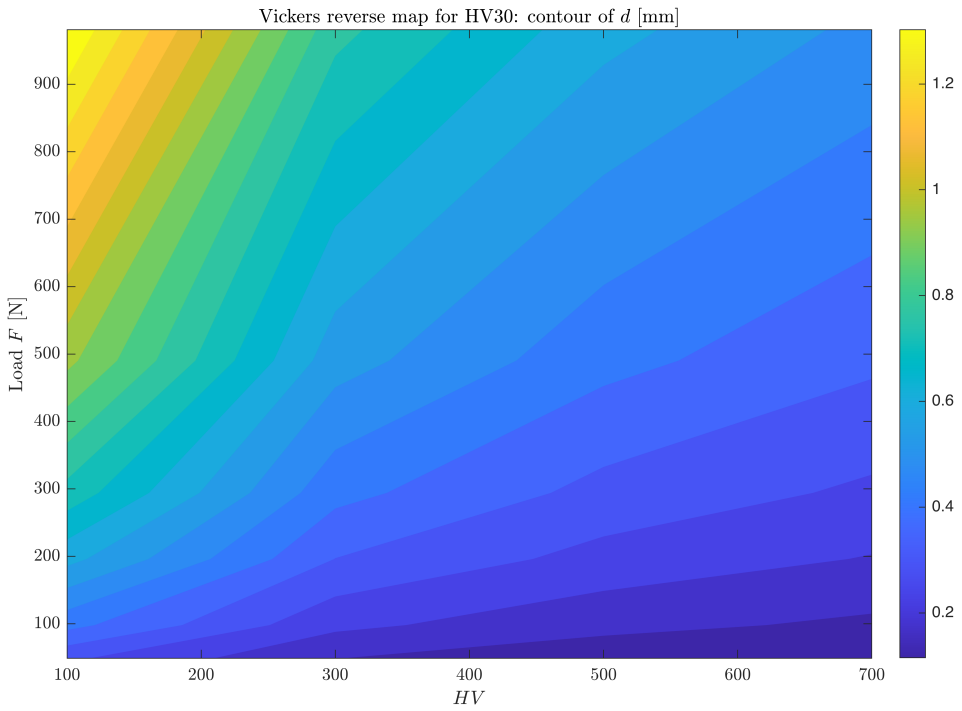

Figure B.9: Vickers reverse-map contour representation

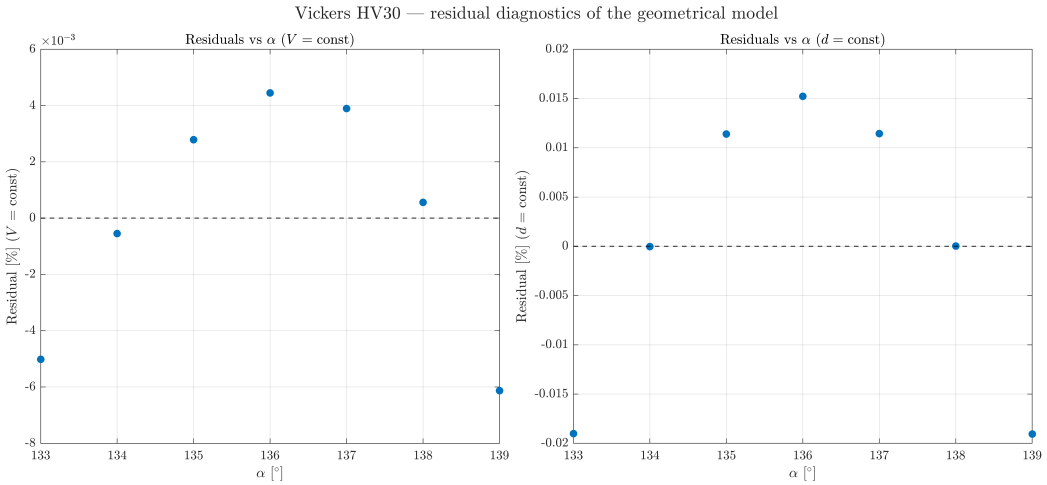

Figure B.10: Residual diagnostics of the Vickers geometrical model

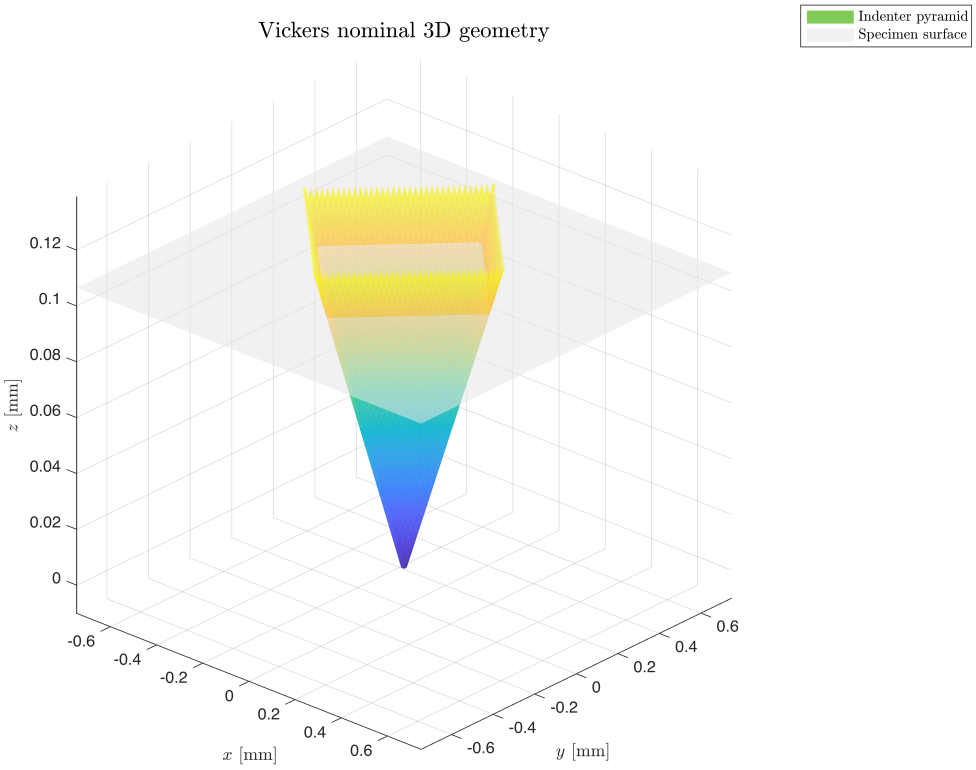

Figure B.11: Nominal Vickers 3D geometry

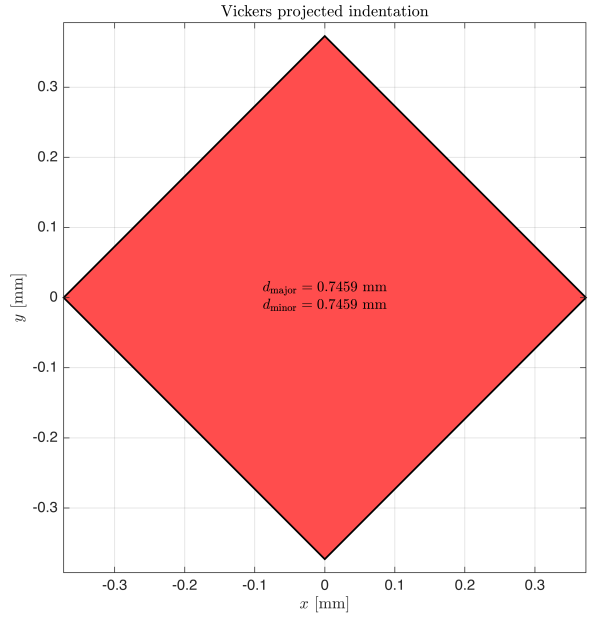

Figure B.12: Nominal Vickers projected indentation

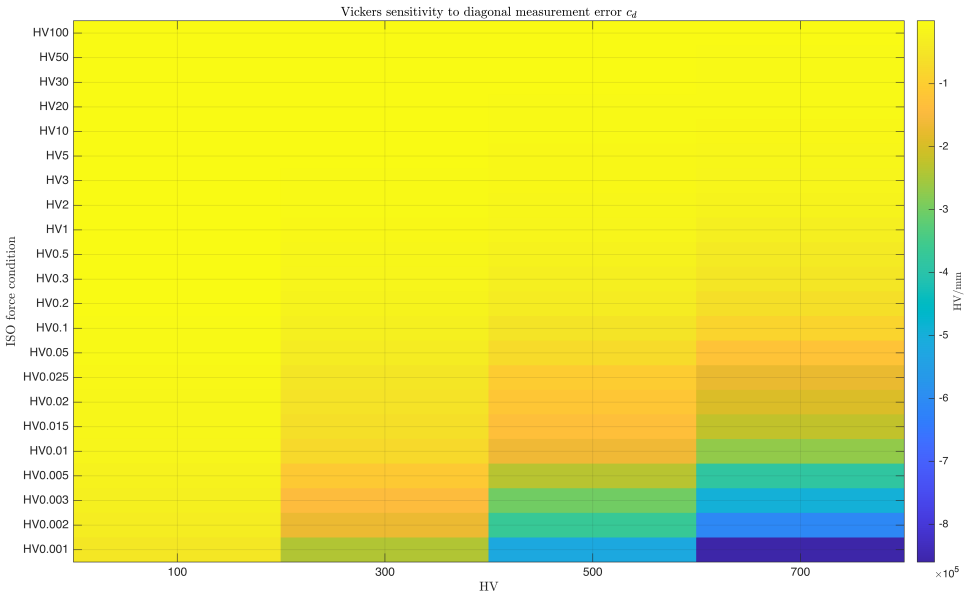

Figure B.13: Vickers sensitivity to diagonal measurement error across ISO force conditions

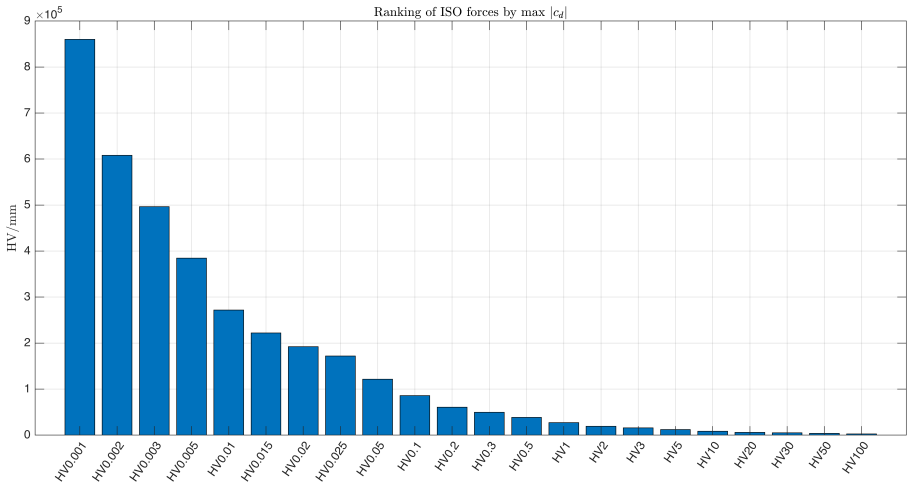

Figure B.14: Ranking of ISO Vickers force conditions by diagonal-error sensitivity

B.4 Vickers supplementary tables

Table B.4: Nominal Vickers diagonal d_0 [mm] for selected ISO force conditions and nominal hardness levels

Condition	HV100	HV300	HV500	HV700
HV0.001	0.0043064	0.0024863	0.0019259	0.0016277
HV0.002	0.0060895	0.0035158	0.0027233	0.0023016
HV0.003	0.0074588	0.0043063	0.0033357	0.0028191
HV0.005	0.0096289	0.0055592	0.0043062	0.0036394
HV0.01	0.013618	0.0078624	0.0060902	0.0051471
HV0.015	0.016678	0.0096292	0.0074588	0.0063038
HV0.02	0.019257	0.011118	0.0086119	0.0072784
HV0.025	0.021533	0.012432	0.0096299	0.0081387
HV0.05	0.030449	0.017580	0.013617	0.011509
HV0.1	0.043064	0.024863	0.019259	0.016277
HV0.2	0.060895	0.035158	0.027233	0.023016
HV0.3	0.074588	0.043063	0.033357	0.028191
HV0.5	0.096289	0.055592	0.043062	0.036394
HV1	0.13618	0.078624	0.060902	0.051471
HV2	0.19257	0.11118	0.086119	0.072784
HV3	0.23587	0.13618	0.10548	0.089149
HV5	0.30449	0.17580	0.13617	0.11509
HV10	0.43064	0.24863	0.19259	0.16277
HV20	0.60895	0.35158	0.27233	0.23016
HV30	0.74588	0.43063	0.33357	0.28191
HV50	0.96289	0.55592	0.43062	0.36394
HV100	1.3618	0.78624	0.60902	0.51471

Table B.5: Sensitivity coefficient $c_d = dHV/dd$ [HV/mm] for selected ISO force conditions

Condition	HV100	HV300	HV500	HV700
HV0.001	-46443	-2.4132e+05	-5.1924e+05	-8.6013e+05
HV0.002	-32843	-1.7066e+05	-3.6720e+05	-6.0826e+05
HV0.003	-26814	-1.3933e+05	-2.9979e+05	-4.9660e+05
HV0.005	-20771	-1.0793e+05	-2.3222e+05	-3.8468e+05
HV0.01	-14686	-76313	-1.6420e+05	-2.7200e+05
HV0.015	-11992	-62310	-1.3407e+05	-2.2209e+05
HV0.02	-10386	-53967	-1.1612e+05	-1.9235e+05
HV0.025	-9288	-48262	-1.0384e+05	-1.7202e+05
HV0.05	-6568.3	-34130	-73436	-1.2165e+05
HV0.1	-4644.3	-24132	-51924	-86013
HV0.2	-3284.3	-17066	-36720	-60826
HV0.3	-2681.4	-13933	-29979	-49660
HV0.5	-2077.1	-10793	-23222	-38468
HV1	-1468.6	-7631.3	-16420	-27200
HV2	-1038.6	-5396.7	-11612	-19235
HV3	-847.94	-4406.0	-9480.2	-15704
HV5	-656.83	-3413.0	-7343.6	-12165
HV10	-464.43	-2413.2	-5192.4	-8601.3
HV20	-328.43	-1706.6	-3672.0	-6082.6
HV30	-268.14	-1393.3	-2997.9	-4966.0
HV50	-207.71	-1079.3	-2322.2	-3846.8
HV100	-146.86	-763.13	-1642.0	-2720.0

B.5 Knoop supplementary figures

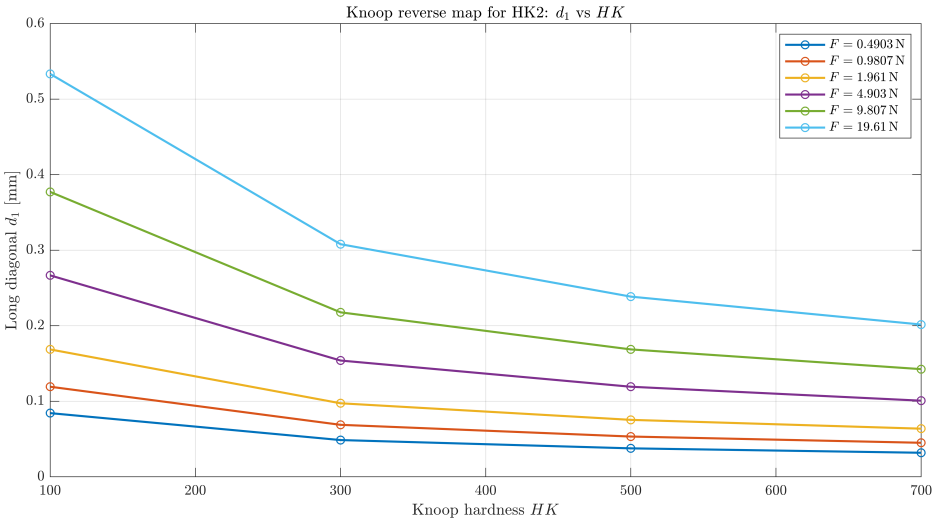

Figure B.15: Knoop reverse map for the HK2 scale: long diagonal d_1 as a function of Knoop hardness and applied force

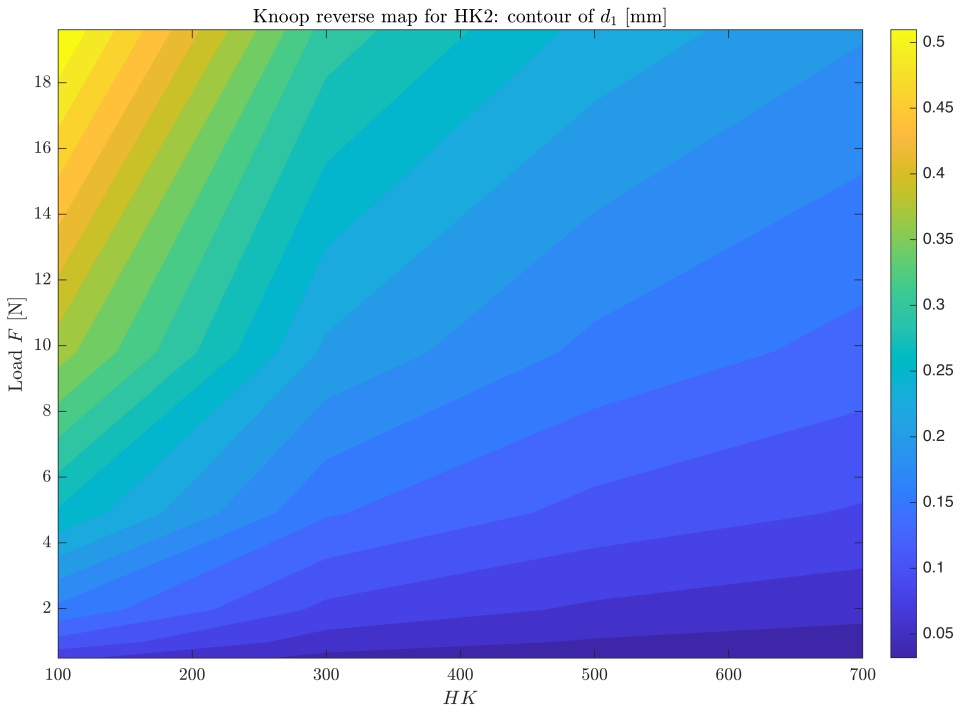

Figure B.16: Knoop reverse-map contour representation

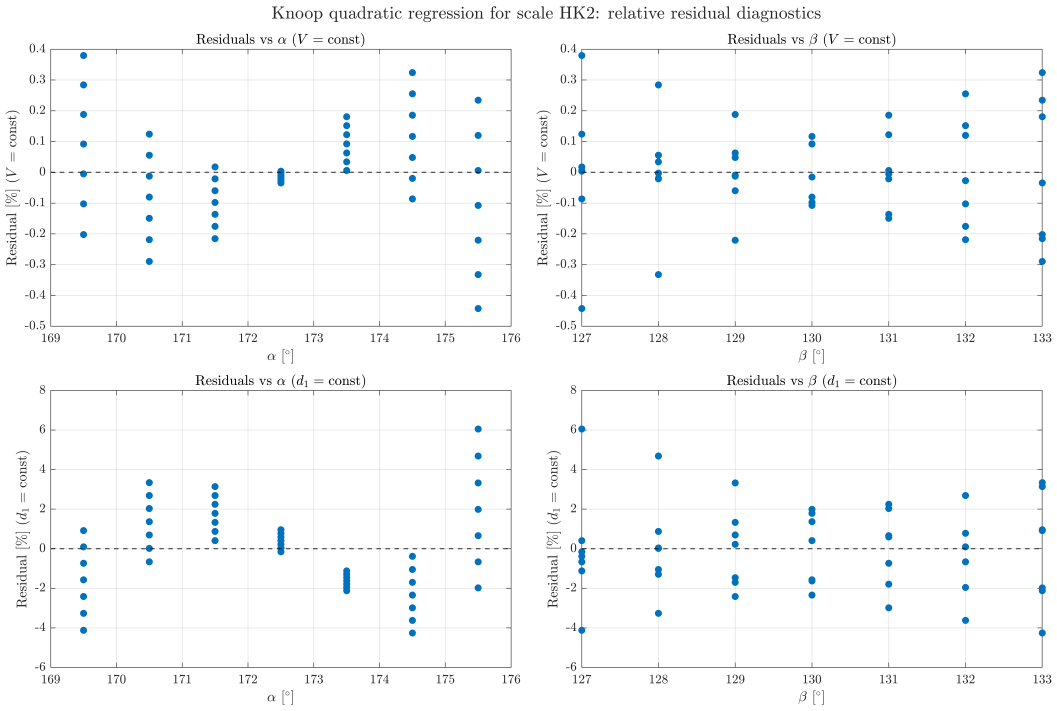

Figure B.17: Residual diagnostics of the quadratic Knoop regression

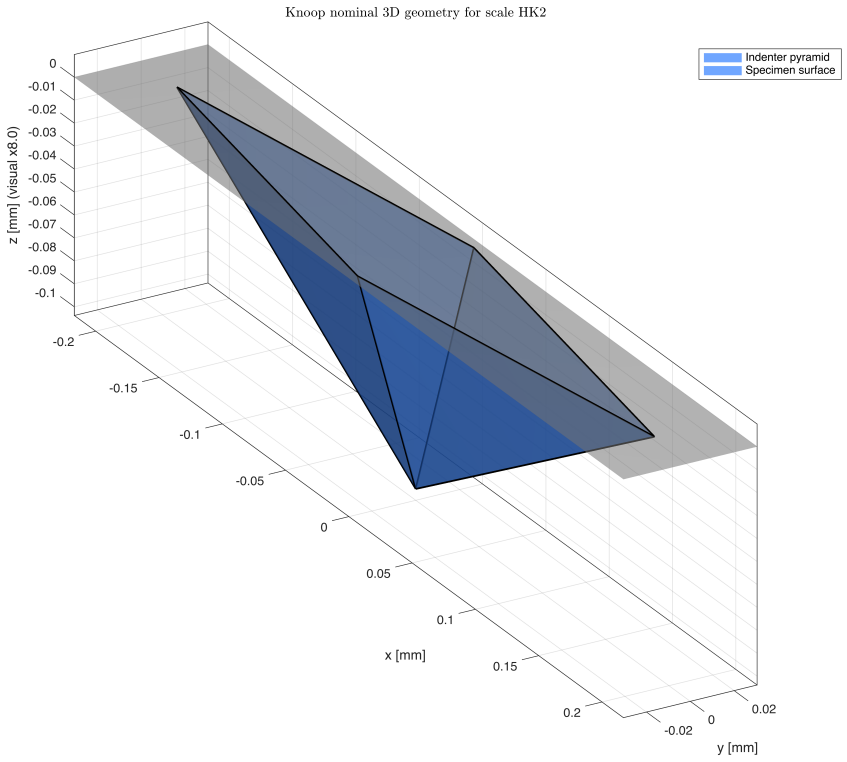

Figure B.18: Knoop indenter geometry: rhomboidal pyramid

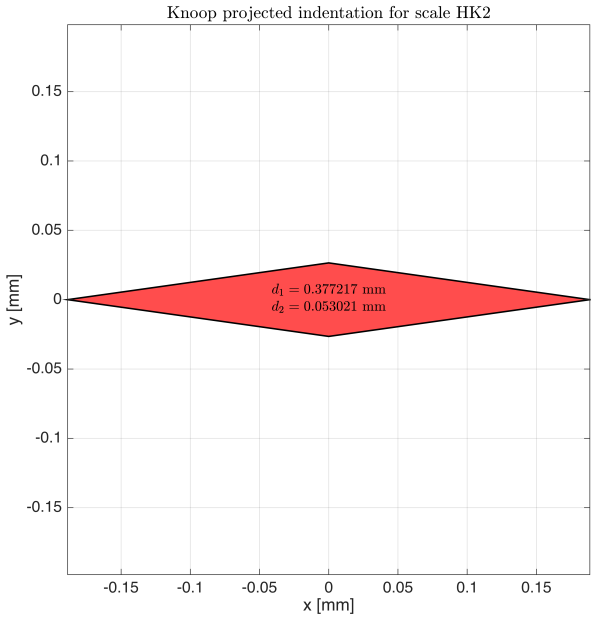

Figure B.19: Nominal Knoop projected indentation

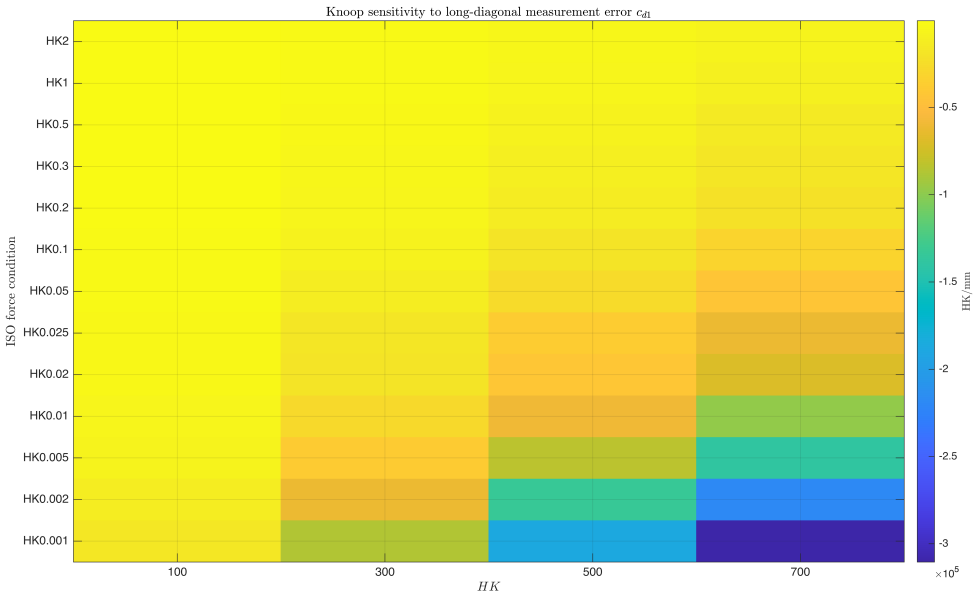

Figure B.20: Knoop sensitivity to long-diagonal measurement error across ISO force conditions

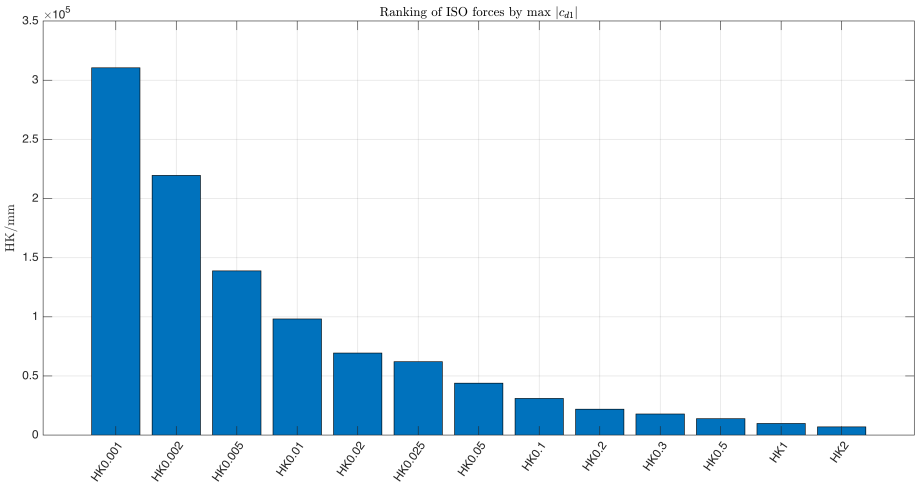

Figure B.21: Ranking of ISO Knoop force conditions by long-diagonal sensitivity

B.6 Knoop supplementary tables

Table B.6: Nominal Knoop long diagonal $d_{1,0}$ [mm] for selected ISO force conditions and nominal hardness levels

Condition	HK100	HK300	HK500	HK700
HK0.001	0.011929	0.0068872	0.0053348	0.0045087
HK0.002	0.016868	0.0097389	0.0075438	0.0063756
HK0.005	0.026673	0.015399	0.011928	0.010081
HK0.01	0.037723	0.021779	0.016870	0.014258
HK0.02	0.053342	0.030797	0.023855	0.020162
HK0.025	0.059648	0.034438	0.026675	0.022545
HK0.05	0.084346	0.048697	0.037721	0.031880
HK0.1	0.11929	0.068872	0.053348	0.045087
HK0.2	0.16868	0.097389	0.075438	0.063756
HK0.3	0.20661	0.11929	0.092400	0.078092
HK0.5	0.26673	0.15399	0.11928	0.10081
HK1	0.37723	0.21779	0.16870	0.14258
HK2	0.53346	0.30800	0.23857	0.20163

Table B.7: Sensitivity coefficient $c_{d_1} = dHK/dd_1$ [HK/mm] for selected ISO force conditions

Condition	HK100	HK300	HK500	HK700
HK0.001	-16766	-87118	-1.8745e+05	-3.1051e+05
HK0.002	-11857	-61608	-1.3256e+05	-2.1959e+05
HK0.005	-7498.3	-38963	-83834	-1.3887e+05
HK0.01	-5301.9	-27549	-59277	-98192
HK0.02	-3749.4	-19482	-41919	-69439
HK0.025	-3353.0	-17423	-37488	-62099
HK0.05	-2371.2	-12321	-26511	-43915
HK0.1	-1676.6	-8711.8	-18745	-31051
HK0.2	-1185.7	-6160.8	-13256	-21959
HK0.3	-968.0	-5029.9	-10823	-17928
HK0.5	-749.83	-3896.3	-8383.4	-13887
HK1	-530.19	-2754.9	-5927.7	-9819.2
HK2	-374.91	-1948.1	-4191.6	-6943.4

Table B.8: Full factorial Knoop grid ($7 \times 7 = 49$ points) around the nominal geometry

α	β	d_1 (mm)	d_2 (mm)	h (mm)	A (mm^2)	HK (V = const)	HK (d_1 = const)	ΔHK (V = const)
169.5	127	0.30794	0.056752	0.014148	0.008738	228.95	152.57	28.897
169.5	128	0.30569	0.057590	0.014044	0.008802	227.27	149.25	27.224
169.5	129	0.30342	0.058453	0.013940	0.008868	225.59	145.96	25.541
169.5	130	0.30114	0.059341	0.013836	0.008935	223.89	142.70	23.846
169.5	131	0.29885	0.060256	0.013730	0.009004	222.19	139.46	22.140
169.5	132	0.29654	0.061200	0.013624	0.009074	220.47	136.25	20.420
169.5	133	0.29421	0.062173	0.013517	0.009146	218.74	133.06	18.687
170.5	127	0.32930	0.054880	0.013681	0.009036	221.40	168.72	21.347
170.5	128	0.32689	0.055691	0.013581	0.009103	219.78	165.05	19.730
170.5	129	0.32447	0.056526	0.013481	0.009170	218.15	161.41	18.102
170.5	130	0.32203	0.057384	0.013379	0.009240	216.51	157.80	16.463
170.5	131	0.31958	0.058269	0.013277	0.009311	214.86	154.22	14.813
170.5	132	0.31710	0.059182	0.013175	0.009383	213.20	150.66	13.150
170.5	133	0.31461	0.060123	0.013071	0.009458	211.52	147.14	11.475
171.5	127	0.35475	0.052875	0.013181	0.009379	213.31	188.65	13.257
171.5	128	0.35216	0.053656	0.013085	0.009448	211.75	184.55	11.698
171.5	129	0.34955	0.054460	0.012988	0.009518	210.18	180.48	10.130
171.5	130	0.34692	0.055287	0.012890	0.009590	208.60	176.44	8.551
171.5	131	0.34428	0.056140	0.012792	0.009664	207.01	172.44	6.961
171.5	132	0.34162	0.057019	0.012693	0.009739	205.41	168.47	5.359
171.5	133	0.33893	0.057926	0.012593	0.009816	203.79	164.52	3.745
172.5	127	0.38573	0.050707	0.012641	0.009780	204.56	213.89	4.513
172.5	128	0.38291	0.051457	0.012549	0.009852	203.07	209.24	3.018
172.5	129	0.38007	0.052227	0.012456	0.009925	201.56	204.63	1.514
172.5	130	0.37722	0.053021	0.012362	0.010000	200.05	200.05	0.000
172.5	131	0.37434	0.053839	0.012268	0.010077	198.52	195.51	-1.525
172.5	132	0.37144	0.054682	0.012173	0.010156	196.99	191.01	-3.061
172.5	133	0.36853	0.055551	0.012077	0.010236	195.44	186.54	-4.609
173.5	127	0.42444	0.048340	0.012051	0.010259	195.01	246.89	-5.039
173.5	128	0.42134	0.049054	0.011963	0.010334	193.58	241.52	-6.464
173.5	129	0.41822	0.049789	0.011874	0.010411	192.15	236.19	-7.898
173.5	130	0.41507	0.050545	0.011785	0.010490	190.71	230.91	-9.341
173.5	131	0.41191	0.051325	0.011695	0.010571	189.25	225.67	-10.795
173.5	132	0.40872	0.052128	0.011604	0.010653	187.79	220.47	-12.259
173.5	133	0.40551	0.052957	0.011513	0.010737	186.31	215.31	-13.735
174.5	127	0.47454	0.045717	0.011397	0.010847	184.43	291.87	-15.620
174.5	128	0.47107	0.046392	0.011314	0.010927	183.08	285.52	-16.968
174.5	129	0.46758	0.047087	0.011230	0.011009	181.73	279.22	-18.324
174.5	130	0.46407	0.047803	0.011145	0.011092	180.36	272.97	-19.689
174.5	131	0.46053	0.048540	0.011060	0.011177	178.99	266.78	-21.063
174.5	132	0.45697	0.049300	0.010975	0.011264	177.60	260.63	-22.448
174.5	133	0.45338	0.050084	0.010889	0.011353	176.20	254.54	-23.844
175.5	127	0.54255	0.042755	0.010658	0.011599	172.48	356.82	-27.568
175.5	128	0.53859	0.043387	0.010581	0.011684	171.22	349.05	-28.828
175.5	129	0.53460	0.044037	0.010502	0.011771	169.95	341.35	-30.096
175.5	130	0.53058	0.044706	0.010423	0.011860	168.68	333.72	-31.373
175.5	131	0.52654	0.045395	0.010344	0.011951	167.39	326.15	-32.658
175.5	132	0.52247	0.046106	0.010264	0.012044	166.10	318.63	-33.953
175.5	133	0.51836	0.046840	0.010183	0.012140	164.79	311.18	-35.259

Chapter C

Supplementary WTLS diagnostics

C.1 Brinell WTLS diagnostics

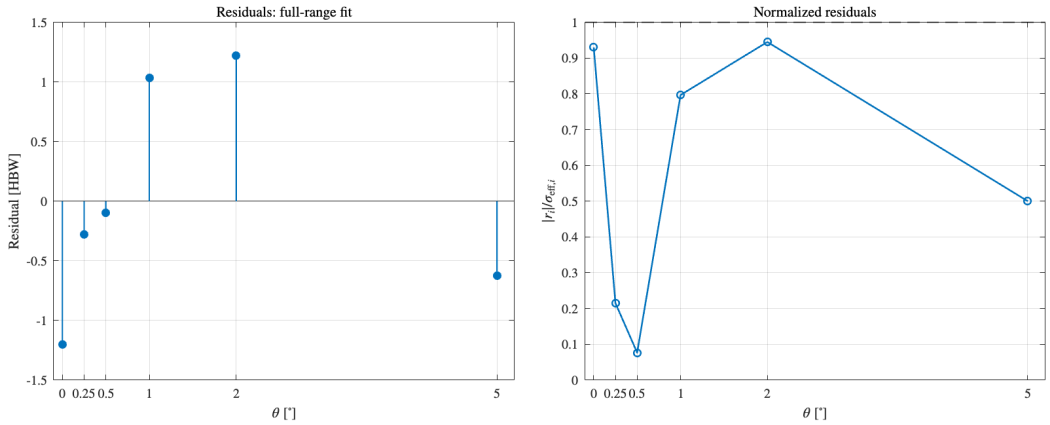

Figure C.1: Residuals and normalized residuals of the Brinell WTLS fit

C.2 Vickers WTLS diagnostics

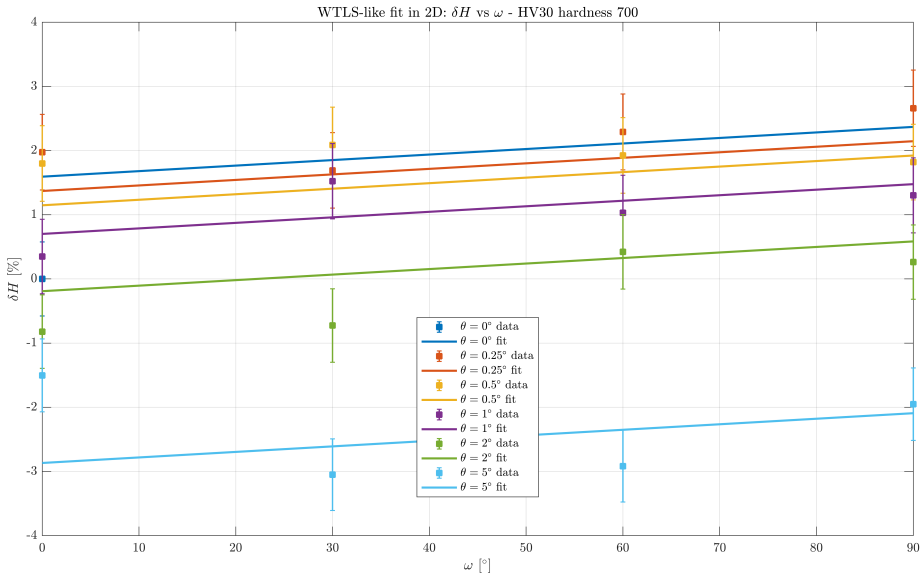

Figure C.2: WTLS-like 2D fit versus ω for the macro-Vickers HV30 hardness 700 block

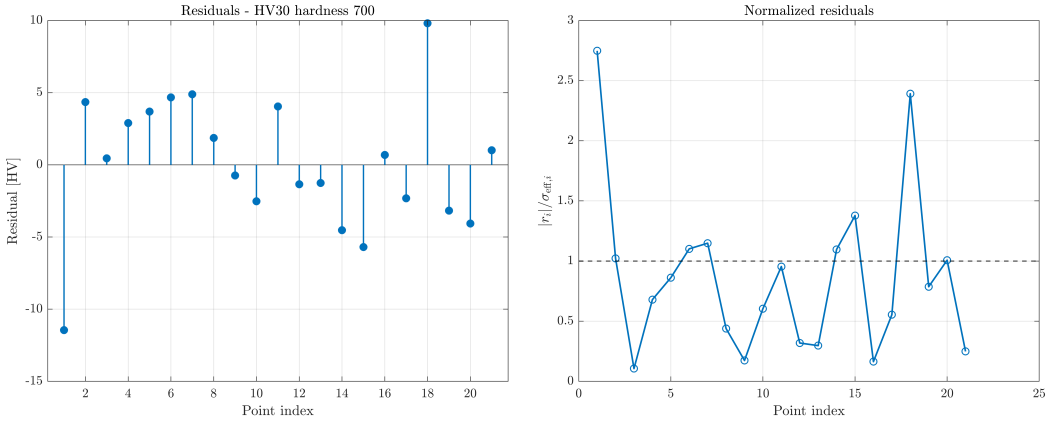

Figure C.3: Residuals and normalized residuals for the macro-Vickers HV30 hardness 700 block

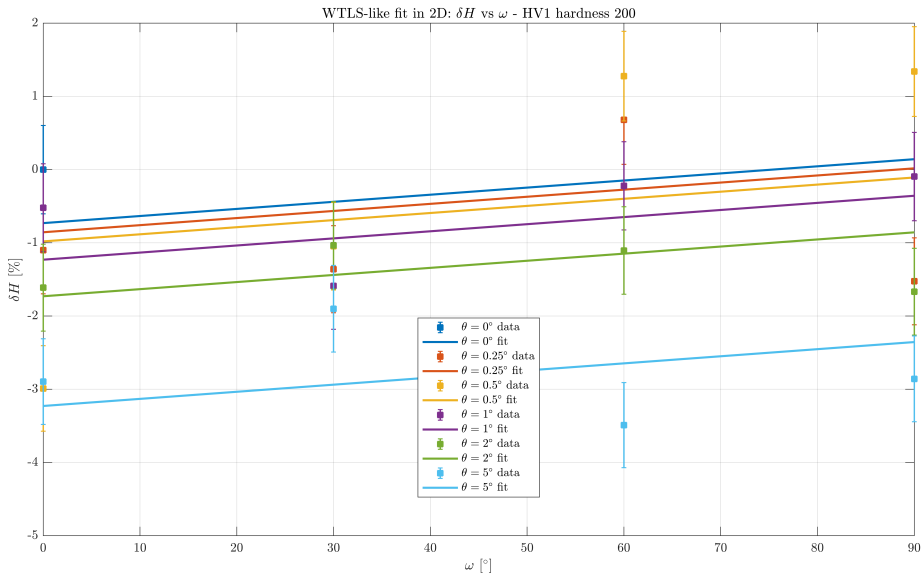

Figure C.4: WTLS-like 2D fit versus ω for the micro-Vickers HV1 hardness 200 block

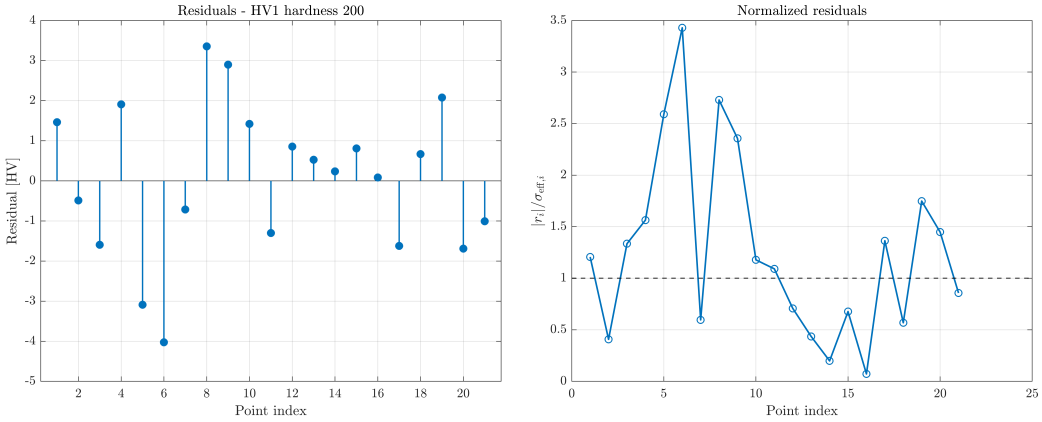

Figure C.5: Residuals and normalized residuals for the micro-Vickers HV1 hardness 200 block

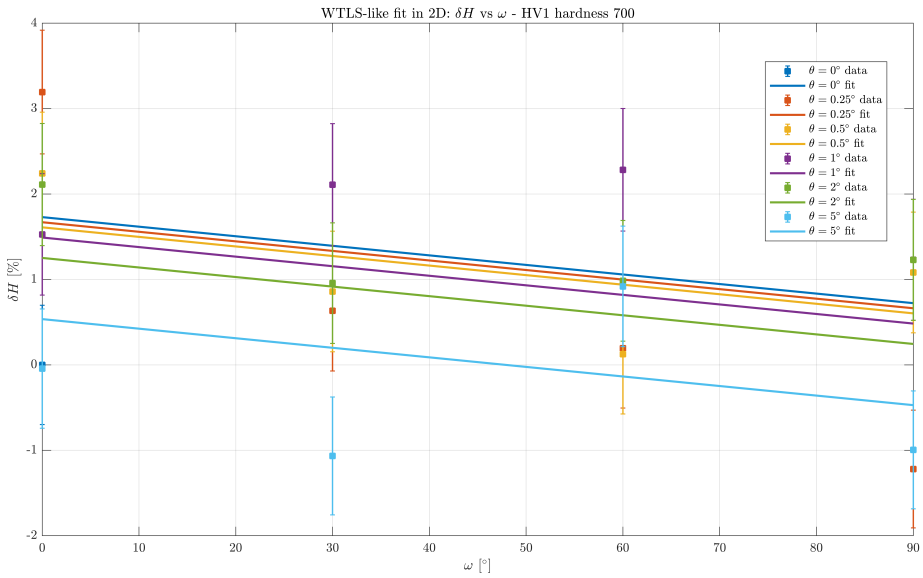

Figure C.6: WTLS-like 2D fit versus ω for the micro-Vickers HV1 hardness 700 block

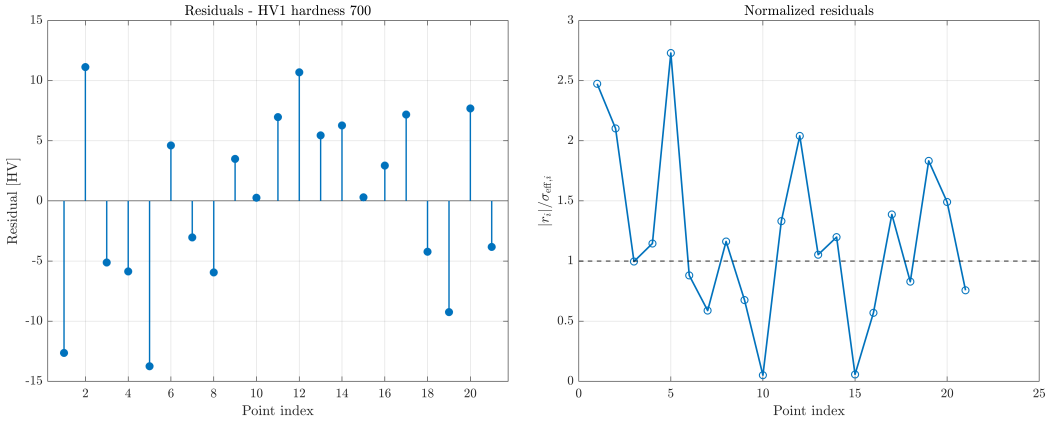

Figure C.7: Residuals and normalized residuals for the micro-Vickers HV1 hardness 700 block

C.3 Knoop WTLS diagnostics

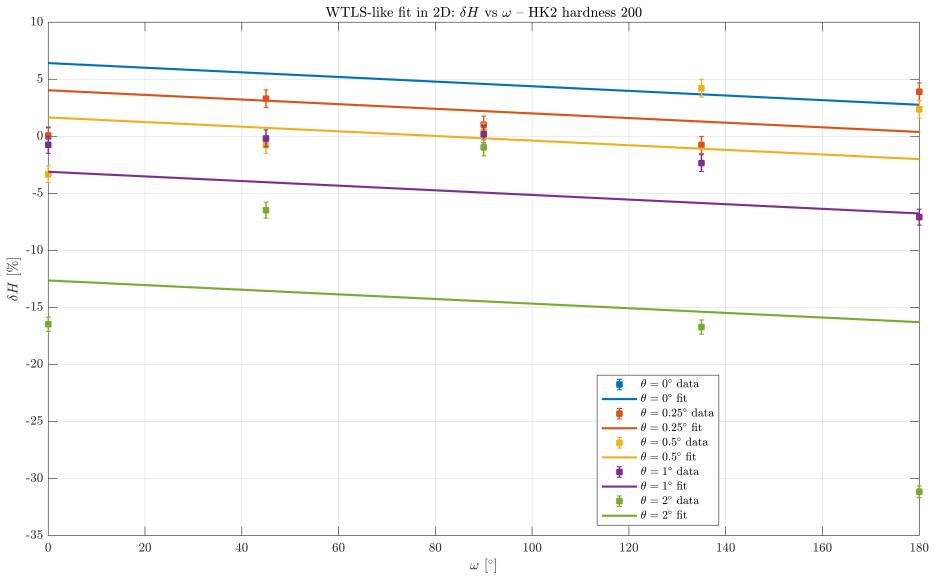

Figure C.8: WTLS-like 2D fit versus ω for the Knoop hardness 200 block

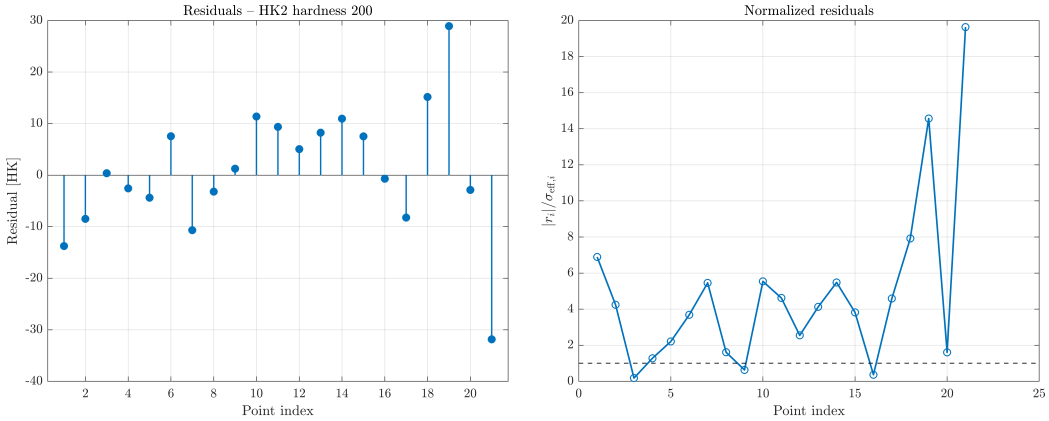

Figure C.9: Residuals and normalized residuals for the Knoop hardness 200 block

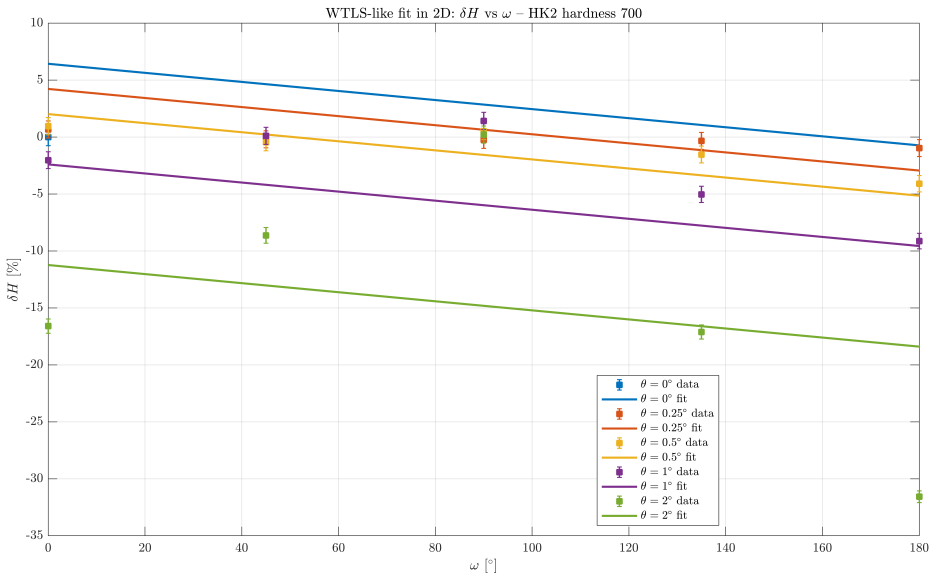

Figure C.10: WTLS-like 2D fit versus ω for the Knoop hardness 700 block

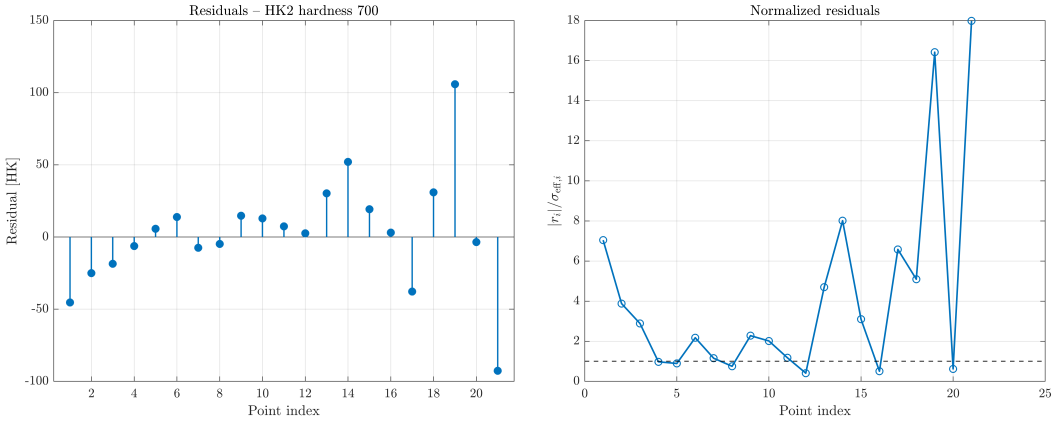

Figure C.11: Residuals and normalized residuals for the Knoop hardness 700 block